THE STRUCTURE AND FUNCTION OF A NOVEL TWO-SITE CALCIUM-BINDING FRAGMENT OF CALMODULIN

by

Theodore Lakowski

B.Sc. (Pharm), The University of British Columbia, 1999

A THESIS SUBMITTED IN PARTIAL FULFILLMENT OF THE REQUIREMENTS FOR THE DEGREE OF

DOCTOR OF PHILOSOPHY

in

THE FACULTY OF GRADUATE STUDIES

(Pharmaceutical Sciences)

UNIVERSITY OF BRITISH COLUMBIA

August 2006

Abstract

Several studies have revealed that calcium-binding EF-hands associate in various arrangements resulting in unique calcium affinities and target interactions, yet similar structures. This study examines the effect of EF-hand association on the structure, calcium-binding, and target-enzyme activation of a novel fragment of calmodulin formed by the association of EF-hands 2 and 3 (CaM2/3). The results from CaM2/3 are compared to those for the N- and C-domain fragments of calmodulin (CaM1/2 and CaM3/4, respectively).

Based on NMR spectroscopic analyses, CaM2/3 is unstructured in the absence of calcium, but upon binding calcium adopts a structure that is similar to both the N- and C-domains of calmodulin. CaM2/3 is composed of four α-helices and a short anti-parallel β-sheet between EF-hands 2 and 3. These EF-hands associate in a manner similar to those in the N- and C-domains of calmodulin. This association is facilitated by the conformationally-flexible hinge region between EF-hands. CaM2/3 exhibits stepwise calcium-binding with a $K_{d1} = 30 \pm 5$ μM to EF-hand 3, and a $K_{d2} = 1800 \pm 400$ μM to EF-hand 2. In native calmodulin, aromatic residues opposite the loop between EF-hands are an important part of its hydrophobic core. It is suggested here that these residues act as an "aromatic zipper" to hold the first and fourth helices of each domain together. In CaM2/3 this "aromatic zipper" is in a structurally redundant position adjacent to the loop between EF-hands, and this may result in weak calcium-binding affinity at EF-hand 2.

Our studies reveal that CaM2/3 binds a peptide corresponding to the calmodulin-binding sequence on skeletal muscle myosin light chain kinase (M13). This affinity is

lower than that measured for both CaM1/2 and CaM3/4. M13 appears to bind to a hydrophobic binding pocket on CaM2/3 in two equally populated conformations.

CaM1/2 and CaM3/4 have little or no ability to stimulate the activity of calcineurin. However, CaM2/3 has a limited ability to stimulate calcineurin, but also appears to inhibit the stimulatory effect of calmodulin on calcineurin.

This investigation leads to a greater understanding of the effect of EF-hand pairing, on structure, calcium-binding affinity, and target interactions in calmodulin.

Table of contents

Chapter 2
The structure and calcium affinity of fragments of calmodulin

Chapter 3
Interaction of fragments of calmodulin with selected targets

List of tables

List of figures

List of abbreviations

φ	the torsion angle formed from rotation around the C^{α}-N bond
ψ	the torsion angle formed from rotation around the C^{α}-C bond
[θ]	mean residue ellipticity
a.m.u.	atomic mass units (same as Da)
AUC	analytical ultracentrifugation
bHLH	basic α-helix-loop-α-helix
bHLHW	the dimer of a peptide representing the CaM-binding region of TCF4
bp	DNA base pairs
%C	percentage (w/w) of bisacrylamide per (acrylamide + bisarcylamide)
C'	the peptide bond carbonyl carbon
CaM	vertebrate calmodulin
CaM1/2	vertebrate calmodulin EF-hands 1 and 2 residues 1-80
CaM2/3	vertebrate calmodulin EF-hands 2 and 3 residues 46-113
CaM3/4	vertebrate calmodulin EF-hands 3 and 4 residues 81-148
CaM3	vertebrate calmodulin EF-hand 3
CaMKIIα	a peptide corresponding to the CaM-binding sequence on CaM-dependant kinase IIα
CaMKK	a peptide corresponding to the binding CaM-binding sequence on CaM-dependant kinase kinase
CD	circular dichroism
C. I. L.	Cambridge Isotope Laboratories Inc.
Da	Daltons (same as a.m.u)
dH_2O	de-ionized H_2O
dNTP	deoxynucleotide triphosphate
EGTA	ethylene glycol bis(2-aminoethyl ether)-N,N,N'N'-tetraacetic acid
h	hour
HLH	α-helix-loop-α-helix
HMQC	heteronuclear multiple quantum coherence
$^1H^N$	peptide bond amide hydrogen
HSQC	heteronuclear single quantum correlation
IMAC	immobilized metal affinity chromatography
IQ	CaM-binding sequence beginning with isoleucine and glutamine
K	association constant
K_d	dissociation constant K_d=1/K
kDa	kilo-Daltons (1000 a.m.u)
LB	Luria broth base
M13	a peptide representing the CaM-binding region of skMLCK
m/*z*	mass to charge ratio
MES	2-morpholinoethanesulfonic acid
min	minute
MLCK	myosin light chain kinase
MOPS	(3-[N-morpholino]propanesulfonic acid)
NMR	nuclear magnetic resonance
NOE	nuclear Overhauser effect

NOESY	nuclear Overhauser effect spectroscopy
OD_{600}	optical density at 600 nm
PAGE	polyacrylamide gel electrophoresis
PCR	polymerase chain reaction
PDB	protein data bank (http://www.rcsb.org/pdb/)
PDB ID	protein data bank accession code
ppm	parts per million
R	gas constant
R_1	$1/T_1$, the rate of T_1 relaxation
R_2	$1/T_2$, the rate of T_2 relaxation
R_n	the average rate of T_n relaxation
R20	a peptide representing the CaM-binding region of smMLCK
RDC	residual dipolar coupling
r.m.s.d.	root mean squared deviation
RP-HPLC	reverse phase high-performance liquid chromatography
rpm	revolutions per minute
S	sedimentation coefficient ($s=dr/dt(1/\omega^2 r)$) in Svedbergs ($s/10^{-13}$sec)
s	second
S^2	The square of the order parameter
SDS	sodium dodecyl sulfate
sec	second
skCaK	a peptide fragment corresponding to the CaM-binding sequence of the small-conductance Ca^{2+} activated potassium channel
skMLCK	skeletal muscle myosin light chain kinase
smMLCK	smooth muscle myosin light chain kinase
T	absolute temperature (Kelvin)
TFA	trifluoroacetic acid
TCF4	a bHLH transcription factor (A.K.A. E2-2)
%T	percentage (w/v), of both acrylamide and bisacrylamide
T_1	relaxation characterized by the longitudinal (Z dimension) return of the net magnetization to its ground state in the direction of the magnetic field
T_2	relaxation characterized by the loss of phase coherence in the transverse plane (XY plane).
τ_m	NOE mixing time
TnC	troponin C
TnC3	troponin C EF-hand 3
TnC4	troponin C EF-hand 4
TOCSY	total correlation spectroscopy
TR1C	vertebrate calmodulin tryptic fragment (residues 1-77)
TR2C	vertebrate calmodulin tryptic fragment (residues 78-148)
Tricine	N-[Tris(hydroxymethyl)methyl]glycine
Tris	Tris(hydroxymethyl) methylamine
U	units
UV	ultraviolet
xg	centrifugal force relative to gravity.

See Appendix A for a list of amino acids

Acknowledgment

I would like to thank my research supervisor Dr. Ron Reid for his guidance and support throughout my research. I would like to thank my supervisory committee members Drs. Stelvio Bandiera, Marc Levine, Lawrence McIntosh, and Chris Overall. I would also like to thank Roland Burton for help with the Mass Spectrometer, Calvin Yip for performing the light scattering experiments, Barbara Lelj-Garolla for performing the analytical ultracentrifugation experiments and Dr. Greg Lee for assistance with many of the NMR experiments. Special thanks are due to Dr. Grant Mauk for the use of the CD spectropolarimeter and to Dr. Federico Rosell for teaching me how to use it. Thanks are also due to Dr. Mark Okon for teaching me to use the NMR spectrometer and how to process NMR data, and once again to Dr. Greg Lee who showed me how to assign NMR spectra. Finally special thanks are due to Dr. Lawrence McIntosh who gave me support, guidance, many helpful suggestions, and near unfettered access to the Laboratory of Molecular Biophysics (LMB) NMR spectrometers.

I would like to thank the many members of my family who have given me support and encouragement throughout the years especially my Mum and Dad. Most importantly, I would like to thank my wife Margot Lakowski who provided love, support, and encouragement.

Financial assistance was provided by Merck-Frosst and The UBC University Graduate Fellowship. Instrument support for the LMB was provided by The Protein Engineering Network of Centers of Excellence (PENCE), The Canada Foundation for Innovation (CFI), the BC Knowledge Development Fund (BCKDF), and the Blusson Gift.

Chapter 1

Introduction

1.1 The biological roles of calcium

Calcium (Ca^{2+}) has many roles in the cell that include signal transduction, haemostasis, muscle contraction, immune function, and bone mineralization (Mann 1988; Strynadka and James 1989; McPhalen et al. 1991). At the molecular level, Ca^{2+} binds to proteins for three purposes: to stabilize protein structure, to buffer Ca^{2+} concentrations, and to mediate signal transduction (Strynadka and James 1989; McPhalen et al. 1991). Examples of enzymes stabilized by Ca^{2+} include thermatase and proteinase K (McPhalen et al. 1991). Proteins involved in Ca^{2+}-buffering and Ca^{2+} signal transduction generally fall into the EF-hand category. Calbindin D_{9k} and parvalbumin are examples of EF-hand Ca^{2+} buffering proteins, while calmodulin (CaM) and troponin C (TnC) are examples of EF-hand proteins that are involved in Ca^{2+} signal transduction (Kretsinger and Nockolds 1973; Goodman et al. 1979; Herzberg and James 1985; Szebenyi and Moffat 1986; Babu et al. 1988).

CaM is a highly conserved, ubiquitous EF-hand Ca^{2+}-binding protein involved in the regulation of more than 100 target proteins in response to Ca^{2+} signals (Lewit-Bentley and Rety 2000; Yamniuk and Vogel 2004). The interaction between CaM and these targets is generally strong, having dissociation constants on the order of 0.01 to 100 nM (Klee 1988). Rather than having many proteins, each with a Ca^{2+} sensing domain, CaM has evolved as a protein that can detect a Ca^{2+} stimulus and respond by activating a diverse set of target proteins. In this way, CaM is exceptional in the biological world because of its high affinity and diverse target recognition (Yamniuk and Vogel 2004).

1.2 The EF-Hand motif

CaM is part of a larger subset of proteins known as the CaM superfamily. Members of this superfamily share a common Ca^{2+}-binding α-helix-loop-α-helix (HLH) structure known as the EF-hand motif (Figure 1) (Moncrief et al. 1990; Nakayama et al. 1992). The typical EF-hand motif is 29 residues long and is composed of two α-helices (labeled E and F in Figure 1) separated by a 9 residue loop (Babu et al. 1988). The Ca^{2+}-binding segment consists of the loop and the first three residues of the second α-helix: 12 residues in total, 6 of which are Ca^{2+}-chelating residues and the other 6 non-chelating residues. When the six chelating residues are aligned along the Cartesian coordinates X, Y, and Z, a pentagonal bipyramidal ligation structure is formed between the chelating residues and a Ca^{2+} ion (Figure 1B and 1C). Residues 1 (+X), 3 (+Y), and 5 (+Z), each chelate via a single direct coordination of the side chain carboxyl oxygen with Ca^{2+} (Strynadka and James 1989). The 12 (-Z) position has two coordination points through both oxygens of a glutamate side chain carboxyl (because there are two coordination points, this glutamate is called bidentate). The backbone carbonyl oxygen of position 7 (-Y) coordinates Ca^{2+} directly, and the side chain of position 9 (-X) coordinates Ca^{2+} indirectly via a water molecule (Figure 1) (Strynadka and James 1989).

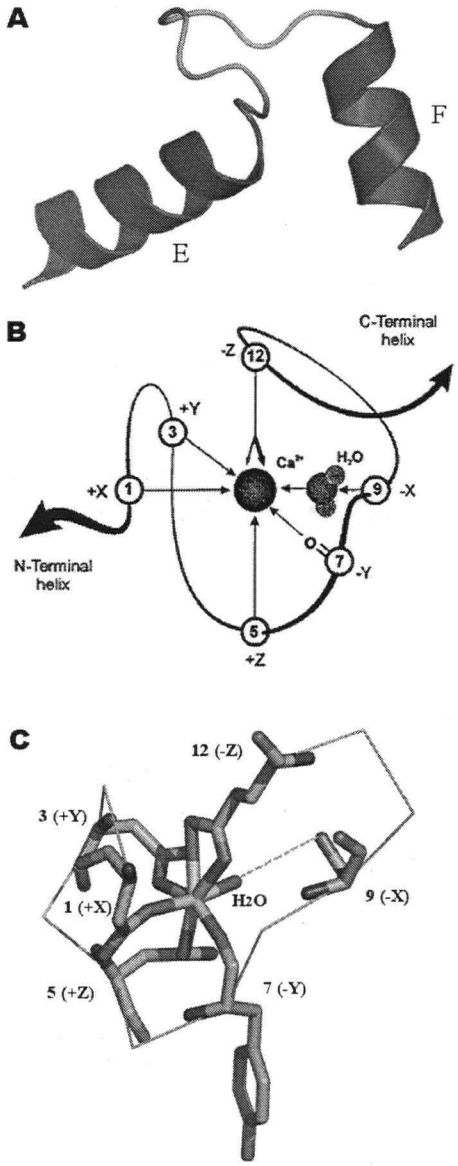

Figure 1. The EF-Hand motif. **(A)** A ribbon diagram of a single EF-hand; the helices are labeled E and F from the N- to C-terminals. **(B)** A diagram of the EF-hand chelating segment showing the residues in the pentagonal bipyramidal chelating structure. **(C)** The EF-hand 3 chelating segment residues from a crystal structure of CaM (3CLN) (Babu et al. 1988). All residues are bound to Ca^{2+}, and the dashed line is a hydrogen-bond from the position 9 residue side chain to water. The structures for A and C were rendered using the program Pymol (DeLano 2002).

The original description of the EF-hand was based on the structure of parvalbumin. The EF-hand has subsequently been identified in numerous proteins including TnC, CaM, and calbindin D_{9k} (Kretsinger and Nockolds 1973; Herzberg and

James 1985; Babu et al. 1988). There is also a variant of the EF-hand known as the pseudo-EF-hand present, for example, in calbindin D_{9k}. The pseudo EF hand differs from the canonical EF-hand in that the Ca^{2+}-binding segment is composed of 14 residues and exhibits a modified chelation structure involving mostly backbone carbonyl oxygens. However, as with canonical EF hands the last chelating residue of the pseudo-EF-hand is usually a bidentate glutamate (Szebenyi and Moffat 1986).

Several studies have determined the propensity for amino acids to occupy positions in the chelating segment of the EF-hand. The results of such a study are summarized in Table 1 (Falke et al. 1994). Positions 1 (+X) and 12 (-Z) are highly conserved, usually being aspartate and glutamate, respectively. Mutations at these positions reduce Ca^{2+}-affinity (Maune et al. 1992b; Falke et al. 1994). The majority of the residues found at chelating positions 3 (+Y) and 5 (+Z) are aspartates. In contrast, positions 7 (-Y) and 9 (-X) show the greatest diversity of the Ca^{2+}-chelating residues. Some residues, not directly involved in chelation, also show some sequence conservation (Moncrief et al. 1990). For example, Position 8 is almost always a branched aliphatic hydrophobic amino acid, whereas positions 4 and 6 are usually glycines (Moncrief et al. 1990).

Table 1. Summary of residue propensity for 567 EF-Hand loop sequences

Coordinate	+X		+Y		+Z		-Y		-X			-Z
Loop Position	**1**	**2**	**3**	**4**	**5**	**6**	**7**	**8**	**9**	**10**	**11**	**12**
Consensus	**D**	**K**	**D**	**G**	**D**	**G**	**T**	**I**	**D**	**F**	**E**	**E**
Consensus%	**100**	**29**	**76**	**56**	**52**	**96**	**23**	**68**	**32**	**23**	**29**	**92**
# Observed	D567	K163	D432	G319	D295	G541	T130	I384	D181	F131	E164	E523
		A46	N130	K69	S131	D9	F90	V94	S116	Y64	D108	D44
		Q45	S5	R48	N123	N8	K70	L74	T79	A59	K70	
		T56		R47	T9	K4	Q54	M11	E65	T53	A54	
		V46		Q22	G8	R2	Y51	C4	N57	L44	P47	
		I39		A15	E1	H2	E36		G56	V43	N35	
		S36		H13			R27		Q9	E37	Q24	
		E32		S11			S26		C4	K35	S20	
		R30		D7			I15			S19	R7	
		L16		E7			C13			P17	G7	
		F9		T5			D11			I14	T7	
		M8		M3			L11			R13	Y7	
		Y5		C1			V11			G10	L5	
		N3					A8			W7	V5	
		C3					H6			N5	H4	
		D1					M5			Q5	M3	
		G1					N3			M5		
										D3		
										C2		
										H1		

The propensity for amino acids to occupy specified EF-Hand loop positions. The consensus sequence is in bold. The one letter code is used followed by the number of occurrences of that residue. This table is adapted from the summary of 576 EF hand sequences from (Falke et al. 1994).

There have been many attempts to estimate the Ca^{2+}-affinity of particular Ca^{2+}-binding sites in EF-hand proteins (Wang and Cheung 1985; Williams et al. 1986; Reid 1987b; Linse et al. 1991). However, affinity can depend not only on the sequence and structural context of a specific EF hand within a given protein but also on the ionic strength, pH, and presence of low affinity competing ligands such as magnesium (Mg^{2+}) and potassium (K^{+}) in the buffer (Haiech et al. 1981). High ionic strength buffers reduce Ca^{2+}-affinity by screening the negative charge of the chelating residues. Indeed, the concentration of the EF-hand protein itself has been shown to affect Ca^{2+}-affinity through the same mechanism (Linse et al. 1995). The affinities of most EF-hand proteins remain

approximately constant over the range of pH 6.4 to 8.3 (Svensson et al. 1993). However, both significantly higher and lower pH solutions can reduce affinity by altering the ionization state of chelating residues and the state of Ca^{2+} (e.g. $Ca(OH)_2$). Mg^{2+} can bind to some EF-hand proteins but with considerably reduced affinity (approximately 10^4 fold less than for Ca^{2+}). However, at sufficiently high concentration Mg^{2+} can reduce the apparent affinity for Ca^{2+} by competition for binding sites.

1.3 The acid pair hypothesis

Several attempts have been made to show a relationship between the Ca^{2+}-affinity of EF hands and the amino acids in the chelating segments. The acid pair hypothesis correlates Ca^{2+}-affinity with both the number and coordination position of acidic amino acids in the Ca^{2+}-binding segment of EF-hand proteins (Reid and Hodges 1980). One of the first model systems used to test this hypothesis was a synthetic peptide fragment corresponding to EF-hand 3 of CaM (CaM3), and mutants thereof (Reid 1990). The acid pair hypothesis states that the Ca^{2+}-affinity of EF-hands will increase if acidic residues (aspartate and glutamate) are paired along the axial vertices of the resulting pentagonal bipyramidal arrangement of chelating residues in the Ca^{2+}-binding segment (Reid 1990). This hypothesis predicts that the highest affinity occurs when positions 1, 9, 5, and 12 (+X, -X, +Z, -Z) of the Ca^{2+}-binding segment are occupied by acidic residues. The hypothesis also predicts that because the position 7 (-Y) residue coordinates Ca^{2+} via its backbone carbonyl oxygen, a Y-axis acid pair will not increase Ca^{2+}-affinity (Reid 1990). Further refinement of the initial hypothesis showed that the Z-axis acid pair produced larger increases in Ca^{2+}-affinity over X-axis acid pairs, and that increasing the number of acidic residues from 3 to 4 by replacing an asparagine in the +Y position with an

aspartate increased affinity from 2 to 38 fold (Procyshyn and Reid 1994a; b). Fragments of CaM were used for initial testing of the acid pair hypothesis, but testing was also extended to mutants of native CaM. These studies largely confirmed the previous studies with single Ca^{2+}-binding site synthetic EF-hand protein fragments (Wu and Reid 1997b; a). Furthermore, these studies show that mutation of one site decreases affinity of a neighboring Ca^{2+}-binding site (Wu and Reid 1997b). These studies also confirm that increasing the number of acid pairs from 0 to 1 and even 2 increases Ca^{2+}-affinity, and that Z-axis acid pairs produce the greatest increase in affinity (Wu and Reid 1997b). Further investigations using mutants of CaM also confirm the acid pair hypothesis (Black et al. 2000). They reveal that increasing the number of axial acid pairs by 1 or 2 increases the affinity of CaM for Ca^{2+}. An increase in the number of acid pairs from 0 to 1 results in a 4.6 fold increase in Ca^{2+}-affinity and an increase from 0 to 2 acid pairs results in an 8 fold increase in Ca^{2+}-affinity (Black et al. 2000). A Z-axis acid pair produces the highest increase in Ca^{2+}-affinity by a single acid pair, while the highest increase in affinity with 2 acid pairs is observed when they are aligned along the Y and Z axes (Black et al. 2000). This contradicts the acid pair hypothesis because the addition of a Y-axis acid pair increases the Ca^{2+}-affinity. Increasing the number of acid pairs from 2 to 3 did not significantly increase Ca^{2+}-affinity in CaM (Black et al. 2000).

1.4 Cooperativity in EF-hand proteins

With few exceptions EF-hand Ca^{2+}-binding proteins do not exist as single EF-hand motifs in nature. EF-hands are normally paired to form EF-hand domains. The interaction of these paired EF-hands within the resulting domains can lead to cooperativity in Ca^{2+}-binding (Linse and Forsen 1995). In any given Ca^{2+}-binding EF-

hand domain, if Ca^{2+}-binding to the first EF hand promotes binding to the second EF-hand, the cooperativity is considered positive. If Ca^{2+}-binding to the first EF-hand decreases affinity at the second EF-hand, the cooperativity is negative. Most Ca^{2+}-binding proteins including, CaM, oncomodulin, and calbindin D_{28k} exhibit positive cooperativity between paired EF-hands (Linse and Forsen 1995).

Scheme 1 shows the two-site Ca^{2+}-binding scheme in a typical EF-hand domain where K_I, K_{II}, $K_{I,II}$ and $K_{II,I}$ are microscopic equilibrium Ca^{2+}-affinity constants. Positive cooperativity is said to occur when $K_{I,II} > K_I$ (or $K_{II,I} > K_{II}$) and negative cooperativity is defined as $K_{I,II} < K_I$ (or $K_{II,I} < K_{II}$) (Linse and Forsen 1995). However, a more common definition of cooperativity is the difference in the free energy of Ca^{2+}-binding between EF-hands in a given EF-hand domain (equation 1). The Ca^{2+}-binding sites are positively cooperative if $\Delta\Delta G < 0$, negatively cooperative if $\Delta\Delta G > 0$, and cooperativity is not present if $\Delta\Delta G = 0$ (or $K_{I,II} = K_I$ or $K_{II,I} = K_{II}$).

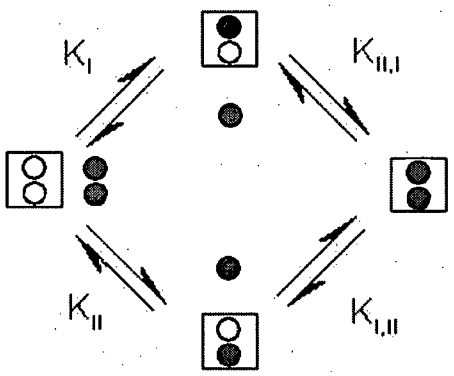

Scheme 1. A schematic of a cooperative interaction. The rectangles represent a Ca^{2+}-binding EF-hand domain, and the black spheres represent Ca^{2+}. K_I, K_{II}, $K_{I,II}$, and $K_{II,I}$ are microscopic equilibrium affinity constants.

$$\Delta\Delta G = -RT\ln\left(\frac{K_{I,II}}{K_I}\right) = -RT\ln\left(\frac{K_{II,I}}{K_{II}}\right) \qquad [1]$$

In practice it is difficult to measure the site-specific microscopic affinity constants. Rather, one measures the macroscopic affinity constants corresponding to the net binding of the first Ca^{2+} to either site ($K_1=K_I+K_{II}$), followed by binding to the remaining site (K_2). It is relatively straightforward to determine the macroscopic equilibrium affinity constants, as specified in scheme 2 and equations 2 and 3, with titrations monitored using spectroscopic techniques or methods such as equilibrium dialysis (Linse et al. 1991; Linse and Forsen 1995). In the case where the microscopic and macroscopic association constants are known, then one can calculate $\Delta\Delta G$ using equation 4 (where $\eta = K_{II}/K_I$). However, as the microscopic affinity constants are generally unknown, an upper limit of $\Delta\Delta G$ ($\Delta\Delta G_{\eta=1}$) is usually defined instead. Given that K_{II} and K_I are similar in magnitude, the last term in equation 4 will be 0 (because η 1 when K_{II} K_I) and an upper limit of $\Delta\Delta G$ ($\Delta\Delta G_{\eta=1}$) can be defined with equation 5 (Linse and Forsen 1995). $\Delta\Delta G_{\eta=1}$ is considered an upper limit because the second term of equation 4 is always ≥ 0 regardless of the value of η and therefore the value of the true $\Delta\Delta G$ may be lower than the $\Delta\Delta G_{\eta=1}$ but not higher. Thus, if $\Delta\Delta G_{\eta=1}$ is negative the system binds Ca^{2+} with positive cooperativity, whereas positive values for $\Delta\Delta G_{\eta=1}$ reveal nothing about cooperativity without further knowledge of the value of η (Linse and Forsen 1995). When the microscopic affinity constants differ widely such that $K_I >> K_{II}$ (or $K_I << K_{II}$), Ca^{2+}-binding is stepwise or sequential (Linse and Forsen 1995). Problems arise in detecting cooperativity in this case because it is not possible to measure the affinity constant of the low affinity site when the high affinity site is Ca^{2+}-free, and one cannot measure the affinity constant of the high affinity site when the lower affinity site is occupied (Forsen and Linse 1995; Linse and Forsen 1995). If stepwise Ca^{2+}-binding is

present, cooperativity can sometimes be assessed using different ligands such as Cd^{2+} and La^{3+} to occupy the higher affinity sites while Ca^{2+} is titrated into the low affinity site (Linse and Chazin 1995).

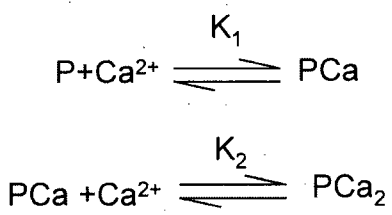

Scheme 2. A schematic of the macroscopic equilibrium of a two-site Ca^{2+}-binding protein. P is the two EF-hand Ca^{2+}-binding protein. PCa and PCa_2 are the Ca^{2+}-binding protein with one and two Ca^{2+} bound, respectively. Equations 2 and 3 are the macroscopic equilibrium affinity constants K_1 and K_2, that govern the steps of the scheme. Equations 2 and 3 also show the relationship between the macroscopic and microscopic equilibrium affinity constants.

$$K_1 = \frac{[PCa]}{[P][Ca^{2+}]} = K_I + K_{II} \qquad [2]$$

$$K_2 = \frac{[PCa_2]}{[PCa][Ca^{2+}]} = \frac{K_I K_{II,I}}{(K_I + K_{II})} \qquad [3]$$

$$\Delta\Delta G = -RT\ln\left(\frac{4K_2}{K_1}\right) - RT\ln\left[(\eta+1)^2/4\eta\right] \text{ where } \eta = K_{II}/K_I \qquad [4]$$

$$\Delta\Delta G_{\eta=1} = -RT\ln\left(\frac{4K_2}{K_1}\right) \qquad [5]$$

Cooperativity can also be measured using the Hill coefficient (n_H) as in equation 6, where *fsat* is the fractional saturation of the Ca^{2+}-binding protein, and $[Ca^{2+}]$ is the free Ca^{2+} concentration. The value of the Hill coefficient at half factional ($n_{H1/2}$) saturation is frequently reported using equation 7 (Forsen and Linse 1995). However, this equation

provides no direct physical relationship between the microscopic Ca^{2+}-affinity constants (K_I, K_{II}, $K_{I,II}$ and $K_{II,I}$) and the Hill coefficient. For this reason, $\Delta\Delta G$ is considered a better measure of cooperativity (Forsen and Linse 1995). In addition, when comparing the effects of mutations and truncations on EF-hand Ca^{2+}-binding proteins, the changes in cooperativity are better reflected by $\Delta\Delta G$ than n_H (Forsen and Linse 1995). It should be noted that in constructing a Hill plot of $\ln(fsat/(1- fsat))$ versus $\ln[Ca^{2+}]$, there must be knowledge of the point of saturation (maximal *fsat*), which is not always easy to determine. Finally, another qualitative method for assessing cooperativity is the shape the Scatchard plots (constructed *fsat* versus $fsat/[Ca^{2+}]$). This method is not ideal because it requires the mixing of dependant and independent variables for construction of the curves (Dahlquist 1978).

$$n_H = \frac{d \ln \frac{fsat}{1 - fsat}}{d \ln[Ca^{+2}]} \qquad [6]$$

$$n_{H1/2} = \frac{4\sqrt{(K_2 / K_1)}}{1 + 2\sqrt{(K_2 / K_1)}} \qquad [7]$$

1.5 The crystal structure of Ca^{2+}-ligated CaM

The structure of Ca^{2+}-ligated CaM can vary depending on the method of structural determination but there is some general consensus on the overall fold. CaM is composed of four Ca^{2+}-binding EF-hands paired into its N- and C-terminal domains, which are connected by a flexible loop known as the hinge (Figure 2) (Babu et al. 1988; Barbato et al. 1992). The four EF-hands are designated 1 through 4 and the helices are labeled A through H from the N- to the C- terminal. A short β-sheet exists between the paired EF-

hands (arrows in Figure 2) facilitating the formation of each domain (Babu et al. 1988). Beyond being linked by the intervening hinge, the domains do not interact.

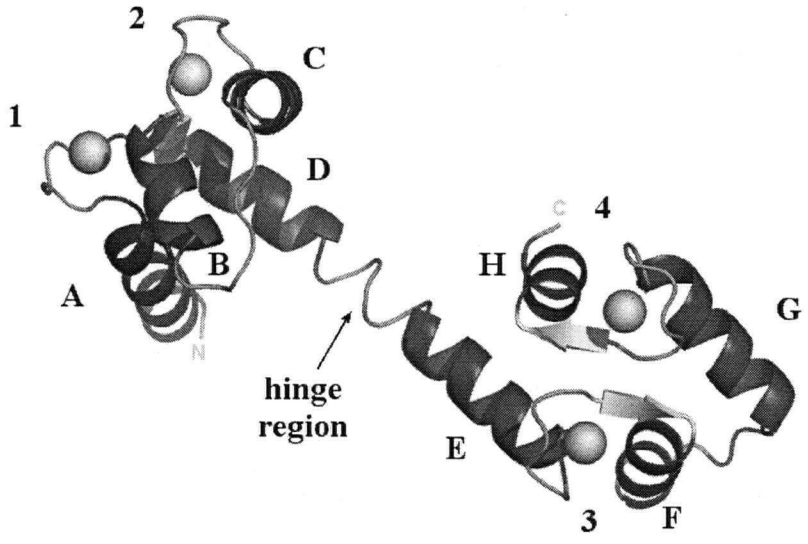

Figure 2. The structure of Ca^{2+}-ligated CaM. A crystal structure of CaM (PDB ID 3CLN) (Babu et al. 1988). The helices are labeled A through H. Ribbons with arrows represent short anti-parallel β-sheets. The Ca^{2+} are represented as spheres, within EF-hands 1 through 4. The coil regions are lines. The hinge region is indicated, along with the N- and C- terminals (gray N and C). The shape of CaM roughly resembles a dumbbell. The structure was rendered using the program Pymol (DeLano 2002).

1.5.1 The open crystal structures of Ca^{2+}-ligated CaM

The known structures of CaM can be divided into three groups, namely Ca^{2+}-ligated CaM, Ca^{2+}-free CaM, and CaM-target complexes. Structures from all three of the groups have been determined using both NMR spectroscopy and X-ray crystallography. The Ca^{2+}-ligated crystal structures of CaM are further subdivided into two groups, denoted open and closed. There are several open crystal structures of Ca^{2+}-ligated CaM that take the form of the well-known "dumbbell" structure shown in Figure 3. Consistent with their sequence similarities the open structures of CaM from rat, human and *Paramecium tetraurelia* have mean backbone r.m.s.d. (over residues 5-146) of 0.43 ±

0.17Å (Babu et al. 1988; Chattopadhyaya et al. 1992; Wilson and Brunger 2000). Although the hinge region between domains appears as a single continuous α-helix (sometimes called the central α-helix) the φ and ψ angles and the hydrogen-bond lengths from residues 79 to 81 are indicative of "unwinding" in this region. In addition, residues 76 to 82 in the central α-helix of the open crystal structures of CaM have high temperature crystallographic B-factors indicating conformational flexibility (Babu et al. 1988; Chattopadhyaya et al. 1992; Wilson and Brunger 2000). These properties suggest that the classical "dumbbell" shape of CaM may not be adopted in solution.

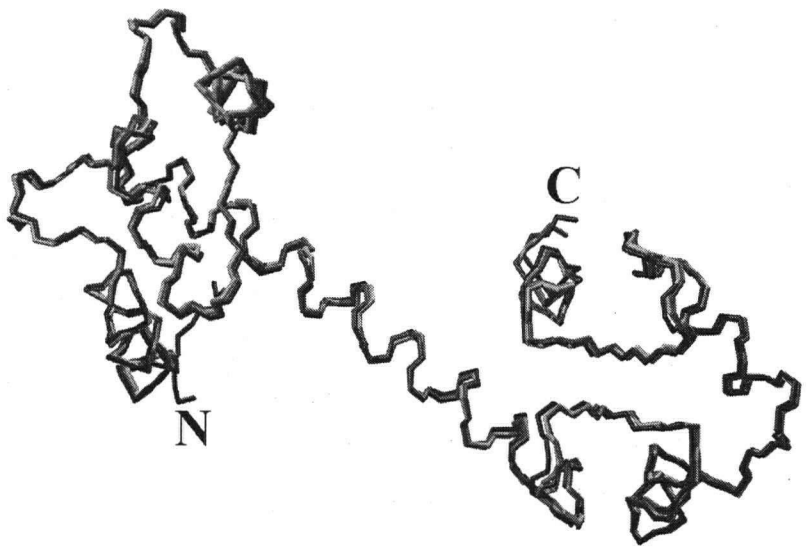

Figure 3. The open crystal structures of Ca^{2+}-ligated CaM. Three open crystal structures of CaM. Rat (light gray) (PDB ID 3CLN), human (gray) (PDB ID 1CLL), and *Paramecium tetraurelia* (black) (PDB ID 1EXR) CaM structures (Babu et al. 1988; Chattopadhyaya et al. 1992; Wilson and Brunger 2000). The structures are aligned along the helices and the backbone (C^{α}, C , N) pair wise r.m.s.d. is 0.43 ± 0.17Å indicating a high degree of structural conservation that is consistent with the 89% residue identity between vertebrate and *Paramecium* calmodulin. The N- and C-terminal ends of the molecule are indicated. The structures were rendered using MOLMOL (Koradi et al. 1996).

The anti-parallel β-sheet between EF-hands in each domain is formed around two direct hydrogen-bonds. In the N-terminal domain, hydrogen-bonds are formed between

the amide hydrogen and carbonyl oxygens of position 8 Ca^{2+}-chelating residues I27 and I63, and similar hydrogen-bonds are observed in the C-terminal domain between position 8 Ca^{2+}-chelating residues I100 and V136. Additional hydrogen-bonds in the anti-parallel β-sheet are indirect as they are bridged with water molecules through the amide hydrogen and carbonyl oxygens of residues neighboring the above listed residues (Babu et al. 1988; Chattopadhyaya et al. 1992; Olsson and Sjolin 2001). The paired EF-hands are connected by a loop region composed of residues 38 to 45 in the N-domain and residues 112 to 117 in the C-domain. Both loops contain turns facilitated by two hydrogen-bonds from the amide hydrogens of G40 and G113, respectively (Chattopadhyaya et al. 1992).

The hydrophobic cores of each domain of CaM are formed through the packing of hydrophobic residues on neighboring α-helices. Especially important are the hydrophobic interactions between the first and fourth α-helices in each domain (Shaw and Sykes 1996). Key to these interactions are aromatic residues that are arranged such that the planes of their aromatic rings are stacked nearly perpendicular to each other (Babu et al. 1988; Chattopadhyaya et al. 1992; Wilson and Brunger 2000). This is sometimes referred to as the T-shaped aromatic stacking arrangement (Misura et al. 2004). Four aromatic residues make up this stacking interaction and each aromatic ring is nearly perpendicular to its neighbor. The first is located four residues before the termination of the first α-helix, the second is the terminating residue of the first α-helix, and the third and fourth are located at Ca^{2+}-binding segment position 10 and just after position 12 of the second Ca^{2+} binding segment (residues F16, F19, F65 and F68 from the N terminal domain and residues F89, F92, Y138 and F141 from the C-terminal domain) (Babu et al. 1988; Chattopadhyaya et al. 1992).

1.5.2 The closed crystal structures of Ca^{2+}-ligated CaM

A recent crystal structure of Ca^{2+}-ligated CaM shows marked differences from the open structures and has been called a closed structure (Figure 4) (Fallon and Quiocho 2003). Although open crystal structures of CaM suggest that there is conformational-flexibility in the hinge region. The closed structure of CaM exhibits a hinge region comprised of residues 78 to 81 that forms a type I reverse turn rather than an α-helix (Fallon and Quiocho 2003). Unlike the open crystal structures, the closed crystal structure of CaM shows inter-domain contacts between the N-terminal α-helix A and the C-terminal α-helices G and H. These inter-domain contacts take the form of 16 hydrogen bonds and 24 van der Waals interactions. These interactions produce a globular structure rather than the dumbbell-shaped open structures of Ca^{2+}-ligated CaM (Fallon and Quiocho 2003). Most of the residues identified as inter-domain contacts are also involved in CaM-target interactions leading to the proposal that this structure facilitates the formation of CaM-target complexes (Fallon and Quiocho 2003).

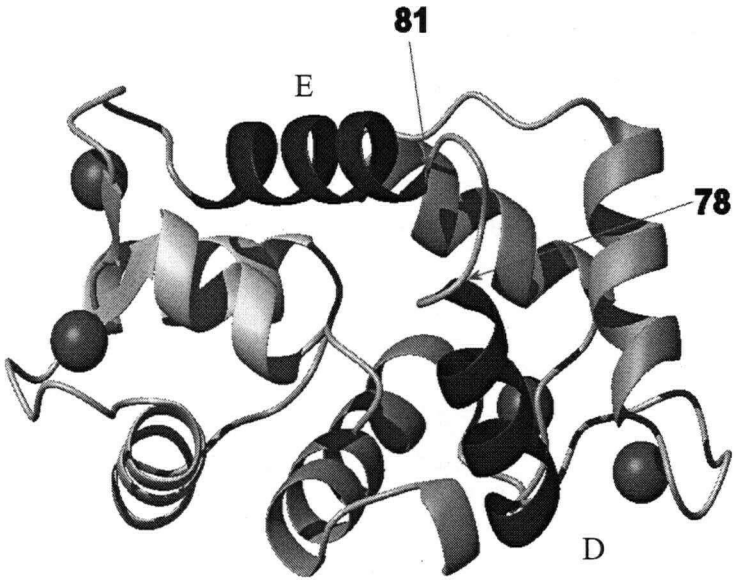

Figure 4. The closed crystal structure of Ca^{2+}-ligated CaM. A closed crystal structure of CaM (PDB ID 1PRW) (Fallon and Quiocho 2003). The α-helices D and E are labeled. The residues delimiting the hinge region with the intervening type I reverse turn are labeled. The β-sheet is represented with ribbons with arrows and the black spheres represent Ca^{2+} ions. The structure was rendered using MOLMOL (Koradi et al. 1996).

1.6 The NMR derived structure of CaM

Structural studies using NMR spectroscopy have improved the understanding of CaM. Arguably the most important initial discovery is that the central α-helix observed in the open crystal CaM structures is highly flexible from K77 to S81 (Barbato et al. 1992). This led to the discovery that the two domains of CaM tumble independently in solution, and thus do not adopt a consistent orientation with respect to each other (Barbato et al. 1992). Chou *et al.* used residual dipolar couplings (RDC) to determine an NMR structure for CaM in solution (Chou et al. 2001b). Each domain of this NMR-derived structure exhibited significant similarity to that of the crystal structures of CaM as reflected by a backbone r.m.s.d. of 0.9Å. However, there is greater similarity still

between the domains of this NMR structure as reflected in a backbone r.m.s.d. of 0.65Å (Chou et al. 2001b). All of the aromatic residues were found to be in a single rotomer with $\chi 1$ dihedral angles similar to those in the repeated crystal structures of CaM. The $\chi 1$ angles for methionine and leucine residues were also found to be similar to existing crystal structures. However, significant rotomer averaging was observed with leucine ($\chi 2$) as well as methionine ($\chi 3$) rotomers (Chou et al. 2001b). This hydrophobic aliphatic side chain flexibility is thought to aid in the diverse target recognition of CaM. The angles between neighboring α-helices in this NMR structure were found to be larger than in previously described CaM structures leading to a compact overall fold in each domain (Chou et al. 2001b).

1.7 The Ca^{2+}-free structures of CaM

Initial attempts to crystallize Ca^{2+}-free CaM were unsuccessful, and as a consequence most of the existing Ca^{2+}-free CaM structures have been solved using NMR. The secondary structure of Ca^{2+}-free CaM in solution is essentially the same as that of Ca^{2+}-ligated CaM. The four residues at the N-terminal ends of each of α-helices B through H show $^{13}C^{\alpha}$ and $^{13}C^{\beta}$ chemical shifts, as well as inter-proton NOE patterns, that are characteristic of α-helix N-capping boxes (Kuboniwa et al. 1995; Zhang et al. 1995). Backbone amide hydrogen exchange and $^{13}C^{\alpha}$ chemical shifts indicate that the α-helices are less stable in the Ca^{2+}-free form of CaM compared to the Ca^{2+}-ligated state. As with previously described structures of CaM, there appear to be no contacts between the domains of Ca^{2+}-free CaM, and the domains of Ca^{2+}-free CaM tumble independently of each other in solution (Figure 5A) (Zhang et al. 1995). The hinge region of Ca^{2+}-free CaM is flexible, but there is evidence that it may transiently adopt an α-helical structure

(Kuboniwa et al. 1995). The most important difference between the Ca^{2+}-ligated and Ca^{2+}-free structures of CaM is the angles between adjacent α-helices. In the Ca^{2+}-free NMR structures the angles between adjacent α-helices are large and they are packed nearly anti-parallel to each other (Kuboniwa et al. 1995; Zhang et al. 1995). This anti-parallel conformation produces a tightly packed four α-helical bundle that prevents exposure of the hydrophobic core residues to the solvent (Table 2) (Kuboniwa et al. 1995; Zhang et al. 1995). In Ca^{2+}-ligated CaM structures the angles between adjacent α-helices are nearly perpendicular resulting in a more open structure (Table 2) (Babu et al. 1988).

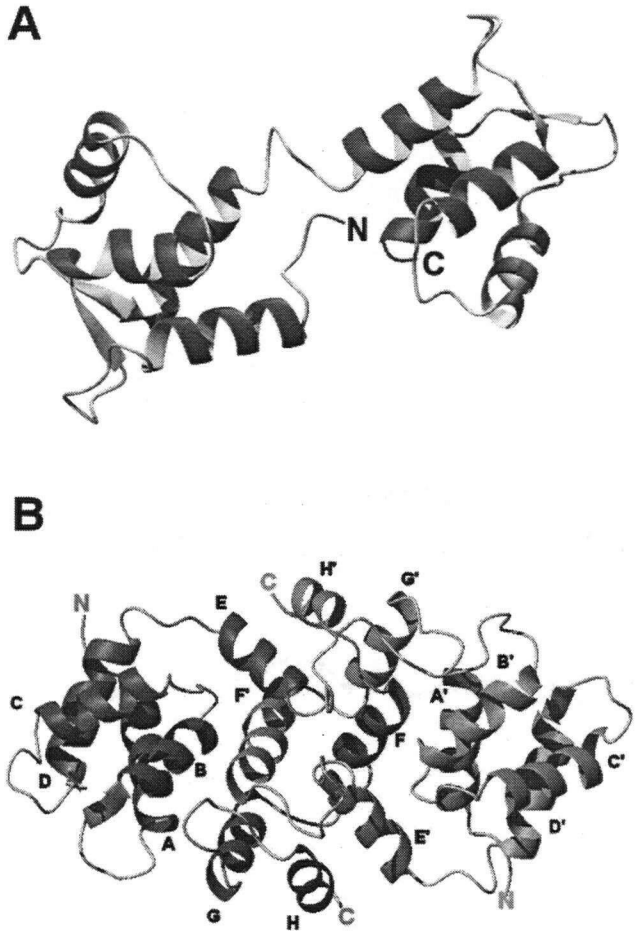

Figure 5. The Ca^{2+}-free structures of CaM. **(A)** The NMR derived structure of Ca^{2+}-free CaM (PDB ID 1CFD). The α-helices are represented as coiled ribbons, the β-strands as arrows and the N- and C-terminals are labeled. The domain structure is more compact and the angles between adjacent α-helices are nearly perpendicular to each other. Due to the flexibility of the hinge region this is only a "snapshot" of the ensemble of possible orientations of the N- and C- domains relative to one another. **(B)** The crystal structure of Ca^{2+}-free CaM (PDB ID 1QX5). The structure exists as a dimer formed by the association of EF-hands from the C-terminal domains of two CaM monomers. For one monomer the α-helices are labeled A' through H', and for the other monomer the α-helices are labeled A through H. For both structures the β-sheet structures are represented as arrows and the N- and C-terminals are labeled. All structures were rendered using MOLMOL (Koradi et al. 1996).

Table 2. Inter-helical angles for CaM structures

Structure method	Organism	Ca^{2+} state	PDB ID	Helical pairings and resulting angles							
				A/B	C/D	B/C	A/D	E/F	G/H	F/G	E/H
X-ray (open)	*Homo sapiens*	$+Ca^{2+}$	1CLL	89	88	109	106	102	95	112	115
X-ray (open)	*Rattus rattus*	$+Ca^{2+}$	3CLN	87	88	112	107	102	95	112	115
X-ray (open)	*Paramecium tetraurelia*	$+Ca^{2+}$	1EXR	87	97	100	88	111	101	109	138
X-ray (closed)	*Bos taurus*	$+Ca^{2+}$	1PWR	108	119	115	109	97	86	117	126
NMR	*Homo sapiens*	$+Ca^{2+}$	1J7O	103	100	107	110	-	-	-	-
NMR	*Homo sapiens*	$+Ca^{2+}$	1J7P	-	-	-	-	108	103	116	121
NMR	*Xenopus laevis*	$-Ca^{2+}$	1F70	131	131	123	128	-	-	-	-
NMR	*Xenopus laevis*	$-Ca^{2+}$	1F71	-	-	-	-	140	125	140	154
NMR	*Xenopus laevis*	$-Ca^{2+}$	1CFD	134	129	128	128	135	136	139	139
X-ray	*Rattus norvegicus*	$-Ca^{2+}$	1QX5	128	134	124	138	-	-	-	-

The angles are in degrees. The column labeled "Structure method" lists the method of CaM structural determination. Where it applies, X-ray structures are listed as "open" or "closed" in parenthesis. The column labeled "Organism" has the name of the organism from which the CaM protein or gene is derived. The column labeled "Ca^{2+} state" lists, "$+Ca^{2+}$" for Ca^{2+}-ligated structures, and "$-Ca^{2+}$" for Ca^{2+}-free CaM structures. The column labeled "PDB ID" gives the protein data bank accession codes for each CaM. NMR structures include average angels for structural ensembles of both the N- and C-terminal domains of Ca^{2+}-ligated CaM (1J7O and 1J7P respectively), and the N- and C-terminal domains of human Ca^{2+}-free CaM (1F70 and 1F71 respectively). The columns labeled "Helical parings and resulting angles" gives the adjacent helices for which angles are calculated and the resulting angles. The helices of CaM are labeled from N- to C-terminal A, B, C, D, E, F, G, and H. Structural files 1J70, 1J7P, 1F70, and 1F71 only contain one domain of CaM and as such 4 helical angles are left blank. The file 1QX5 has no angles listed for the C-terminal domain because this domain is involved in inter-molecular EF-hand swapping (Schumacher et al. 2004). All helical angles were calculated using the program interhlx (Yap 1995; Yap et al. 2002).

A Ca^{2+}-free crystal structure of CaM was recently solved, and unlike any previous CaM structure, it exists as an "EF-hand-swapped" dimer (Schumacher et al. 2004). The dimer formation is achieved by interchanging EF-hands from the C-terminal domain. The C-terminal domain EF-hands interchange such that EF-hand 3 from one CaM monomer pairs with EF-hand 4 of another and *vise versa* (Figure 5B) (Schumacher et al. 2004). Most of the interactions forming this dimer are between the swapped EF-hands but some interactions, including those between helices F and B', are thought to be important for dimer formation (Schumacher et al. 2004). In addition, dimerization results in unusual contacts between domains within a monomer. For example, α-helix A is positioned against α-helix G and as a consequence there is a hydrogen-bond between residues T34 and D133. The dimer interface is rich in glutamate and aspartate residues

and this has led to the proposal that Ca^{2+}-free CaM may exist *in vivo* as a monomer to dimer equilibrium depending on the cellular conditions such as pH (Schumacher et al. 2004).

Once again, the secondary structure of this Ca^{2+}-free CaM dimer is similar to previously solved Ca^{2+}-free and Ca^{2+}-ligated CaM structures. The hinge region encompasses residues 77-80 and is not helical. However, unlike previous Ca^{2+}-ligated CaM structures, it is well ordered (Schumacher et al. 2004). As with other Ca^{2+}-free structures, the angle between α-helices in the N-terminal domain are large resulting in nearly anti-parallel arrangements (Table 2). As a result, the N-terminal domain is similar to previously described Ca^{2+}-free CaM structures reflected in a backbone r.m.s.d. of 1.1Å (Zhang et al. 1995; Schumacher et al. 2004).

As described above, the angles between adjacent α-helices in Ca^{2+}-free CaM structures are large (Table 2) resulting in a nearly anti-parallel arrangement of α-helices. However, upon Ca^{2+} binding the conformation changes such that the adjacent helices in Ca^{2+}-ligated CaM are nearly perpendicular to each other. This change in conformation upon Ca^{2+}-binding is facilitated by the +X aspartate and bidentate -Z glutamate residues in the chelating segment of each EF-hand. In the Ca^{2+}-free state the –Z glutamate is displaced far away from its chelating partners. When the EF-hand binds Ca^{2+} the –Z glutamate and +X aspartate move toward each other thereby changing the angle between the α-helixes to which they are a part of (Finn et al. 1995; Kuboniwa et al. 1995; Zhang et al. 1995). Therefore, within both domains of CaM, Ca^{2+}-coordination produces a lever-like motion in the α-helices, so the ends of the α-helices next to the chelating loops move closer together and the other ends of the α-helices move further away from each other

(Finn et al. 1995). This causes the hydrophobic core of the domain to become exposed to the solvent in the region that is opposite the Ca^{2+}-binding sites. The exposed hydrophobic residues form a hydrophobic pocket that can interact with hydrophobic ligands (Finn et al. 1995; Kuboniwa et al. 1995; Zhang et al. 1995).

1.8 CaM-target complexes

The interaction between CaM and its target enzymes is linked to the conformational change observed in CaM upon Ca^{2+}-binding. In the Ca^{2+}-free state, the angles between neighboring α-helices of CaM are large producing a roughly anti-parallel and compact arrangement of α-helices in each domain. Upon Ca^{2+}-binding, the angles between neighboring α-helices change exposing a hydrophobic pocket in each domain of CaM that can bind to specific hydrophobic residues of the CaM-binding sequence of the CaM-target. The flexibility of the hinge region of CaM allows each domain to bind to different hydrophobic residues on the target enzyme CaM-binding sequence. Therefore, CaM wraps around the target enzyme CaM-binding sequence, and this places the N- and C-domains of CaM in close proximity. The CaM-binding sequence usually takes the form of a short amphiphilic α-helix that is often part of an auto-inhibitory domain, or pseudo-substrate for the target enzyme. By sequestering the auto-inhibitory domain or pseudo-substrate, the active site of the target enzyme becomes free and the enzyme becomes fully active. Thus, through CaM, these target enzymes are Ca^{2+}-regulated.

Although there are few sequence identities among the many CaM-binding sequences that have been discovered, there are some recurring structural features. CaM-binding sequences are usually short (14-26 residues), basic, and form amphiphilic α-helices (Crivici and Ikura 1995). Most of these sequences are continuous peptides, but

there are examples of discontinuous binding sequences (Crivici and Ikura 1995). The positions of key, hydrophobic residues in the CaM-binding sequences are conserved. These hydrophobic residues bind to the solvent-exposed hydrophobic pockets on Ca^{2+}-ligated CaM resulting in a CaM-target complex (Yamniuk and Vogel 2004).

Many attempts have been made to categorize all of the CaM-target complexes. However, the diversity of identified targets means that some of the CaM-target complexes do not fall into a defined structural category. Nevertheless, many of the CaM-target complexes described so far can be organized into four classes based on the CaM-binding sequence. The four classes are known as the IQ, 1-14, 1-10, and 1-16 motifs (Yap et al. 2000; Yamniuk and Vogel 2004). The IQ class is so named because many of the binding sequences of this class begin with isoleucine and glutamine. The 1-14, 1-10, and 1-16 classes are so numbered because they delimit the positions of the key bulky hydrophobic "anchor" residues such as isoleucine, leucine, valine, phenylalanine, tyrosine, or tryptophan (Table 3) (Rhoads and Friedberg 1997; Yamniuk and Vogel 2004). These residues are called anchor residues because they are the principal residues that fit into the hydrophobic binding pockets in each domain of Ca^{2+}-ligated CaM.

CaM is able to bind to a diverse array of CaM-binding sequences because of the flexibility of the hinge region and the structural "plasticity" of the domains. The flexibility of the hinge region of CaM allows for multiple and independent positioning of the hydrophobic binding pockets in each domain (Vetter and Leclerc 2003; Yamniuk and Vogel 2004). The plasticity of the hydrophobic binding pockets on each domain is also central to the diverse activity of CaM. The high number of methionines in CaM mediates this plasticity. In addition, the high polarizability of the methionine sulfur atoms

promotes the formation of strong van der Waals interactions, but also makes methionine more compatible with the surrounding aqueous environment than other hydrophobic residues (Chou et al. 2001b). Finally, the long, flexible methionine side chain makes the binding pocket conformationally adaptable (Yamniuk and Vogel 2004).

Table 3. Alignment of selected CaM-binding sequences

Classification	Sequence
IQ class	**---ΦQ---BG---B--Φ---**
myosin V IQ1	CIRIQKTIRGWLLRKRYLCM
myosin V IQ2	AITVQRYVRGYQARCYAKFL
1-14 class (1-5-8-14)	**---Φ---Φ--Φ-----Φ---**
skMLCK (M13)	KRRWKKN**F**IA**V**SAANRFKKI
calcineurin A	RRAIKNK**I**LA**I**GRLSRVFQV
1-14 class (1-8-14)	**---Φ------Φ-----Φ---**
smMLCK (R20)	RRKWQKTGHA**V**RAIGRLSSS
spectrin	ASPWKSARLM**V**HTVATFNSI
1-10 class (1-5-10)	**---Φ---Φ----Φ-----**
CaMKII	RRKLKGA**I**LTTMLATRNF
CaMKI	KSKWKQA**F**NATAVVRHMR
1-16 class	**---Φ----------BBB-Φ--**
CaMKKα	IPSWTTVILVKSMLRKRSFGN
CaMKKβ	IPSLATVILVKTMIRKRSFGN
Other class	
PDE1A2	TEKMWQRLKGILRCLVKQEK
TCF4 (E2-2)	KERRMANNARERLRVRG

The alignment is made based on the position of the first anchor residue where it is known. The classes of CaM targets (bold on the left) are listed with the positions of all hydrophobic residues in parentheses. Consensus sequences are in bold and conserved residues are indicated with their one letter code. The positions of conserved hydrophobic residues are indicated with **Φ**, and the positions of conserved basic residues (arginine and lysine) are indicated with **B**. Key hydrophobic anchoring residues are highlighted gray, and additional important hydrophobic resides are in bold. This table is based on a similar table from (Yap et al. 2000).

1.8.1 The IQ motif CaM target class

Table 3 shows the consensus sequence for the IQ class CaM-binding sequence. A key difference between the IQ class and other CaM-binding classes is that, in many cases, CaM-binding to the IQ class is Ca^{2+}-independent (Rhoads and Friedberg 1997). In addition, some specific IQ sequences differ from the other CaM-binding sequences in that they do not adopt an α-helical structure. For example, the IQ-sequence for inducible nitric oxide synthase (iNOS) in a complex with Ca^{2+}-free CaM, takes the form of a type II β-turn (Yamniuk and Vogel 2004). The addition of Ca^{2+} induces a change in conformation of this complex such that the IQ sequence takes on an α-helical structure (Yamniuk and Vogel 2004). Enzymes such as glycogen phosphorylase (b) kinase (GbK) and iNOS have IQ sequences that bind CaM in the absence and presence of Ca^{2+}. In addition, there are also members of the IQ class that have differing affinities for CaM based on the presence or absence of Ca^{2+}. Neuromodulin is an example of a membrane bound IQ class CaM-target protein that binds CaM with high affinity in the absence of Ca^{2+} and low affinity in the presence of Ca^{2+}. This has led to speculation that neuromodulin is a CaM storage protein. Therefore, in the absence of Ca^{2+}, neuromodulin concentrates CaM at the membrane in specific locations for rapid release in response to a Ca^{2+} signal (Yamniuk and Vogel 2004).

1.8.2 The 1-14 CaM target class

The 1-14 CaM-target class is further subdivided into the 1-8-14 and 1-5-8-14 sub-classes, denoting the positions of important hydrophobic residues (Table 3). The CaM-binding sequence for smooth muscle myosin light chain kinase (smMLCK) is a representative of the 1-8-14 sub-class. A crystal structure of CaM bound to a peptide corresponding to the smMLCK CaM-binding sequence (R20) has been determined (PDB ID 1CDL) (Meador et al. 1992). Position 1 of the R20 sequence is occupied by tryptophan, position 8 is a valine, and position 14 is a leucine. The side chains of the two bulky hydrophobic anchor residues (1 and 14) point approximately 180° with respect to each other in this crystal structure (Meador et al. 1992; Yap et al. 2000). The structure of the CaM-R20 complex is compact and ellipsoidal. The hinge region of CaM in the complex is unwound and the C- and N-domains are in close proximity (Figure 6A). The R20 peptide lies in a hydrophobic channel running diagonal to the long axis of the ellipsoidal complex. There are 185 contacts between CaM and the R20 peptide, 80% of which are van der Waals interactions. Not surprisingly, all nine methionine residues of CaM are involved in forming this complex (Meador et al. 1992). The structures of the N- and C-terminal domains of CaM in the CaM-R20 complex are similar to N- and C-terminal domains of Ca^{2+}-ligated CaM. The most significant change occurs in the hinge region where residues 73 to 77 are in an extended conformation, thereby facilitating the wrapping of CaM around the R20 peptide (Figure 6A) (Meador et al. 1992).

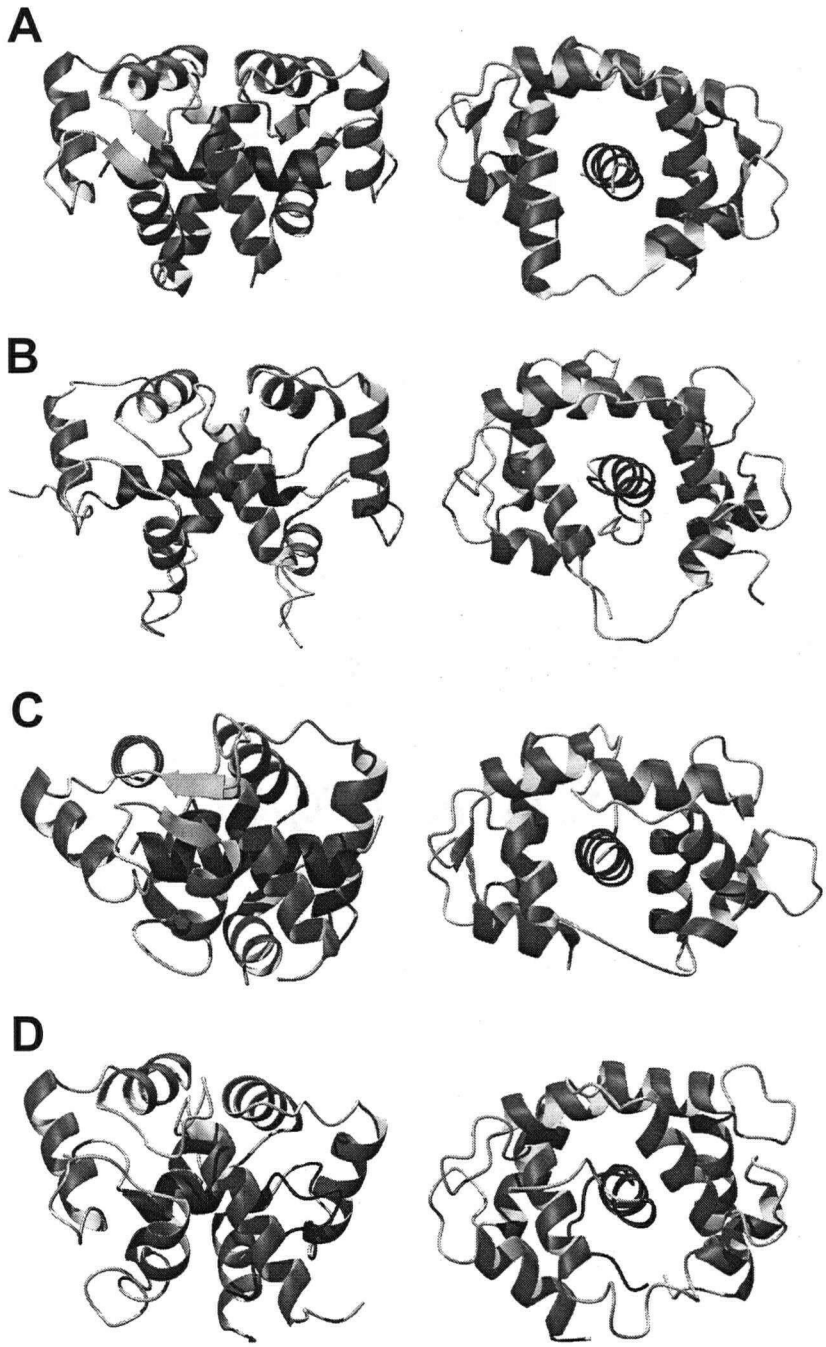

Figure 6. CaM-target peptide complex structures. The structure of CaM bound to a peptide fragment of the CaM binding site for: **(A)** smMLCK, **(B)** skMLCK, **(C)** CaMKIIα, and **(D)** CaMKK. The structures are from the PDB coordinate files: 1CDL, 2BBM, 1CDM, and 1CKK, respectively. All complex structures on the left are presented from N- to C-terminal looking into the page with the hinge region facing down. The structures on the right are rotated approximately 90°. The α-helices of CaM are represented as coiled ribbons, and the β-sheets as arrows (secondary structures are as defined in the PDB files). Ca^{2+} ions are not included in this figure. All structures were rendered using MOLMOL (Koradi et al. 1996).

A representative of the 1-5-8-14 CaM-binding sub-class is the binding site from skeletal muscle myosin light chain kinase (skMLCK) (Table 3). An NMR structure of CaM in a complex with a peptide corresponding to the skMLCK CaM-binding sequence (M13) has been determined (Figure 6B) (PDB ID 2BBM) (Ikura et al. 1992). Position 1 of the M13 peptide is occupied by tryptophan, 5 by phenylalanine, 8 by valine, and position 14 by phenylalanine. The side chains of the two bulky hydrophobic anchor residues (1 and 14) point approximately 180° with respect to each other in this complex (Ikura et al. 1992; Yap et al. 2000). The shape of the CaM-M13 complex is similar to that of the CaM-R20 complex, and once again the structures of N- and C-terminal domains are similar to the same domains in Ca^{2+}-ligated CaM. The hinge region takes the form of a flexible loop from residues 74 to 82. CaM covers about 80% of the surface area of the M13 peptide, and 71 of the 78 identified contacts (91%) are hydrophobic (Ikura et al. 1992). The complex is compact, and the domains of CaM are staggered such that the C-terminal of CaM mainly contacts the N-terminal of the M13 peptide, whereas the N-terminal of CaM mainly contacts the C-terminal of M13 peptide. A similar binding arrangement is observed in the CaM-R20 complex (Ikura et al. 1992). This binding arrangement is called anti-parallel (Crivici and Ikura 1995; Yamniuk and Vogel 2004).

1.8.3 The 1-10 CaM target class

The 1-10 CaM-target class is also known as the 1-5-10 binding class (Table 3) (Yap et al. 2000). A representative of this class is seen in the structure of CaM with a peptide corresponding to the CaM-binding site on CaM-dependant kinase IIα (CaMKIIα), (Figure 6C) (PDB ID 1CDM) (Meador et al. 1993). As with the previously described

structures, the complex is ellipsoidal, compact, and 80% of the contacts take the form of van der Waals interactions (Figure 6C). The binding is also anti-parallel, however, a cluster of basic residues before the first hydrophobic anchor in the peptide binds to both domains of CaM (Meador et al. 1993). Positions 1 and 10 of the CaMKIIα peptide are occupied by leucine, and position 5 by isoleucine. The side chains of the two bulky hydrophobic anchor residues (1 and 10) point approximately 180° with respect to each other in the complex (Meador et al. 1993). Both position 1 leucine, and position 5 isoleucine bind to the C-terminal domain hydrophobic pocket of CaM, and position 10 leucine fits into the N-terminal hydrophobic pocket of CaM (Meador et al. 1993). Note that the difference in the distances between hydrophobic anchors for the 1-10 and 1-14 CaM-binding sequences requires that CaM vary the positioning of its domains. This is mediated through the hinge region of CaM and in the case of the CaM-CaMKIIα peptide complex, this region is disordered from residues 73 to 83 (Meador et al. 1993). For most of the CaM-target complexes described thus far, the flexible hinge region in CaM begins at residue 73 but does not unwind N-terminal to this residue. It is thought that this is because of the importance of the positioning of residues M71 and M72 in the N-terminal hydrophobic binding pocket of CaM (Meador et al. 1993).

1.8.4 The 1-16 CaM target class

The first structure determined in the 1-16 CaM target class is that of CaM bound to a peptide corresponding to the CaM-binding site on CaM-dependant kinase kinase (CaMKK) (Figure 6D) (PDB ID 1CKK) (Osawa et al. 1999). Position 1 of the CaMKK peptide is occupied by tryptophan, position 16 by phenylalanine, and the side chains of these two bulky hydrophobic anchor residues point approximately 90° with respect to

each other in the CaM-CaMKK peptide structure (Table 3 and Figure 6D) (Osawa et al. 1999). As with the previously described structures, the conformation of the N- and C-terminal domains of CaM in the complex CaM-CaMKK are essentially the same as the N- and C-terminal domains of Ca^{2+}-ligated CaM (backbone r.m.s. deviations of 0.96 and 1.32Å respectively) (Osawa et al. 1999). As with other complexes, the hinge region of CaM forms a flexible loop allowing CaM to wrap around the target peptide. In this particular complex structure the hinge encompasses residues 75 to 82.

In most of the previously mentioned Ca^{2+}-ligated CaM-complexes, the target peptide forms an α-helix upon binding to CaM. The CaMKK peptide differs from this paradigm because it forms two distinct structural regions: an 11 residue α-helix connected to a C-terminal hairpin-like loop that folds back on to the α-helical portion of the peptide (Osawa et al. 1999). The CaM-CaMKK peptide complex also differs from previously determined CaM-complex structures because the binding of the peptide is parallel. That is, the N-terminal portion of CaM binds to the N-terminal end of the peptide while the C-terminal portion of CaM binds to the C-terminal end of the peptide (Osawa et al. 1999).

The parallel binding orientation of the CaM-CaMKK peptide complex prompted the development of a theory to explain the binding orientation of all target peptides in CaM-complexes (Osawa et al. 1999). The CaMKK peptide lies in a hydrophobic channel running through CaM. At the ends of each channel are the so-called channel outlets. Channel outlet 1 (CO1) is formed by helices B, C, and D from the N-domain and helix E of the C-domain of CaM. Channel outlet 2 (CO2) is composed of helix A from the N-domain and helix E, F, and G of the C-domain of CaM (Osawa et al. 1999). The hinge

region of CaM partially covers CO1 making it smaller than CO2. CO1 has a net charge of –3, and CO2 has a net charge of –8 (Osawa et al. 1999). The characteristics of the channel outlets help to determine the orientation of the CaMKK peptide within the hydrophobic channel in CaM. For example, in the CaM-CaMKK peptide complex, the CaMKK peptide is bulkier at its C-terminal due to the hairpin-like structure, and thus it can only fit into CO2 (Osawa et al. 1999). In addition, the CaMKK peptide has a net positive charge at the C-terminus, so it binds preferentially to the more negatively charged CO2 (Osawa et al. 1999). In contrast, because the N-termini of the M13, R20, and CaMKIIα peptides have a greater net positive charge, their N-termini favor binding to CO2 (Table 3). This explains the anti-parallel binding observed in the previous complexes (Osawa et al. 1999).

1.9 Atypical CaM target complexes

There are many examples of CaM-binding sequences that do not fall into the above mentioned classes. Most of these CaM-binding sequences have little or no sequence similarity to any of the above mentioned target classes or to each other and as such cannot be classified. In these cases, the targets are said to be "other class" or "atypical" (Table 3) (Yap et al. 2000; Yamniuk and Vogel 2004).

A structure of a peptide from the atypical CaM-binding site of the small-conductance Ca^{2+} activated potassium channel (skCaK) and CaM has recently been solved (Schumacher et al. 2001). The structure is unique among CaM-complexes being a symmetrical 2:2 dimer formed with 2 skCaK peptides and 2 CaM molecules (Figure 7A) (Schumacher et al. 2001). In this complex, both of the two skCaK peptides adopt an HLH structure (Figure 7A). As a result, both of the CaM molecules in the complex are

wrapped around 3 helices of an skCaK peptide dimer (Schumacher et al. 2001). The structure of the N-terminal domain of CaM in the CaM-skCaK complex is similar to the N-terminal domain of previously described Ca^{2+}-ligated CaM structures as reflected in the backbone r.m.s.d. of 0.58Å (Schumacher et al. 2001). Similar to other CaM complexes, the binding of the N-terminal domain of CaM to skCaK is mediated by hydrophobic interactions. A leucine residue on the skCaK dimer peptide plays a similar role as the previously described hydrophobic anchor residues, binding to the N-terminal hydrophobic binding pocket of CaM (Schumacher et al. 2001). However, unlike previously described CaM-target complexes, the N-terminal domain of CaM in the CaM-skCaK complex interacts with both peptides of the skCaK dimer helping to stabilize the complex. Also unlike previously described CaM-target complexes, the hydrophobic binding pocket of the C-terminal domain of CaM in the CaM-skCaK complex binds to two α-helices (Figure 7A) (Schumacher et al. 2001). Therefore, the backbone conformation of the C-terminal domain of CaM in the complex with skCaK is unlike previously described Ca^{2+}-ligated CaM structures as evidenced by a backbone r.m.s.d. of 2.8Å (Schumacher et al. 2001). The C-terminal domain of CaM in the CaM-skCaK complex is Ca^{2+}-free. As a result, the conformation of this domain is similar to that of Ca^{2+}-free CaM, and this is reflected by a backbone r.m.s.d. of 1.7Å (Schumacher et al. 2001). Therefore, it is proposed that in the Ca^{2+}-free state, the C-terminal domains of two CaM molecules bind to two separate regulatory domains of a single small-conductance Ca^{2+} activated potassium channel. However, when Ca^{2+} is present, the regulatory domains dimerize via CaM and this causes the potassium channel to open (Schumacher et al. 2001).

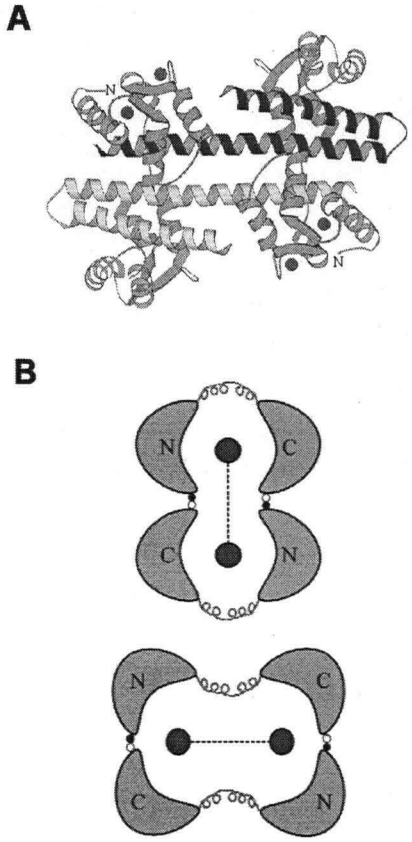

Figure 7. Atypical CaM-target peptide complexes. (A) The structure of two CaM molecules bound to two skCaK peptides. The skCaK peptides are in black and light gray. Two CaM molecules are shown in gray, and the spheres are bound Ca^{2+}. The complex is an symmetrical 2:2 dimer formed from 2 skCaK peptides and 2 CaM molecules. The C-terminal domains of the CaM molecules are Ca^{2+}-free and wrapped around two α-helices from each skCaK peptide. This figure was adapted from (Schumacher et al. 2001). **(B)** A schematic structure of two proposed CaM-bHLHW complexes. Large black circles represent the helices of the bHLHW peptide perpendicular to the page, and the dashed-line between them is a disulfide bond holding them together. CaM domains are labeled as C and N, and the coil between them is the hinge region. Two CaM molecules wrap around one bHLHW peptide, facilitated by interactions between L112 (small white circle) in the C-domain of one CaM molecule and the M36 (small black circle) in the N-domain of another CaM molecule. This figure was adapted from (Larsson et al. 2001).

In an effort to confirm this proposed mechanism, the structure of Ca^{2+}-free CaM complexed with the skCaK peptide was also determined (Schumacher et al. 2004). The secondary and tertiary structure of CaM in this complex is similar to that of Ca^{2+}-free

CaM as determined by NMR spectroscopy (Kuboniwa et al. 1995; Zhang et al. 1995; Schumacher et al. 2004). In accordance with the proposed mechanism of gating for the small-conductance Ca^{2+} activated potassium channel, only the C-terminus of Ca^{2+}-free CaM appears to bind to the skCaK peptide. A single tryptophan hydrophobic anchor residue (W432) from the skCaK peptide is involved in this interaction. This same residue is involved in binding to the hydrophobic pocket of the C-terminus of CaM in the Ca^{2+}-ligated CaM-skCaK structure (Schumacher et al. 2004). Only a short sequence of amino acids in the skCaK peptide around the hydrophobic anchor residue appear to adopt an α-helical conformation and the rest of the peptide is disordered in the Ca^{2+}-free state (Schumacher et al. 2004). The chief difference between the Ca^{2+}-free and loaded complex is the orientation of the skCK peptide with respect to the C-terminus of CaM. In the Ca^{2+}-ligated complex the position of the skCaK peptide shifts by 90° allowing the movement necessary for the proposed gating mechanism (Schumacher et al. 2004).

Another example of an atypical CaM-target is that of the basic HLH (bHLH) transcription factors (Corneliussen et al. 1994). The bHLH transcription factors are composed of two distinct parts; namely an HLH dimerization domain and a basic DNA binding region. In addition, the bHLH transcription factors come in two classes; A and B, that can hetero or homodimerize. Ca^{2+}-ligated CaM can bind to and inhibit several class A homodimeric bHLH transcription factors including TCF4 (E2-2), E12 and E47 (Corneliussen et al. 1994; Onions et al. 1997; 2000). In contrast class B homodimers are resistant to CaM binding (Onions et al. 1997; 2000). The CaM-binding sequence on bHLH transcription factors has been localized to the basic DNA binding region, and does not conform to any of the above CaM-target categories (Corneliussen et al. 1994).

Furthermore, binding only occurs to the dimerized bHLH transcription factors, as a monomeric peptide corresponding to this basic DNA binding region has very low affinity for CaM. However, if two such peptides are covalently bound together by a disulfide bond, as a surrogate of the HLH dimerization domain, CaM binds with high affinity (Corneliussen et al. 1994; Onions et al. 1997; 2000). CaM-bHLH complexes dissociate in high salt concentrations. This behavior is unique among CaM-target complexes as it suggests that ionic interactions are more important in the CaM-bHLH complex than the hydrophobic interactions observed in previously discussed CaM-target complexes (Onions et al. 2000). In addition, traditional CaM inhibitors, such as trifluoperazine, fail to inhibit CaM-bHLH interactions (Onions et al. 1997; 2000).

Although no structure of a CaM-bHLH transcription factor complex is known, an attempt was made to solve the structure of CaM with a peptide dimer of the DNA binding region of the bHLH transcription factor TCF4 (bHLHW) using NMR spectroscopy (Larsson et al. 2001). In this CaM-bHLHW complex, the hinge region in CaM extends from residues 77 to 80 (Larsson et al. 2001). This is shorter than in all of the previously discussed CaM-target complexes, suggesting that CaM does not wrap around bHLH transcription factors, as it does with other targets (Larsson et al. 2001). In addition, unlike previously described CaM complex structures, the bHLHW peptide does not adopt a clearly defined α-helical structure upon binding with CaM.

The interaction between bHLHW and CaM involves the interaction of two CaM molecules with one bHLHW (or one bHLH monomer peptide to one CaM) (Larsson et al. 2001). This unique interaction is facilitated by interaction between L112 in the C-terminal domain of one CaM molecule and M36 in the N-terminal domain of another

CaM molecule (the white and black circles respectively in Figure 7B). Thus, two CaM molecules appear to wrap around a bHLH dimer and make contact with each other (Figure 7B) (Larsson et al. 2001). However, NMR studies failed to produce a more detailed structure for the CaM-bHLH complex (Larsson et al. 2001).

1.10 EF-hand protein fragments

1.10.1 Isolated single EF-hand protein models

As mentioned previously, Ca^{2+}-binding proteins composed of a single EF-hand motif do not exist in nature. However, because all EF-hand proteins are thought to have evolved by gene duplication from a single progenitor EF-hand, the properties of many single EF-hand motifs have been characterized by several investigators (Moncrief et al. 1990; Nakayama et al. 1992; Kawasaki et al. 1998). Some of the studies focused on Ca^{2+}-binding, and others focused on structural issues. These structural and Ca^{2+}-binding studies quickly demonstrated that peptide models of single EF-hand motifs do not exist as monomers in solution. Rather, these peptide models form homodimers with folded structures similar to that of a domain in an EF-hand protein (Kay et al. 1991; Finn et al. 1992; Shaw et al. 1992). Furthermore, homodimers of EF-hand peptide models have lower Ca^{2+}-affinities than do their respective native proteins. In the case of the troponin C EF-hand 3 (TnC3) homodimer, there is a higher affinity Ca^{2+}-binding site (K_{d1} = 3μM) and a low affinity site (K_{d2} >1mM) (Shaw and Sykes 1996). The global dissociation constant for the troponin C EF-hand 4 (TnC4) homodimer is around 1 mM (Kay et al. 1991). In addition, the global dissociation constant for a CaM EF-hand 3 (CaM3) homodimer is 878 μM (Reid 1987a; Franchini and Reid 1999b). Heterodimers of EF-hand peptide models also exhibit Ca^{2+}-affinities that are lower than in their respective

original proteins. However, both Ca^{2+}-binding sites in EF-hand heterodimers generally have higher affinity than those seen in the corresponding homodimers. Furthermore, the Ca^{2+}-affinities are in the more physiologically meaningful micromolar range. For example, a heterodimer composed of TnC3 and TnC4 has a global dissociation constant of between 2 and 3 μM, however, the C-terminal domain of native TnC has dissociation constants in the 0.1 μM range (Potter and Gergely 1975; Shaw and Sykes 1996). Another example is that of a heterodimer composed of calbindin D_{9k} EF-hand fragments which has dissociation constants of 1.25 and 5 μM, yet these constants are 100 times higher than those observed in native calbindin D_{9k} (Finn et al. 1992). Finally, EF-hand heterodimers are formed in preference to homodimers (Finn et al. 1992; Shaw and Sykes 1996).

Much of the structural work in the area of EF-hand homo- and heterodimers has been done using the EF-hand protein troponin C (TnC). However, because the structures of TnC and CaM are very similar (sharing 51% residue identity), many of the findings are applicable to CaM. The structure of a homodimer of TnC3 was solved using NMR spectroscopy (Shaw et al. 1992) (Figure 8A). In the absence of Ca^{2+} the TnC3 homodimer is unstructured. However, upon addition of Ca^{2+} a single monomer of TnC3 binds Ca^{2+} and this event is coupled to both dimerization with a Ca^{2+}-free TnC3 monomer and folding (Shaw et al. 1991). Additional Ca^{2+} is needed to completely saturate the second weak affinity site (Scheme 3) (Shaw et al. 1991). The TnC3 homodimer adopts a secondary structure similar to that of a domain of TnC, there are four α-helices and a short anti-parallel β-sheet between the Ca^{2+}-binding sites (arrows Figure 8). Contacts between hydrophobic residues at the interface between monomers

help to stabilize this interaction (Shaw et al. 1992). Both monomers adopt a similar structure having a backbone r.m.s.d. of 0.3Å, and the dimer complex is similar to the C terminal domain of TnC having a backbone r.m.s.d. of 1.33Å (Shaw et al. 1992).

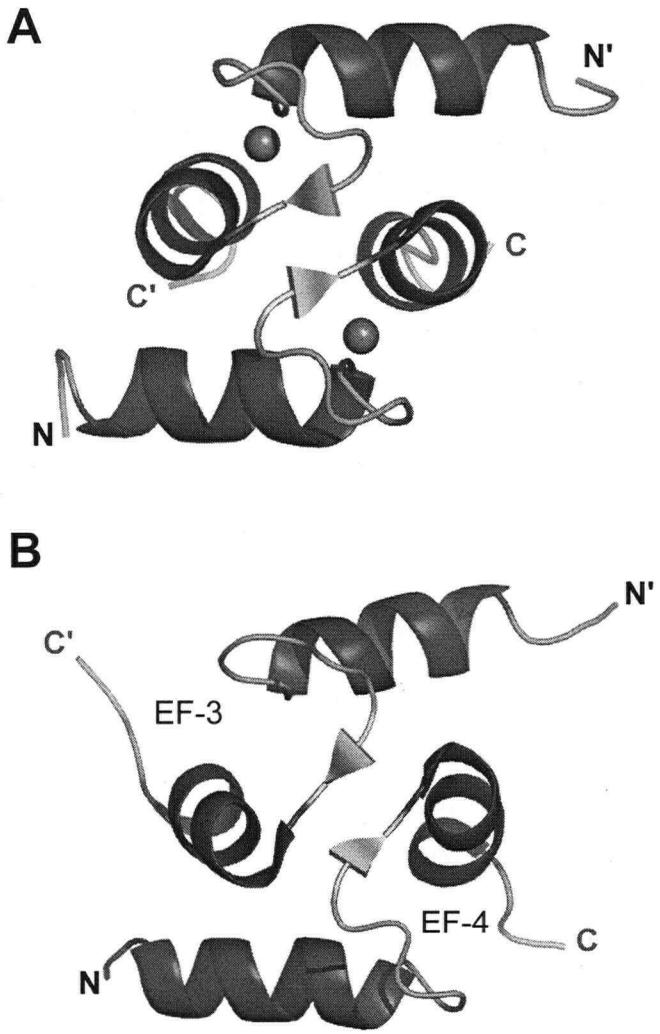

Figure 8. The structures of a TnC homodimer and heterodimer. Shown are the NMR derived structures of the (**A**) TnC3 homodimer (PDB ID 1CTA) (Shaw et al. 1992), and the (**B**) TnC3 and TnC4 heterodimer (TnC3/4) (PDB ID 1PON) (Shaw and Sykes 1996). The EF-hands 3 and 4 of the heterodimer are indicated with EF-3 and EF-4, respectively. The structure for the TnC3/4 heterodimer was solved in the presence of Ca^{2+} but coordinates for Ca^{2+} were not included in the model. The black spheres in A are Ca^{2+}. For both structures the α-helices are represented as coiled ribbons and the small anti-parallel β-sheets as arrows. The N- and C-terminals are indicated. These structures were rendered using the program Pymol (DeLano 2002).

$$2P + Ca^{2+} \overset{K_{d1}}{\rightleftharpoons} P^*Ca + P \overset{K_{dimer}}{\rightleftharpoons} P^*_2Ca + Ca^{2+} \overset{K_{d2}}{\rightleftharpoons} P^*_2Ca_2$$

Scheme 3. The homodimerization of TnC3. P represents the unfolded TnC3 monomer, P*Ca the folded monomer with one bound Ca^{2+}, P^*_2 Ca the folded homodimer of TnC3 with a single bound Ca^{2+}, and P^*_2 Ca_2 is the folded homodimer with two bound Ca^{2+}. The dissociation constants governing this equilibrium are K_{d1} (3μM) and K_{d2} (>1mM). The constant K_{dimer} is the dissociation constant for dimerization of TnC3. The species P*Ca cannot be detected and the first Ca^{2+}-binding event and dimerization cannot be separated. This scheme is adapted from (Shaw et al. 1991).

The structure of a homodimer of TnC4 was solved using NMR spectrometry (Kay et al. 1991). As with the TnC3 homodimer, the TnC4 homodimer is unstructured in the absence of Ca^{2+} and folding is induced by the addition of Ca^{2+}. However, more than 20 equivalents of Ca^{2+} are needed to completely saturate both Ca^{2+}-binding sites and induce complete folding of the TnC4 homodimer (Kay et al. 1991). This phenomena yielded a high global Ca^{2+} dissociation constant for the TnC4 homodimer (1 mM) (Kay et al. 1991). An overall decrease in solvent exposed hydrophobic residues (15%) upon dimerization drives dimerization (Kay et al. 1991). The secondary structure of the TnC4 homodimer is similar to that of the TnC3 homodimer and by extension to that of both domains of TnC (Kay et al. 1991). The tertiary structure of the TnC4 homodimer is similar to a crystal structure of TnC having a backbone r.m.s.d. of 0.9Å (Kay et al. 1991).

A structure of a heterodimer of EF-hand monomers TnC3 and TnC4 was solved using NMR spectroscopy (Shaw and Sykes 1996) (Figure 8B). The heterodimer of TnC3 and TnC4 reconstructs the C-terminal domain of TnC. It is not surprising then, that the tertiary structure of the TnC3/TnC4 heterodimer is similar to the C-terminal domain of TnC having a backbone r.m.s.d. of 1.40Å (Shaw and Sykes 1996). The α-helical angles are also similar to that of the C-terminal domain of TnC, but the distances between

helices are greater in the heterodimer, leading to a more open structure (Shaw and Sykes 1996).

1.10.2 Tryptic fragments of CaM

It was observed that the domains of CaM do not adopt a specific orientation with respect to each other, but tumble independently in solution (Barbato et al. 1992). Further evidence for the independence of the domains comes from studies of the proteolytic cleavage of CaM. If Ca^{2+}-ligated CaM is treated with trypsin, a single cleavage site is cut midway between the two domains, yielding two fragments the N terminal TR1C (residues 1-77), and the C terminal TR2C (residues 78-148) (Drabikowski et al. 1982). Consistent with their structural independence, Ca^{2+}-binding studies have shown that TR1C and TR2C have similar characteristics with respect to Ca^{2+}-affinity and cooperativity when compared to the same domains in intact CaM (Linse et al. 1991). The fragments have also been shown to bind to CaM-targets and can act as agonists and antagonists of CaM-target enzymes (Newton et al. 1984).

The structure of the TR1C fragment has been solved using NMR spectroscopy (Bentrop et al. 1997). The secondary, and tertiary structure of the TR1C fragment is similar to that of the N-terminal domain of CaM, as evidenced by a backbone r.m.s.d. of 1.28Å (Bentrop et al. 1997). As with the N-terminal domain of CaM, a short β-sheet structure is formed between EF-hands 1 and 2 centered around I27 and I63 (Bentrop et al. 1997). In addition, the region between the first α-helix and the β-strand, in each EF hand of TR1C exhibits high flexibility as evidenced by a high r.m.s.d. in this region (Babu et al. 1988; Bentrop et al. 1997). However, the region with the highest flexibility in the TR1C CaM fragment occurs in the loop between EF hands 1 and 2. Excluding the hinge

region, this is also consistent with the N- and C-terminal domains of native CaM (Bentrop et al. 1997).

The structure of the TR2C fragment has been solved by both X-ray and NMR spectroscopic techniques. Both structures resemble the C-terminal domain of native CaM as evidenced by r.m.s. deviations of 0.66 and 1.4 Å for the X-ray and NMR structures, respectively (Finn et al. 1995; Olsson and Sjolin 2001). As with the C-terminal domain of native CaM, a short anti-parallel β-sheet structure is observed between EF hands 3 and 4 centered around residues I100 and V136 (Finn et al. 1995; Olsson and Sjolin 2001).

The NMR structure of TR2C was solved in both the Ca^{2+}-free and Ca^{2+}-ligated states. Similar changes in the angles between adjacent α-helices are observed in the transition from the Ca^{2+}-free to ligated state as are observed with native CaM (Table 2) (Finn et al. 1995). As with native CaM, the transition from Ca^{2+}-free to bound state for TR2C results in a 59% increase in solvent exposure of some hydrophobic residues. These exposed residues form the previously described hydrophobic pocket that is essential for binding to CaM-target sequences (Finn et al. 1995).

Some key differences between this crystal structure for TR2C and previous CaM structures include the movement of the side chain of M144 so that it extends over the exposed hydrophobic pocket, and a decrease in solvent exposure for residue L116 (Olsson and Sjolin 2001). In addition, with respect to the crystal structure of TR2C, the N-terminal end of helix E is about 1 Å closer to the C-terminal end of helix H making TR2C a slightly more compact structure than the C-terminal domain of native CaM.

The studies on the typtic fragments of CaM show that despite being cut out of native CaM, the TR1C and TR2C fragments of CaM are nearly identical, in structure and

Ca^{2+}-affinity, to the N- and C-terminal domains of native CaM (Finn et al. 1995; Bentrop et al. 1997; Olsson and Sjolin 2001).

1.11 Hypothesis

CaM has been the focus of intense scrutiny. Various CaM structures have been solved with and without Ca^{2+}, and with target peptides. Structures of the N-terminal (TR1C) and C-terminal (TR2C) tryptic fragments of CaM have also been determined. There are still, however, diverse opinions concerning of the following: (1) the relationship between EF-hand association and Ca^{2+} affinity, (2) the presence of Ca^{2+}-binding cooperativity between CaM domains (3) the mechanism of cooperativity between Ca^{2+}-binding EF-hands, and (4) the mechanism of the diverse target recognition of CaM (Lewit-Bentley and Rety 2000; Yamniuk and Vogel 2004).

The arrangement of EF-hands in CaM is thought to be a consequence of its evolution from a progenitor EF-hand by gene duplication. In this theory, a progenitor EF-hand gave rise to a progenitor EF-hand domain that evolved into a two-domain progenitor EF-hand protein that then evolved into CaM and TnC among others (Goodman et al. 1979; Moncrief et al. 1990; Nakayama et al. 1992). In this theory, EF-hands 1 and 3 are related as are EF-hands 2 and 4 because both domains evolved from a single progenitor domain (Nakayama et al. 1992). Therefore, EF-hand 1 has evolved to associate with EF-hand 2, and EF-hand 3 has evolved to associate with EF-hand 4. This behavior suggests that there is a structural motivation behind the evolutionary mandated paring of EF-hands 1 and 2, and EF-hands 3 and 4 in CaM. However, there is also considerable plasticity in the association between EF-hands. In particular, peptide models of single EF-hands will associate to form homodimers and heterodimers, with

globular structures similar to those of intact EF-hand domains (Reid 1987b; Shaw et al. 1990; Kay et al. 1991; Shaw et al. 1991; Franchini and Reid 1999a). Yet the affinity of these EF-hand structures for Ca^{2+} can vary many orders of magnitude depending on the associating EF-hands. Taken together, this demonstrates that there is a relationship between the particular EF-hands that associate to form an EF-hand domain and the affinity and cooperativity of that EF-hand domain for Ca^{2+} and for target sequences.

To investigate the effect of EF-hand association on the structure, Ca^{2+}-affinity, and target peptide recognition of CaM we divided CaM into three regions containing two Ca^{2+}-binding EF-hands each. CaM1/2, which corresponds to the N-terminal domain, CaM3/4 which corresponds to the C-terminal domain, and CaM2/3 which is a novel peptide composed of EF-hands 2 and 3 (one EF-hand from each domain) (Figure 9). As mentioned, there are extensive studies on the structure, target peptide recognition and Ca^{2+}-binding of the tryptic fragments of CaM representing the N- and C-terminal domains (Drabikowski et al. 1982; Guerini et al. 1984; Newton et al. 1984; Gillis 1985; Klee et al. 1986; Onions et al. 2000). However, no such studies have been reported on the novel CaM2/3 peptide, which represents the central portion of CaM and contains the hinge region that is critical for target peptide recognition. In CaM2/3 the sequence for EF-hands 2 and 3 are tethered together through the hinge region; this forces association of EF-hands 2 and 3, and generates an EF-hand paring not observed in native CaM.

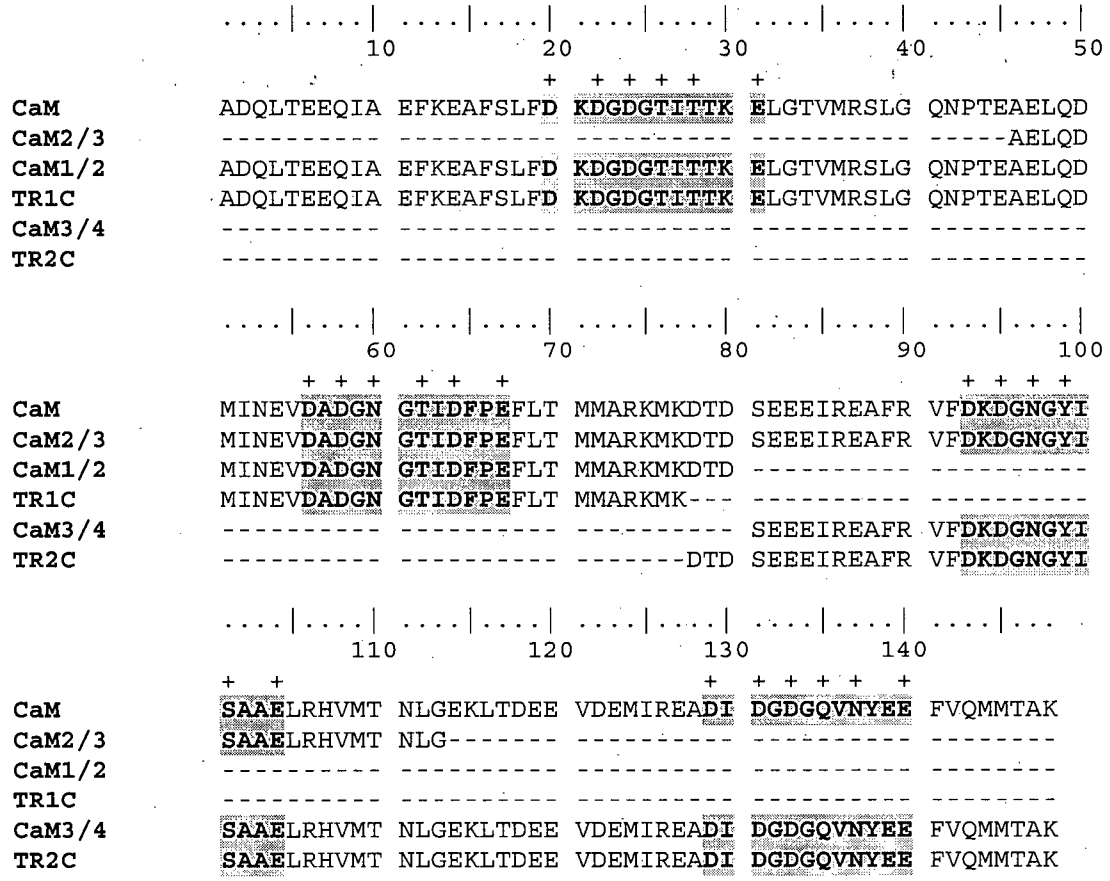

Figure 9. The sequences of CaM and CaM fragments. The protein sequences of CaM2/3, CaM1/2, CaM3/4, and the tryptic fragments TR1C and TR2C aligned on the sequence of CaM. The Ca^{2+}-binding segments are highlighted and the chelating residues are indicated with a + above the sequence. From left to right the indicated chelating residues are 1 (+X), 3 (+Y), 5 (+Z), 7 (-X), 9 (-Y), 12 (-Z). The sequence of CaM2/3 encompasses residues 46-113 and is composed of EF-hands 2 and 3 as well as the entire sequence for the hinge region. CaM2/3 has an estimated net charge of –9 at pH 7.0. CaM1/2 encompasses residues 1-80 (EF-hands 1 and 2) and has an estimated net charge of –12 at pH 7.0. It has three additional residues over TR1C (residues 1-77). CaM3/4 encompasses residues 81-148 (EF-hands 3 and 4) and has an estimated net charge of –12 at pH 7.0. The boundaries of CaM1/2 and CaM3/4 were chosen to yield fragments with the same net charge.

The addition of 3 more residues to CaM1/2, relative to the tryptic fragment TR1C is expected to increase Ca^{2+}-binding activity and target enzyme binding due to stabilization of the N-terminal α-helices (Reid and Hodges 1980). In addition, the C- and

N-terminal peptides CaM1/2 and CaM3/4 have the same predicted net charge of –12 at pH 7.0. In contrast, the tryptic fragment TR1C has a net charge of -10 where as TR2C has a net charge of –14 at pH 7.0. The normalization of net charges for CaM1/2 and CaM3/4 (with respect to TR1C and TR2C) may eliminate any bias when comparing the N- and C-terminal domains for CaM-target sequence binding.

Studies using these CaM fragment peptides will help to illuminate the relationship between EF-hand association to form domains and the Ca^{2+}-affinity, and cooperativity of these domains. These CaM fragments will also assist in understanding the mechanism of the diversity of target enzyme binding, and enzyme stimulation by CaM. These studies will also provide further insights into the evolution of EF-hand proteins.

1.12 Objectives

The objectives of this study were to determine the structure, Ca^{2+}-binding, cooperative interactions and select target peptide interactions of the CaM1/2, CaM2/3 and CaM3/4 fragments of CaM. These were achieved by using NMR spectroscopy to solve the structure of the CaM2/3 fragment and comparing it to known structures of CaM and its constituent domains. Ca^{2+}-affinity was measured in the CaM1/2, CaM2/3 and CaM3/4 fragments using titrations monitored by circular dichroism (CD) spectrometry and also in the case of CaM2/3, by NMR spectrometry. The CaM-target interactions of CaM1/2, CaM2/3 and CaM3/4 were examined with a peptide fragment of myosin light chain kinase (M13) and a dimerized peptide fragment of the basic helix-loop-helix transcription factor TCF4 (bHLHW). These interactions were measured using titrations monitored by fluorescence spectrometry and chemical cross-linking followed by SDS PAGE. In addition, the interaction between M13 and CaM2/3 was studied in depth using NMR and

analytical ultracentrifugation (AUC). Finally calcineurin was used as a model for the assessment of enzyme activation by these CaM fragments.

Chapter 2

The structure and calcium affinity of fragments of calmodulin [1]

2.1 Introduction

In nature, EF-hands associate pair wise into folded domains. An EF-hand domain is composed of two EF-hands connected by a flexible loop and is stabilized by an anti-parallel β-sheet and by the packing of hydrophobic side chains from neighboring α-helices. A key feature of this packing is the presence of four stacked aromatic residues found on the first and the fourth α-helices (Babu et al. 1988; Shaw and Sykes 1996). CaM is a dumbbell-shaped protein formed from the association of four Ca^{2+}-binding EF-hand motifs: EF-hands 1 and 2 associate to form the N-terminal domain, and EF-hands 3 and 4 associate to form the C-terminal domain (Babu et al. 1988).

Although EF-hand proteins have evolved to specifically pair into domains, there is considerable plasticity in the association of EF-hands (Moncrief et al. 1990; Kay et al. 1991; Nakayama et al. 1992). This plasticity is evidenced by the peptide models of single EF-hands that self-associate to form homodimers. Examples of this type of homodimerization include single EF-hand peptides of CaM3, TnC3, TnC4, and chimeras of parvalbumin and CaM, (Reid 1987b; Shaw et al. 1990; Kay et al. 1991; Shaw et al. 1991; Franchini and Reid 1999a). The structures of the homodimers of both TnC3 and TnC4 are very similar to the C-terminal domain of native TnC and, by extension, all EF-hand proteins (Kay et al. 1991; Shaw et al. 1992).

---

[1] A version of this chapter has been submitted for publication to the Journal of Biological Chemistry. Lakowski, T. M., Lee, G. M., Okon, M., Reid, R. E., and McIntosh, L. P., 2006. Calcium-Induced Folding of a Fragment of Calmodulin Composed of EF-Hands 2 and 3.

Despite the similarity between the homodimers and the native structures of EF-hand proteins, Ca^{2+}-binding and cooperativity are negatively affected in the homodimer EF-hand models (Reid 1987b; Kay et al. 1991; Shaw et al. 1991). However the heterodimers of single EF-hand peptides, have improved Ca^{2+}-affinities (Finn et al. 1992; Shaw and Sykes 1996). Therefore, there is a poorly understood relationship between the particular EF-hands that associate to form an EF-hand domain and Ca^{2+}- affinity and cooperativity in that EF-hand domain.

To better understand how EF-hand association affects the structure, Ca^{2+}-affinity, and cooperativity of CaM, we examined three fragments of CaM containing two EF-hands each. We expressed three fragments of CaM: CaM1/2, CaM2/3 and CaM3/4, and used circular dichroism (CD) monitored Ca^{2+} titrations to measure the Ca^{2+}-affinity and cooperativity of these fragments. We solved the NMR structure of the novel CaM2/3 peptide, and demonstrated that its overall fold is similar to both the N- and C-terminal domains of CaM. NMR and CD titration studies show that CaM2/3 binds Ca^{2+} in a stepwise manner, and that many additional equivalents of Ca^{2+} are required to completely saturate the second Ca^{2+}-binding site of CaM2/3. In contrast, CaM1/2 and CaM3/4 retain both high affinity for Ca^{2+} and exhibit positive cooperativity as observed in native CaM.

Our results stress the importance of the aromatic stacking interactions in EF-hand proteins: we attribute the low Ca^{2+}-affinity of the second Ca^{2+}-binding site of CaM2/3 to the lack of native-like stacking interactions between aromatic residues on the first and fourth α-helices. This investigation leads to the conclusion the optimal paring of EF-hands to produce high affinity Ca^{2+}-binding requires aromatic stacking interactions between residues on the first and fourth α-helices of EF-hand domains. The presence of

such stacking interactions opposite the loop between EF-hands is important for domain stabilization and this in turn affects Ca^{2+}-affinity.

2.2 Materials and Methods

2.2.1 Construction of the CaM, CaM3/4 and CaM1/2 genes

The gene for human CaM was amplified from human liver cDNA (Invitrogen). The primers used contained additional DNA sequence that allowed for the incorporation of 5′ *Bam*HI and 3′ *Hind*III DNA restriction sites with sufficient overhanging nucleotides to allow for efficient digestion by both restriction enzymes (Figure 10). A Factor Xa protein restriction site was also incorporated 5′ to the CaM gene, so that a free N-terminal peptide could be produced. A modified version of the "Touchdown" technique was performed in a MJ Research Peltier thermal cycler (PTC-200) (Appendix B) (Don et al. 1991). The reaction contained 30 ng cDNA, 2.5 U Pfx DNA polymerase (Invitrogen), 0.3 μM of both primers, 1 mM $MgSO_4$ (Invitrogen), a 0.2 mM of a mixture of all four dNTP's (Invitrogen), and the appropriate Pfx buffer (Invitrogen) in sterile dH_2O (producing a final volume of 50 μL). The results of the reaction were visualized on 2% agarose (Invitrogen) gel with 0.1 μg/mL ethidium bromide (Sigma), run at 100V, and a band corresponding to approximately 500 bp was observed. The remaining reaction was purified using a phenol/chloroform extraction, followed by ethanol precipitation. The purified gene was digested with *Bam*HI, and *Hind*III (Invitrogen) overnight, according to the manufacturer's instructions, and then purified by phenol/chloroform extraction, followed by ethanol precipitation. The pET28a+ vector (Novagen) was digested with the same enzymes, and the cut vector was purified with a 1% agarose gel. The DNA was extracted from the excised band using the Geneclean II kit (Bio 101). The digested CaM gene was ligated into the pET28a+ vector overnight at 4 °C using T4 DNA ligase (Invitrogen), according to the manufacturer's instructions. A 2 μL aliquot of this ligation

was transformed into DH5α *E. coli* (Invitrogen), according to the manufacturer's instructions, plated on LB agarose plates containing 30 μg/mL kanamycin (Sigma), and incubated overnight. Single colonies from this incubation were randomly picked and used as templates in a typical PCR reaction (Appendix B). The primers used were the T7 promoter primer and the T7 terminator primer because they bordered the CaM insert on the pET28a+ vector. The results of the PCR reaction were visualized on a 2% agarose gel, 3 bands with molecular weights corresponding to the CaM insert were randomly selected. Colonies corresponding to the randomly selected bands were used to inoculate three culture (Falcon) tubes with 5 mL of LB media and 30 μg/mL kanamycin, for an overnight culture. Plasmid DNA (i.e. the pET28a+ vector with the CaM insert) was extracted from the overnight cultures using the Wizard Plus SV Miniprep DNA purification system (Promega) according to the manufacturer's instructions. The CaM gene was sequenced with the BigDye terminator v3.1 cycle sequencing kit (Applied Biosystems) using a T7 terminator primer, and the results were analyzed at the Nucleic Acid Protein Service (NAPS) Unit DNA sequencing facility at the University of British Columbia, Canada. Miniprep plasmid DNA with the correct sequence (i.e. the pET28a+ vector with the CaM insert) was stored at –20 °C, and colonies with plasmids having the correct CaM sequence were stored as 10% glycerol stocks at –80 °C. The CaM gene in the pET28a+ vector was also transformed into the expression host BL21 star DE3 *E. coli* (Invitrogen) and stored as above.

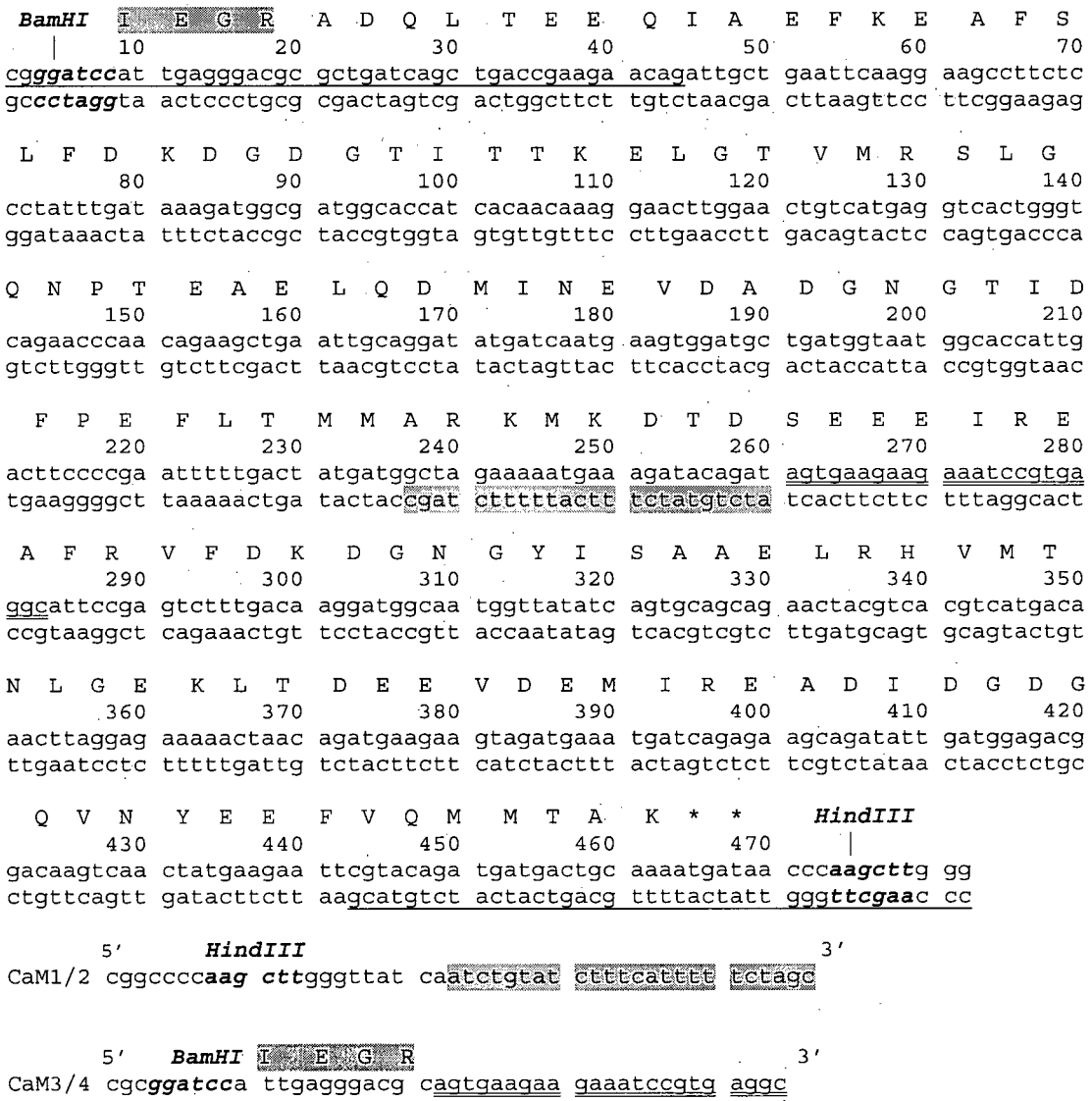

Figure 10. DNA Sequence of CaM, CaM1/2 and CaM3/4 with primers. The DNA sequence of the CaM gene amplified from human liver cDNA. The DNA sequence is presented double stranded and in lower case. DNA restriction sites *Bam*HI and *Hind*III are labeled and the DNA sequences italicized. The stop codon is indicated with an asterisk. The primers used for amplification of CaM are single underlined. The protein sequence is listed above the DNA sequence in uppercase, and the Factor Xa protein restriction site is highlighted in gray. CaM1/2 was amplified from the CaM gene using the first primer in the CaM sequence and the one listed below as CaM1/2; the gray highlighted DNA sequences indicate where the second primer anneals to the CaM sequence. CaM3/4 was amplified from the CaM gene using the second primer in the CaM sequence and the one listed below as CaM3/4; the double underlined sequence of DNA indicates where this second primer anneals to the CaM sequence.

The genes for CaM1/2 and CaM3/4 were constructed using the above protocol for the CaM gene except that the purified CaM gene in the pET28a+ vector was used as the template instead of the human liver cDNA (Figure 10). The genes for CaM1/2 and CaM3/4 were ligated into the pET28a+ vector, from mini-prep DNA (i.e. the pET28a+ vector with the CaM1/2 or CaM3/4 insert) according to the protocols for the CaM gene. Their sequences and the primers used are shown in Figure 10. These genes were also transformed into the expression host BL21 star DE3 *E. coli* as described above and stored as glycerol stocks.

2.2.2 Construction of the CaM2/3 Gene.

The gene for CaM2/3 was constructed using an extensively modified version of the technique of mutually-priming long oligonucleotide primers (Moore 1987; Uhlmann 1988). Along with the gene sequence encoding CaM2/3 these primers included the DNA restriction sites for *Nco*I and *Hind*III, and a Factor Xa cleavage site (Figure 11). The reaction was performed in two stages in a thermal cycler. In the first stage, two separate reactions were performed with the primers identified in Figure 11 at concentrations of 0.5 μM with 2.5 U *Taq* DNA polymerase (Invitrogen), 3 mM $MgCl_2$ (Invitrogen), a 0.2 mM of a mixture of all four dNTP's, and the appropriate buffer (Invitrogen) in 50 μL of sterile dH_2O (final volume). A gradient annealing thermal cycler program was used (Appendix B). The products of both reactions were visualized on 2% agarose gels and bands corresponding to approximately 120 bp were observed. The products of both reactions were purified by phenol/chloroform extraction followed by ethanol precipitation. Finally the products of both reactions were combined in a second stage reaction with the same reagents as the first stage, except no primers were added because the products of the first

stage were designed to be mutually priming. For the second stage a different gradient annealing thermal cycler program was used (Appendix B). The products of the second stage were visualized on a 2% agarose gel, and bands corresponding to approximately 120 bp and 240 bp were observed. The band at 240 bp was thought to be the gene for CaM2/3 and it was subsequently purified with a 2% agarose gel, and DNA was extracted from the excised band using the Geneclean II kit. The CaM2/3 gene was ligated into the pGEM-T (Promega) vector using the CaM2/3 3′ A and pGEMT 5′ T sticky ends according to the manufacturer's instructions. The CaM2/3 gene and pET41a+ vector (Novagen) were digested with *Nco*I (Invitrogen) and *Hind*III, overnight according to the manufacturer's instructions. The CaM2/3 gene was purified by phenol/chloroform extraction, followed by ethanol precipitation. The double digested pET41a+ vector was purified using a 1% agarose gel, and the DNA extracted from the excised band using the Geneclean II kit. The purified double digested CaM2/3 gene was ligated into double digested pET41a+ using T4 ligase. Subsequent investigations using the pET41a+ vector yielded low protein expression levels, so the CaM2/3 gene was subcloned from the pET41a+ vector to the pET28a+ vector. Figure 12 shows the protocol for the subcloning of CaM2/3 gene into the pET28a+ vector. The CaM2/3 gene in the pET28a+ vector was transformed into the DH5α and BL21 star DE3 strains of *E. coli* and stored in a 10% glycerol stock as above. The CaM2/3 gene was sequenced from mini-prep DNA (i.e. the pET28a+ vector with the CaM2/3 insert) according to the above protocols.

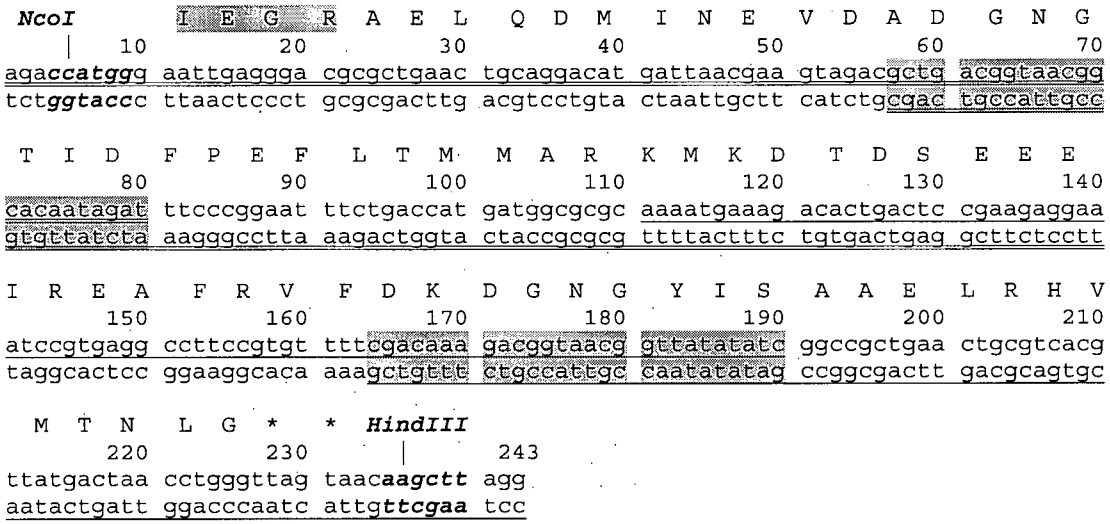

Figure 11. DNA Sequence of CaM2/3 with primers. The DNA sequence of the CaM2/3 gene; the DNA sequence is presented double stranded and in lower case. DNA restriction sites *Nco*I and *Hind*III are labeled and the DNA sequences italicized. The stop codon is indicated with an asterisk. The primers used for construction of CaM2/3 using mutually priming oligonucleotide gene synthesis are underlined. The double underlined primer sequences are used in one reaction for the first stage of gene synthesis and the single underlined sequences are used in the other reaction of the first stage of synthesis. The gray highlighted regions of DNA indicate the regions of overlap for the mutually priming oligonucleotides in the first stage of CaM2/3 gene synthesis. The region where the double-underlined and single-underlined sequences overlap indicate the region of overlap for the mutually priming oligonucleotides in the second stage of CaM2/3 gene synthesis. The protein sequence is listed above the DNA sequence in uppercase, and the Factor Xa protein cleavage site is highlighted in gray.

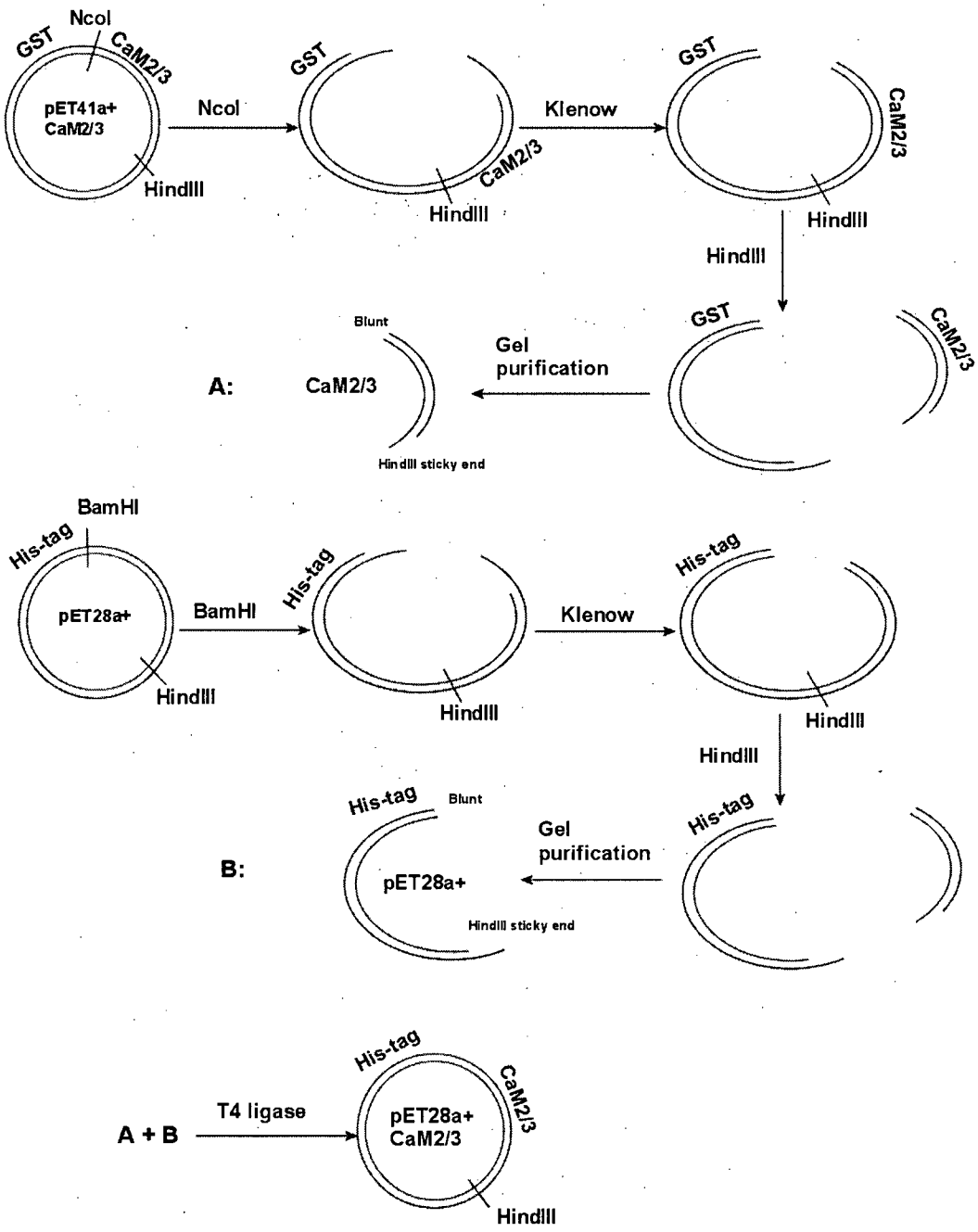

Figure 12. The subcloning of the gene for CaM2/3 from pET41a+ to pET28a+. The pET41a+ vector with the CaM2/3 gene was digested with *Nco*I and purified using phenol / chloroform extraction followed, by ethanol precipitation. This was treated with 6.2 U of the large fragment of DNA polymerase I (Klenow) (Invitrogen) at 0 °C for 30 min, and the enzyme was heat inactivated at 75 °C for 10 min. This was then digested with *Hind*III and the CaM2/3 gene purified using a 2% agarose gel and the Geneclean II kit. The pET28a+ vector was treated as above. The gel purified fragments were combined (A+B) and treated with T4 ligase at 4 °C overnight.

2.2.3 Expression and purification CaM and CaM fragments

2.2.3.1 Optimizing expression parameters

All of the Ca^{2+}-binding proteins were incorporated into the pET28a+ vector to produce an N-terminal poly-histidine affinity tag (His-tag). After purification, the His-tag was removed using the Factor Xa protein cleavage site to produce a free N-terminal peptide. A small-scale trial expression was conducted for each gene to optimize the expression conditions. Test expressions of all genes were performed using the BL21 star DE3 strain of *E coli*. LB plates containing 50 μg/mL kanamycin were streaked with scrapings from glycerol stocks for each of the genes and incubated overnight at 37 °C. A single colony was picked randomly from the plates and used to inoculate 5 mL of LB media containing kanamycin and this was incubated at 37 °C with shaking (200 rpm) in a Lab-Line Environ Shaker. The cultures were used to inoculate pairs of 225 mL Erlenmeyer flasks containing 50 mL LB media and kanamycin. In each pair, one flask acted as a non-induced control and the other was induced with isopropyl-β-D-thiogalactopyranoside (IPTG) (EM Science). Prior to induction, the flasks were incubated until the optical density at 600 nm (OD_{600}) was between 0.7-0.8. One flask was induced with IPTG and both flasks were incubated at 37 °C for 18 h post induction. Samples for each gene (induced and control) were taken at 0, 1, 2, 3, 4 and 18 h. The total amount taken was normalized to 1 mL of culture at an OD_{600} of 0.8 and the samples were centrifuged at 4 °C, and 12000 xg for 10 min, the supernatant discarded and the pellets frozen. Each test expression was repeated using 1 and 2 mM IPTG. The next day the pellets were lysed using 100 μL BugBuster (Novagen) with 1 U/mL benzonase (Novagen) nuclease incubated at room temperature for 20 min, and centrifuged at 4 °C,

and 12000 xg for 10 min. The supernatant was mixed with Tris-Tricine SDS-PAGE loading buffer, and loaded onto a 16.5% Tris-Tricine gel (Schagger and von Jagow 1987). The gel was run at 35 V for 1 h then at 100 V for approximately 6 h. The gel was removed from the apparatus, fixed in 50% ethanol (Fisher) with 8% phosphoric acid (Fisher) for 30 min, and stained with colloidal Brilliant Blue G-250 (BioRad) overnight (see section 3.2.4 for a more detailed protocol). The relative levels of expression were evaluated for all experimental conditions by visual inspection of the gels. For all genes in question, optimal expression levels were attained with 1 mM ITPG, and optimal expression times varied between 1 and 3 hours. In all cases, expression levels dropped off significantly after 4 h and were almost non-existent after 18 h.

2.2.3.2 Expression of CaM and CaM fragments

The protocol for expression of each gene was similar. A 1 mL aliquot of LB media containing 50 μg/mL kanamycin was inoculated with scrapings from the BL21 star DE3 glycerol stock for each gene and incubated at 37 °C, with shaking at 200 rpm for 1 h. This culture was used to streak LB plates containing kanamycin and incubated overnight at 37 °C. A single colony from the overnight plates was used to inoculate a 25 mL LB starter culture with kanamycin and this was incubated overnight at 30 °C with shaking at 200 rpm. The next day the starter culture was centrifuged at 2000 xg for 30 min and the supernatant decanted. The pellet from the starter culture was used to inoculate 1 to 3 L of LB media containing kanamycin. A 20 mL aliquot of this culture was added to a 200 mL Erlenmeyer flask as an un-induced control. The remaining culture was divided into two 3 L baffled Erlenmeyer flasks and incubated at 37 °C with shaking at 200 rpm until the OD_{600} was 0.8 at which time the flasks were induced with

100 mM IPTG such that the final concentration was 1 mM IPTG. Samples were taken from both a control flask and from one of the induced flasks at regular intervals post induction, and the samples were normalized, centrifuged and frozen according to the trial expression protocol. After the appropriate induction time the rest of the culture was centrifuged at 4 °C and 9000 xg for 20 min, the supernatant was decanted, and the pellet frozen overnight at –80 °C. The control and induced samples taken during the post induction incubation were applied to a 16.5% Tris Tricine gel to check for problems during the expression (see section 3.2.4 for a more detailed protocol).

2.2.3.3 Expression of ^{15}N-labeled and ^{15}N/^{13}C-labeled CaM2/3

Uniformly ^{15}N-labeled CaM2/3 (^{15}N-CaM2/3), and uniformly ^{15}N/^{13}C-labeled CaM2/3 (^{15}N/^{13}C-CaM2/3) were expressed similar to the previously described expression protocol. In the case of ^{15}N-CaM2/3, M9 media was supplemented with 1 g/L $^{15}NH_4Cl$ (C. I. L.) and 1 g/L Celtone-N (Spectra Stable Isotopes). In the case of ^{15}N/^{13}C-CaM2/3, M9 media was supplemented with 4 g/L of uniformly-labeled ^{13}C-glucose (C. I. L.), 1 g/L $^{15}NH_4Cl$, and 1.5 g/L Celtone-CN (Spectra Stable Isotopes) (Muchmore et al. 1989; Reilly and Fairbrother 1994). For both ^{15}N-CaM2/3, and ^{15}N/^{13}C-CaM2/3, protein expression was induced at an OD_{600} of ~0.7 with 1 mM IPTG followed by growth for 1 h at 37 °C with shaking at 200 rpm. The resulting cultures were centrifuged at 4 °C and 9000 xg for 20 min, the supernatants were decanted, and the pellets frozen overnight at –80 °C. In both cases, samples of control and induced cultures were taken and analyzed according to the previously described expression protocol to check for problems during the expression.

2.2.3.4 Initial purification with IMAC

The initial purification protocols for both the isotopically-labeled and natural abundance proteins were similar. Frozen pellets were thawed. The cells from the pellets were lysed with 40 mL (per liter of expression culture) of Bugbuster containing 20 mM Tris pH 8.0, 100 μg/mL lysozyme (Sigma) and 4 U/mL benzonase nuclease. The resulting lysate was incubated at room temperature for 20 min then centrifuged at 4 °C and 12000 xg for 20 min.

Initial purification was effected with His Select (Sigma) immobilized metal affinity chromatography (IMAC). The clarified cell lysate was applied to 19 mL of His Select IMAC affinity resin in a 20 mL plastic BioRad column with a Pharmacia peristaltic pump at a flow rate of 1 mL/min. The purification was monitored at 280 nm using a Pharmacia single path UV monitor. After loading, the column was washed with a buffer containing 50 mM Tris pH 7.5, 300 mM NaCl (Fisher), and 1 mM imidazole (Acros) at a flow rate of 4 mL/min. Fractions were collected every 6 min until the absorbance at 280 nm reached a minimum. The His-tagged peptide was eluted with a buffer containing 50 mM Tris pH 7.5, 100 mM NaCl, 250 mM imidazole at a flow rate of 1 mL/min and fractions were collected every 3 min until a peak eluted (typically at 15-18 min).

In order to change the buffer and to remove imidazole, which can inhibit Factor Xa, the fractions corresponding to the His-tagged fusion peptide were pooled (typically about 10-20 mL) and applied to a Pharmacia column with 70 mL of BioGel P-6DG (BioRad) desalting resin. The imidazole free His-tagged fusion peptide was eluted with a buffer composed of 50 mM Tris pH 7.5, and 100 mM NaCl. The purification was

monitored by UV absorbance at 280 nm, the flow rate was 1.5 mL/min and fractions were collected every 3 min. The fractions corresponding to the imidazole-free fusion peptide were pooled. Sufficient 1 M $CaCl_2$ (Fisher) was added to make the final concentration 10 mM, and Factor Xa (Novagen) was added to a final concentration of 2 to 4 U/mL. The resulting cleavage mixture was incubated at room temperature for 24 to 72 h.

2.2.3.5 RP-HPLC purification

Factor Xa cleaved Ca^{2+}-binding peptides were further purified using RP-HPLC. A Zorbax C8 semi-prep column (9.4 X 250 mm) (Agilent Technologies) was connected to a Waters 626 pump, controlled by a Waters 600s controller, and monitored using a Waters 486 absorbance detector. A gradient solvent system was used with the following components: 0.1% aqueous TFA (Fisher) (A) and 0.1% TFA in acetonitrile (Fisher) (B). A linear gradient was developed over 20 min starting with 90% A, 10% B and ending with 10% A, 90% B. The typical injection volume varied from 0.5 to 3 mL, and the flow rate was 2 mL/min. The purification was monitored at 280 nm and a single peak eluted from 16 to 19 min. The eluted fractions were pooled and freeze dried using a Labconco model 77510 lyophilizer. The peptides were purified a second time using the same scheme as above except the gradient was developed over 40 min. A single peak was observed and all the fractions containing the purified peptide were pooled, freeze dried, and the pure peptide stored at –80 °C.

2.2.4 Amino acid analysis, and mass spectrometry

Peptide hydrolysis followed by amino acid analysis was performed to assist in confirming peptide identity and to measure peptide concentrations. Pure peptide samples were dried in a 6 X 50 mm Pyrex tubes (Corning) under vacuum, and purged with nitrogen (Praxair). Amino acid hydrolysis was carried out under vacuum with 6 N HCl (Sigma) at 110 °C for 24 h. Amino acid analysis was performed with the internal standard carboxymethylcysteine at The Hospital for Sick Children Advanced Protein Technology Center at the University of Toronto, Canada (Appendix C).

The molecular weights and purity of all peptides were confirmed using analytical liquid chromatography, mass spectrometry (LCMS) on a Micromass Quattro microelectrospray mass spectrometer. This spectrometer was connected to a Waters Alliance HT 2795 separations module and an YMC ODS aqua RP-HPLC column. A gradient solvent system was used with the following components: 0.1% aqueous formic acid (BDH) (A) and 0.1% formic acid in acetonitrile (B). The linear elution gradient was developed over 11 min starting with 70% A, 30% B and ending with 40% A, 60% B. The typical injection volume varied from 5 to 10 μL and the flow rate was 0.2 mL/min. The mass spec was operated in the single MS mode with a cone voltage of 40 V, scanning for positive ions with m/*z* from 20 to 1500. The masses of the Ca^{2+}-binding peptide samples did not deviate significantly from the expected values, and in all cases, the purity was > 90% by HPLC (Appendix C).

2.2.5 De-calcification of Ca^{2+}-binding peptides

Isotopicaly labeled and natural abundance Ca^{2+}-binding peptides were de-calcified in preparation for structural and Ca^{2+} titration studies. Nano-pure (Barnstead) water was made Ca^{2+}-free by applying it to a 60 mL column of Chelex 100 resin (BioRad) at a flow rate of 1 mL/min; initial fractions were discarded until the pH dropped below 8.0 (typically 1 L). Peptides were dissolved in 50 mM NH_4HCO_3 (Fisher) buffer, pH 8.0, in Ca^{2+}-free water, applied to a 20 mL column containing 19 mL of Chelex 100 resin and eluted with the same buffer at a flow rate of 1 mL/min. The eluted peptides were lyophilized, re-dissolved in Ca^{2+}-free water, and lyophilized again to remove NH_4HCO_3. For the preparation and manipulation of Ca^{2+}-free peptides, we used Nalgene plastic laboratory equipment in place of glassware to avoid contamination of solutions with Ca^{2+} leached from glass.

Standard Ca^{2+} solutions were prepared in a buffer containing 20 mM MOPS (Sigma), 50 mM KCl (BDH) and $CaCl_2$ (Fisher) at pH 7.4. The Ca^{2+} concentrations of the standards were determined by titration with 10 mM EGTA (Sigma) standardized with 0.1 M $CaCl_2$ standard solution (Orion), using hydroxynaphthol blue (BDH) as the indicator (Procyshyn and Reid 1994b).

2.2.6 CD-monitored Ca^{2+}-binding studies

Circular dichroism (CD) monitored Ca^{2+} titrations were performed on a Jasco J720 spectropolarimeter to record the change in ellipticity at 222 nm with increasing Ca^{2+} concentration at 25 °C. The scanning speed was 50 nm/min, the bandwidth was 1 nm, the response was 4 sec, and the number of accumulations was 4. Samples were loaded in a 1 mm path-length 110-QS Hellma quartz cell. The initial concentrations of the Ca^{2+}-free

peptides were 40 μM in 0.3 mL of 20 mM MOPS and 50 mM KCl in Ca^{2+}-free water at pH 7.4. A total volume of 10 μL of a 2.0 mM $CaCl_2$ standard, prepared as described above, was added in 1 μL aliquots. An additional 7 μL of a 20 mM Ca^{2+} standard, and a final 1 μL of a 1 M Ca^{2+} standard were added, producing a 100 fold molar excess of Ca^{2+} at the end of the titration. A far UV-CD scan was recorded from 200 nm to 300 nm at the beginning and end of the titration. The experiments were repeated 4 times for each Ca^{2+}-binding CaM fragment peptide. The data were fit to the two Ca^{2+}-binding site model using the CaLigator software. This program calculates the free Ca^{2+} concentration from the total Ca^{2+} added (Andre and Linse 2002).

2.2.7 NMR derived structure of CaM2/3

2.2.7.1 NMR spectral assignments of Ca^{2+}-ligated CaM2/3

Uniformly labeled ^{15}N- and $^{13}C/^{15}N$-CaM2/3 protein samples were prepared for NMR spectroscopic analysis by dissolving the freeze dried peptide in 10 mL of an NMR buffer composed of 20 mM Tris d11 (C.I.L.), 50 mM KCl, 10 mM $CaCl_2$ (Ca^{2+} was excluded from the buffer if Ca^{2+}-free CaM2/3 was desired), and 10% D_2O (C.I.L.) at pH 7.4. The pH of the protein solution was measured and readjusted to pH 7.4 without correction for isotope effects. This solution was then concentrated using a Centricon plus-20 centrifugal filter (Amicon) to approximately 150-300 μL, and additional NMR buffer was added to make the final volume 500 μL. Prior to NMR spectroscopic analysis studies the CaM2/3 peptide was tested for stability (Appendix D).

NMR experiments were performed using Varian Unity 500 MHz and Inova 600 MHz spectrometers. Data were processed with Felix 2000 (Accelrys, Inc.) or NMRpipe (Delaglio et al. 1995) and analyzed using Sparky (Goddard and Kneeler 1999). Spectra

were acquired at 25 °C with 0.25 to 0.5 mM samples of ^{15}N- and $^{13}C/^{15}N$-CaM2/3. Initially, sensitivity enhanced gradient ^{15}N-HSQC spectra were recorded with 0.37 mM Ca^{2+}-free ^{15}N-CaM2/3 and in the presence of increasing concentrations of Ca^{2+}. All remaining spectra were recorded in the presence of 10 mM $CaCl_2$. The protein backbone connectivity was established using ^{15}N-HSQC, HNCACB, and CBCA(CO)NH spectra (Grzesiek and Bax 1992; 1993; Wittekind and Mueller 1993). The assignment of resonances from most remaining main chain and aliphatic side chain ^{1}H, ^{13}C, and ^{15}N nuclei were obtained from sensitivity enhanced gradient ^{15}N-HSQC, HNCO, C(CO)TOCSY-NH, H(CCO)TOCSY-NH, and HCCH-TOCSY spectra (Logan et al. 1992; Montelione et al. 1992). The resonances from aromatic side chains were obtained using ^{13}C-HSQC, CβHδ and CβHε experiments (Yamazaki et al. 1993).

2.2.7.2 Structure calculations for Ca^{2+}-ligated CaM2/3

Structure calculations were performed using ARIA/CNS v1.2 with torsion angle dynamics (Brunger et al. 1998; Linge et al. 2003). Distance restraints were obtained from a ^{1}H-^{15}N-^{1}H NOESY-HSQC spectrum (τ_m = 150 msec) recorded on ^{15}N-CaM2/3, and from a simultaneous aliphatic ^{1}H-$^{13}C/^{15}N$-^{1}H NOESY-HSQC spectrum (τ_m = 150 msec), an aromatic ^{1}H-^{13}C-^{1}H NOESY-HSQC spectrum (τ_m = 150 msec), and a simultaneous constant-time methyl ^{1}H-$^{13}C/^{15}N$-^{1}H NOESY-HSQC spectrum (τ_m = 150 msec) recorded on $^{13}C/^{15}N$-CaM2/3 in the NMR buffer (Pascal et al. 1994; Jahnke et al. 1995; Zwahlen et al. 1998). Most NOE-peaks were manually assigned prior to intensity calibration in ARIA. Backbone φ and ψ dihedral angles were determined from $^{13}C_\alpha$, $^{13}C_\beta$, $^{13}C'$, $^{1}H_\alpha$, and ^{15}N chemical shifts using the program TALOS (Cornilescu et al. 1999). ^{13}C secondary chemical shifts, TALOS-derived dihedral angles, and a manual

consideration of initial structures were used to define 28 hydrogen bond distance restraints involving residues within α-helices for subsequent rounds of structure calculations.

Residual dipolar couplings (RDC) were measured with a ^{1}H-^{15}N-IPAP-HSQC spectrum recorded on a sample of ^{15}N-CaM2/3 (~0.3 mM final) diffused into a 7% acrylamide gel (29:1 acrylamide:bisacrylamide stock), dialyzed previously against NMR buffer (Chou et al. 2001a). The gel was cast with a 6 mm diameter and stretched ~2 fold lengthwise upon loading into a 5 mm silanized bottomless NMR tube with a gel stretching apparatus purchased from New Era Enterprises, Inc. Before acquisition of the ^{1}H-^{15}N-IPAP-HSQC with the stretched gel the $^{2}HO^{1}H$ splitting was 11.3 Hz, and after acquisition it was 10.8 Hz. The resulting $^{1}H^{N}$-^{15}N RDC restraints ranged from 14.5 to –16.5 Hz. Signals from residues with a $S^2 < 0.6$, and those residues at the C- and N-terminals were excluded in structural calculations. Axial (D_a) and rhombic (R) parameters were estimated by a histogram method using a grid search for minimal SANI violations (Clore et al. 1998). The R parameter was held constant at 0.18 while D_a was varied between –12 to –10 Hz (Figure 13A), and in another set of experiments the D_a was held constant at –11 Hz while the R varied between 0.1 and 0.5 (Figure 13B). Figure 13 shows that the optimized values were D_a = -11 Hz and R = 0.3. The RDC restraints were included after iteration 5 of the ARIA protocol.

Eight distance restraints for chelating residues to bound Ca^{2+} ions were built into the structure. In EF hand 2, these included residues D58 $O^{\delta 1}$, D60 $O^{\delta 1}$, and E67 $O^{\varepsilon 1}$ and E67 $O^{\varepsilon 2}$. In EF-hand 3 the residues were D93 $O^{\delta 1}$, D95 $O^{\delta 1}$, D97 $O^{\delta 1}$ and E104 $O^{\varepsilon 1}$. These restraints were based upon the reported structure of a Ca^{2+}-loaded CaM-peptide

complex (PDB ID 2BBM) (Ikura et al. 1992). The Ca^{2+}-binding restraints were included after iteration 5 of the ARIA protocol. Justification for these restraints is provided in the Results section 2.3.3.

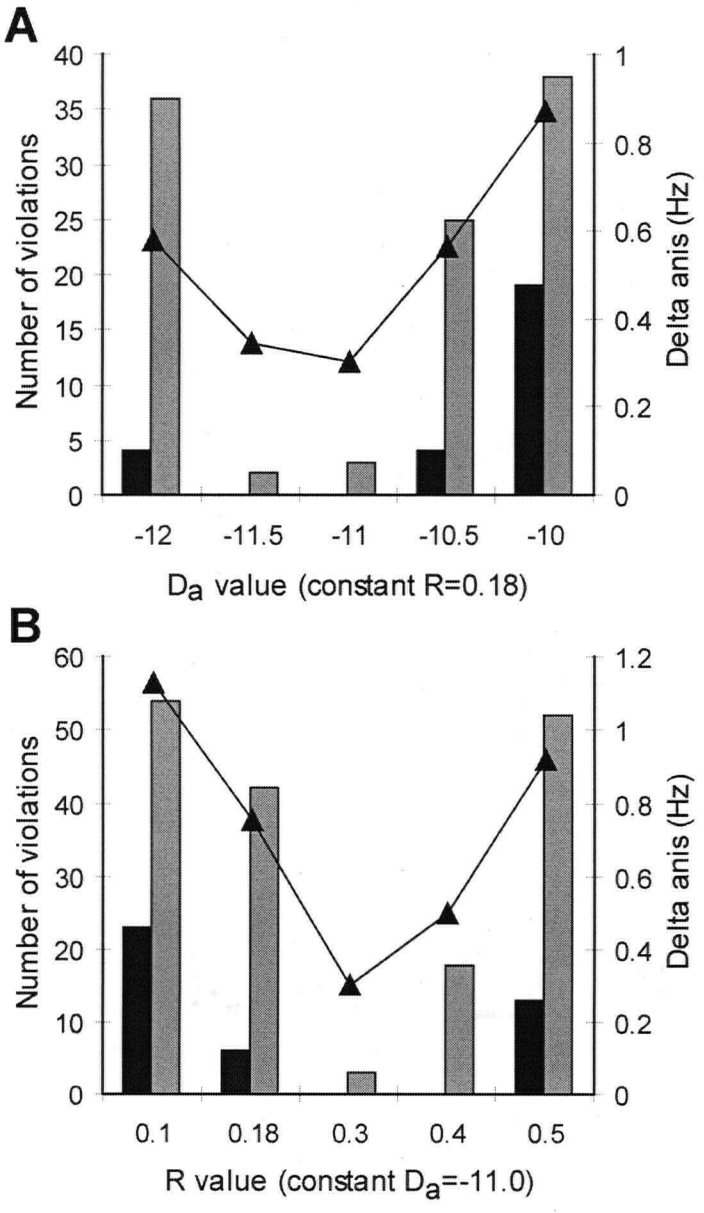

Figure 13. Optimization of axial (D_a) and rhombic (R) parameters for RDC. (A) The optimization of the axial (D_a) parameter using a grid search with the constant rhombic parameter R = 0.18. The black bars indicate the number differences (violations) between calculated and experimentally determined RDC greater than 1 Hz, and the gray bars greater than 0.5 Hz. The black triangles indicate the average difference between calculated and experimentally determined RDC's. **(B)** The optimization of the rhombic parameter (R) parameter using a grid search with the constant axial parameter D_a = -11.0.

The final CaM2/3 structures were calculated using a two-step ARIA protocol. An initial round of ARIA (iterations 0 to 8), started with an unfolded CaM2/3 polypeptide, along with dihedral angle, and NOE restraints. Hydrogen-bond, Ca^{2+}-binding, and RDC restraints were added from iteration 5 onward. A second full ARIA calculation (iteration 0 to 8) was performed, using the structures from the first round and the unambiguous and ambiguous NOE restraint sets from the previous round as the starting parameters. After a final ARIA refinement in a water box using Lennard-Jones potentials, an ensemble of 50 structures was generated and from this the 20 lowest energy structures were selected for subsequent analysis using PROCHECK NMR (Laskowski et al. 1996). The per-residue backbone r.m.s.d. values were calculated using the coordinates for $^{13}C^{\alpha}$, $^{13}C'$ and ^{15}N and the program SupPose (Smith 1997), and the secondary structure of the ensemble of 20 CaM2/3 structures was defined using the program PROMOTIF (Hutchinson and Thornton 1996). Inter-helical angles were calculated according to the method of Kuboniwa *et al.* using the program Interhlx (Kuboniwa et al. 1995; Yap 1995; Yap et al. 1999; 2002). Weighted secondary chemical shifts were calculated using the program CSI with the $^{13}C^{\alpha}$ and $^{13}C^{\beta}$ chemical shifts (Yap and Tomomori 1999). Backbone r.m.s. deviations were calculated using the coordinates for $^{13}C^{\alpha}$, $^{13}C'$ and ^{15}N and MolMol (Koradi et al. 1996). The structures were analyzed and visualized using MolMol (Koradi et al. 1996), and WebLab ViewerPro (Accelrys, Inc.).

2.2.7.3 Backbone amide ^{15}N relaxation studies

Backbone amide ^{15}N relaxation parameters were acquired for Ca^{2+}-saturated ^{15}NCaM2/3 at 25 °C using a 500 MHz NMR spectrometer (Farrow et al. 1994; Farrow et al. 1995). Data points for the T_1 (10, 30.1, 50.2, 100.4, 200.7, 301.1, 451.6, 602.2, 752.7, and 903.2 msec) and T_2 (16.7, 33.4, 50.1, 66.8, 83.5, 100.2, 116.9, 133.6, 150.3, and 167.0 msec) experiments were collected in random order. Steady-state heteronuclear $^1H\{^{15}N\}$-NOE spectra were acquired with and without 2 sec of ^1H saturation and a total recycle delay of 5 sec. All data were processed with NMRpipe and the above data points were fit to a single exponential using Sparky to obtained the T_1 and T_2 parameters (Goddard and Kneeler 1999). Anisotropic diffusion and model-free order parameters (S^2) were calculated with the program Tensor 2.0 using the lowest energy structural model of CaM2/3 (Dosset et al. 2000). Residues for which the $^1H\{^{15}N\}$NOE ratios were < 0.6, and for which the values of $[(\langle R_2 \rangle - R_{2i})/\langle R_2 \rangle) - (\langle R_1 \rangle - R_{1i})/\langle R_1 \rangle)]$ > were 1.5 x the standard deviation of this difference, were excluded from the diffusion tensor calculations due to the possibility of fast internal motions or chemical exchange broadening (Tjandra et al. 1995).

2.3 Results

2.3.1 CD spectra and Ca^{2+}-binding of CaM1/2 and CaM3/4

The CD spectra of CaM1/2 and CaM3/4 exhibit shapes consistent with a significant amount of α-helical secondary structure in both the Ca^{2+}-free and Ca^{2+}-ligated forms (Figure 14) (Johnson 1988). Thus as expected, CaM1/2 and CaM3/4 appear well folded due to their similarity to the N- and C- terminal domains of CaM. A prominent change in molar ellipticity at 222 nm is usually interpreted as an change in overall α-helical content of a protein (Johnson 1988; Pelton and McLean 2000). However, in the case of Ca^{2+}-binding peptides, this difference is more likely reflective of the rearrangement of α-helices and the resulting change in α-helical angles upon Ca^{2+}-binding. The CaM1/2 peptide exhibits a small but significant change in molar ellipticity at 222 nm upon Ca^{2+}-binding. The CaM3/4 peptide shows a larger change in molar ellipticity at 222 nm upon Ca^{2+}-binding compared to CaM1/2 (Table 4).

Table 4. Changes in mean residue ellipticity

	$[\theta]_{222}x10^{-3}$ (deg cm^2 /dmol residue)		
Protein	Ca^{2+}-free	Ca^{2+}-ligated	$\%\Delta[\theta]_{222}$
CaM1/2	-17.3±0.3	-18.3±0.4	5.5
CaM2/3	-7.9±0.01	-11.3±0.1	30.1
CaM3/4	-17.1±0.4	-21.3±0.1	19.7
CaM*	-14.3±0.1	-16.4±0.1	12.8

Each value is the mean ± sd of four replicates. *Values for CaM taken from (Wu and Reid 1997b). $[\theta]_{222}$ is the mean residue ellipticity at 222 nm. $\%\Delta[\theta]_{222}$ is the percent change in mean residue ellipticity at 222.

Figure 14 shows the results of the CD monitored Ca^{2+} titrations for CaM1/2, CaM2/3 and CaM3/4 with the corresponding fits generated by the Caligator software. CaM1/2 and CaM3/4 exhibit relatively high affinity Ca^{2+}-binding. The overall Ca^{2+}-binding affinity of CaM3/4 is higher than for CaM1/2 (Table 5) as evidenced by the ΔG_{tot}=-RTln(K_1K_2), however, the difference is not large. In addition, both CaM1/2 and CaM3/4 demonstrate positive cooperative relationships between the first and second binding sites as evidenced by the negative values of the $\Delta\Delta G_{\eta=1}$. In contrast the CaM2/3 peptide shows markedly different behavior.

Fitting of the CD-monitored Ca^{2+}-titration of CaM2/3 yielded two widely divergent dissociation constants (Table 5 and Figure 14). This behavior is indicative of a sequential, two-step Ca^{2+}-binding model (Li et al. 1995). In addition, the overall Ca^{2+}-affinity of CaM2/3 is much lower than that of CaM1/2 and CaM3/4 as evidenced by the K_d and ΔG_{tot} values.

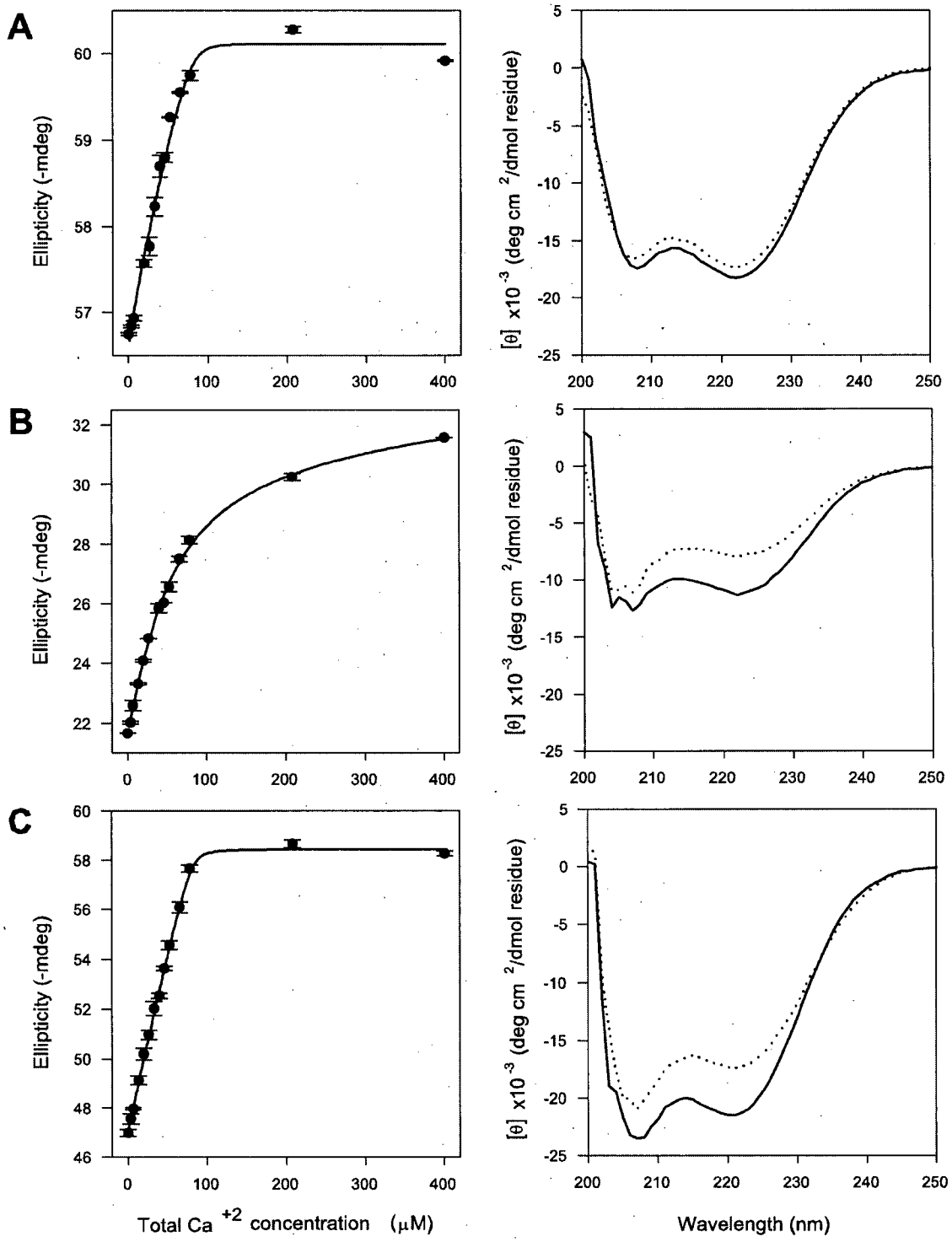

Figure 14. The Ca^{2+} titration curves and CD spectra. The titration curves and CD spectra for (**A**) CaM1/2, (**B**) CaM2/3, and (**C**) CaM3/4. The Ca^{2+} titration curves were fit to a two Ca^{2+}-binding site model using CaLigator (Andre and Linse 2002) on the left

side, and the corresponding CD spectra on the right side. The CD spectra are presented as mean residue ellipticity ([θ]) versus wavelength. The mean residue ellipticity is calculated [θ] = mDeg(10^6)/(#residues C 1mm). Where mDeg is the ellipticity, #residues is the number of residues, C is the concentration of protein (40μM), and 1 mm is the cell path length. The CD spectra exhibit shapes that are consistent with α-helical structure in both the Ca^{2+}-free and ligated forms. The titration curves are presented as the negative of the ellipticity at 222 nm versus the total concentration of Ca^{2+}. The black circles represent the mean and the error bars represent the standard error. The titration curves reveal that the N- and C-terminal domain peptide fragments of CaM (CaM1/2 and CaM3/4) have much higher affinity for Ca^{2+} than the middle fragment, CaM2/3. The titrations of all peptides were carried out to approximately 100 fold molar excess for the curve fitting. However, here the titration curves are presented only to 10 fold molar excess.

Table 5. Caligator fit Ca^{2+} dissociation constants, $\Delta\Delta G_{\eta=1}$, and ΔG_{tot}

Peptide	K_{d1} (μM)	K_{d2} (μM)	$\Delta\Delta G_{\eta=1}$ (kJ/mol)	ΔG_{tot} (kJ/mol)
CaM1/2	10.9±0.6	1.5±0.1	-8.4±0.2	-61.7±0.2
CaM2/3	30±5	1800±400	6.5±0.1	-41.4±1
CaM3/4	7.7±1.3	0.6±0.1	-9.9±0.2	-65.1±1.2

All values are presented as mean ± S.E. for 4 replicates.

ΔG_{tot}=-RTln($K_{d1}K_{d2}$)

$\Delta G_{\eta=1}$=-RTln($4K_{d2}/K_{d1}$)

2.3.2 NMR and CD spectropolarimetry of CaM2/3

NMR spectroscopy and CD spectropolarimetry were used to monitor the behavior of CaM2/3 as a function of Ca^{2+} concentration. As with the CD spectra of both Ca^{2+}-free CaM1/2 and CaM3/4, the CD spectrum of Ca^{2+}-free CaM2/3 shows minima near 208 and 222 nm, indicative of at least some transient α-helical content (Figure 14B). However, the ^{15}N-HSQC spectrum of Ca^{2+}-free CaM2/3 shows poorly resolved amide resonances with ^{1}H chemical shifts clustered near 8.5 ppm (Figure 15A). Therefore, Ca^{2+}-free CaM2/3 does not adopt a defined, folded structure. However, upon the incremental addition of Ca^{2+}, a progressive disappearance of the Ca^{2+}-free peaks, and the appearance of a set of well-dispersed amide peaks was observed in the ^{15}N-HSQC spectra of CaM2/3. These new dispersed peaks corresponded to folded Ca^{2+}-ligated CaM2/3 (Figures 15B and C). In parallel, a significant increase in negative ellipticity was observed by CD upon addition of Ca^{2+} (Figure 14B and Table 4). These results suggest Ca^{2+}-binding causes the co-operative folding of CaM2/3 in the slow exchange regime on the NMR chemical shift timescale.

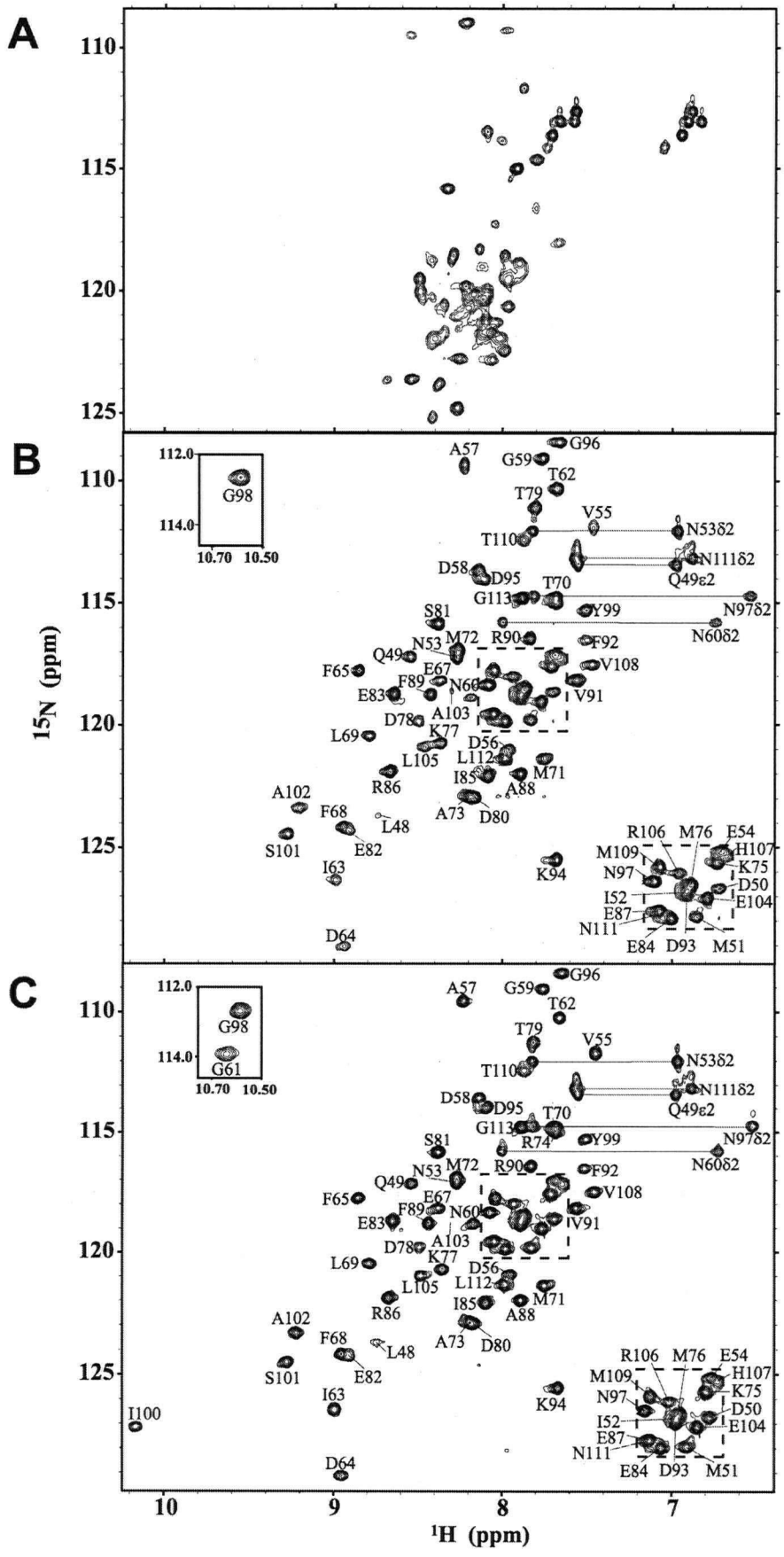
A
B
C
110
115
120
125
^{15}N (ppm)
112.0
114.0
10.70 10.50
G98
G61
A57
G59
G96
T62
T79
V55
T110
N53δ2
N111δ2
Q49ε2
D58
D95
T70
G113
S81
Y99
N97δ2
N60δ2
R90
F92
N53
M72
Q49
V108
F65
E67
F89
N60
V91
E83
A103
D78
K77
L69
D56
L105
L112
I85
M71
R86
A88
A102
F68
A73
D80
L48
S101
E82
I63
K94
D64
R106
M76
E54
H107
M109
K75
N97
D50
I52
E104
E87
N111
E84
D93
M51
R74
I100
10
9
8
7
^{1}H (ppm)

Figure 15. The ^{15}N-HSQC spectra of CaM2/3. (**A**) The unassigned ^{15}N HSQC spectrum of Ca^{2+}-free CaM2/3. The poor $^{1}H^{N}$ dispersion indicates the lack of any predominant structure. The ^{15}N HSQC spectra of 0.37 mM CaM2/3 in the presence of (**B**) 0.74 mM Ca^{2+} and (**C**) 1.8 mM Ca^{2+} (25°C, pH 7.4). Assigned peaks are numbed as in native CaM, with horizontal lines connecting resonances from $^{15}NH_2$ groups. The insets bordered with dashed-lines correspond to the crowded regions near the center of the spectra. The insets bordered with a solid line show the positions of the downfield shifted signals from G98 and G61. The peak for A57 is aliased from 130.9 ppm, and signals corresponding to residues A46 and E47 were not detected. Signals from the amides of G61 and I100 were only observed upon saturation of CaM2/3 with Ca^{2+} (panel **C**) These data indicate that CaM2/3 adopts a globally folded structure upon binding the first Ca^{2+} in EF hand 3, and that subsequent binding of a second Ca^{2+} leads to local stabilization of EF hand 2.

Most of the ^{15}N-HSQC resonances corresponding to folded CaM2/3 were observed in the presence of approximately a 2-fold molar excess of Ca^{2+}, however, several additional equivalents of Ca^{2+} were required to obtain the spectra of the fully Ca^{2+} saturated form of CaM2/3 (Figures 15B and 15C). This is best illustrated by consideration of the amide hydrogen ($^{1}H^{N}$) resonances of G61 and G98. The downfield shift of these resonances is indicative of hydrogen bonds between G61 and G98 $^{1}H^{N}$, and D56 and D93 carboxyl side chains, respectively, and are diagnostic of a Ca^{2+}-ligated EF-hand (Kay et al. 1991). The signal from G98, corresponding to EF-hand 3 in CaM2/3, is observed upon the initial addition of Ca^{2+}, (Figure 15B) whereas that from G61 is not detected until full saturation (Figure 15C). This suggests that binding of Ca^{2+} to EF-hand 3 is linked to the cooperative folding of CaM2/3 to an intermediate, albeit "native-like" structure. Complete folding requires Ca^{2+}-binding to the lower-affinity EF-hand 2. Furthermore, with one Ca^{2+} bound, the signals from residues adjacent to G61, including D56, D58, N60, T62, I63, and D64, were relatively weak. Upon saturation, these signals sharpen yet their chemical shifts do not change (Figure 15B and 14C). This behavior is suggestive of peak broadening in the ^{15}N-HSQC due to localized conformational

exchange, on the msec to μsec timescale, for these residues about an "EF-hand-like" intermediate state. Ca^{2+}-binding stabilizes the conformation of these residues giving rise to the sharp peaks seen in the fully Ca^{2+}-saturated CaM2/3 ^{15}N-HSQC (Figure 15C).

These data confirm the sequential two-step Ca^{2+}-binding that was observed with the CD-monitored Ca^{2+} titration of CaM2/3 (Figure 14). They also confirm that one Ca^{2+}-binding site has low affinity. Based on the Ca^{2+}-dependent spectral changes observed in the ^{15}N-HSQC spectra of CaM2/3 (especially the G61 and G98 $^{1}H^{N}$ resonances) (Figure 15B and 15C), the high affinity site is assigned to EF-hand 3, and the low affinity site to EF-hand 2.

2.3.3 The Structure of CaM2/3

NMR spectroscopy was used to determine the monomeric tertiary structural ensemble of Ca^{2+}-saturated CaM2/3. The atomic coordinates of the CaM2/3 ensemble (PDB ID 2HF5) have been deposited in the Protein Data Bank, Research Collaboratory for Structural Bioinformatics, Rutgers University, New Brunswich, NJ (http://www.rcsb.org/). The NMR chemical shift list (accession code 7190) has been deposited in the BioMagResBank at www.bmrb.wisc.edu/. Analytical ultracentrifugation, (Chapter 3 section 3.2.5) light scattering, and isotope-filtered NOE experiments confirm that CaM2/3 is monomeric under the experimental conditions of this study (Appendix E). As discussed below, ^{15}N relaxation measurements also corroborate this conclusion.

The statistics of the CaM2/3 structural ensemble are presented in Table 6 and the structures are shown in Figure 16. CaM2/3 contains four α-helices (helix C, residues 48-55; D, 65-73; E, 82-92; and F, 102-109) and one small anti-parallel β-sheet centered on

I63 and I100 (Figure 16A). This secondary structure, which is nearly identical to that found for the corresponding sequence in native CaM (Chattopadhyaya et al. 1992; Chou et al. 2001b), confirms that residues 48-72 and 82-109 form EF-hand motifs in CaM2/3. These motifs associate through the β-strand pairing and hydrophobic side chain packing (Figure 16B), thereby stabilizing the globular tertiary structure of CaM2/3.

Table 6 Structural statistics for CaM2/3

Summary of restraints	
NOE restraints	
Intra-residue	358 (13)
Sequential (|i-j| = 1)	132 (55)
Medium-range (|i-j| < 4)	95 (59)
Long-range (|i-j > 5)	126 (68)
Total NOE's	711 (195)
RDC's	57
Hydrogen bonds	14 x 2
Ca^{2+}-coordinating	8
Dihedral angle restraints ϕ, ψ	52, 52
Ramachandran plots residues in: (%)	
Most favored regions	85
Additional allowed regions	14.8
Generously allowed regions	0.2
Structure Statistics (mean and s.d.)	
Violations	
NOE restraints (Å)	0.034±0.0034
Dihedral angle restraints (°)	2.34±0.51
RDC restraints (Hz)	0.32±0.17
Max. dihedral angle violation (°)	3.37
Deviations from idealized geometry	
Bond lengths (Å)	0.0043±0.00016
Bond angles (°)	0.63±0.019
Impropers (°)	1.98±0.14
Average pairwise r.m.s.d. (Å)	
Side chain heavy atoms *	1.27±0.26
Backbone ($^{13}C^{\alpha}$, $^{13}C'$, ^{15}N) *	0.58±0.14

The distance restraints are listed as unambiguous and ambiguous in parentheses.
*Pair wise r.m.s.deviations were calculated for the 20 refined structures by alignment of residues 48-71, 82-106 roughly corresponding to EF-hands 2 and 3 respectively. Backbone r.m.s. deviations were calculated using the coordinates for $^{13}C^{\alpha}$, $^{13}C'$ and ^{15}N and side chain r.m.s. deviations were calculated using heavy atoms. All r.m.s.deviations were calculated with MolMol (Koradi et al. 1996).

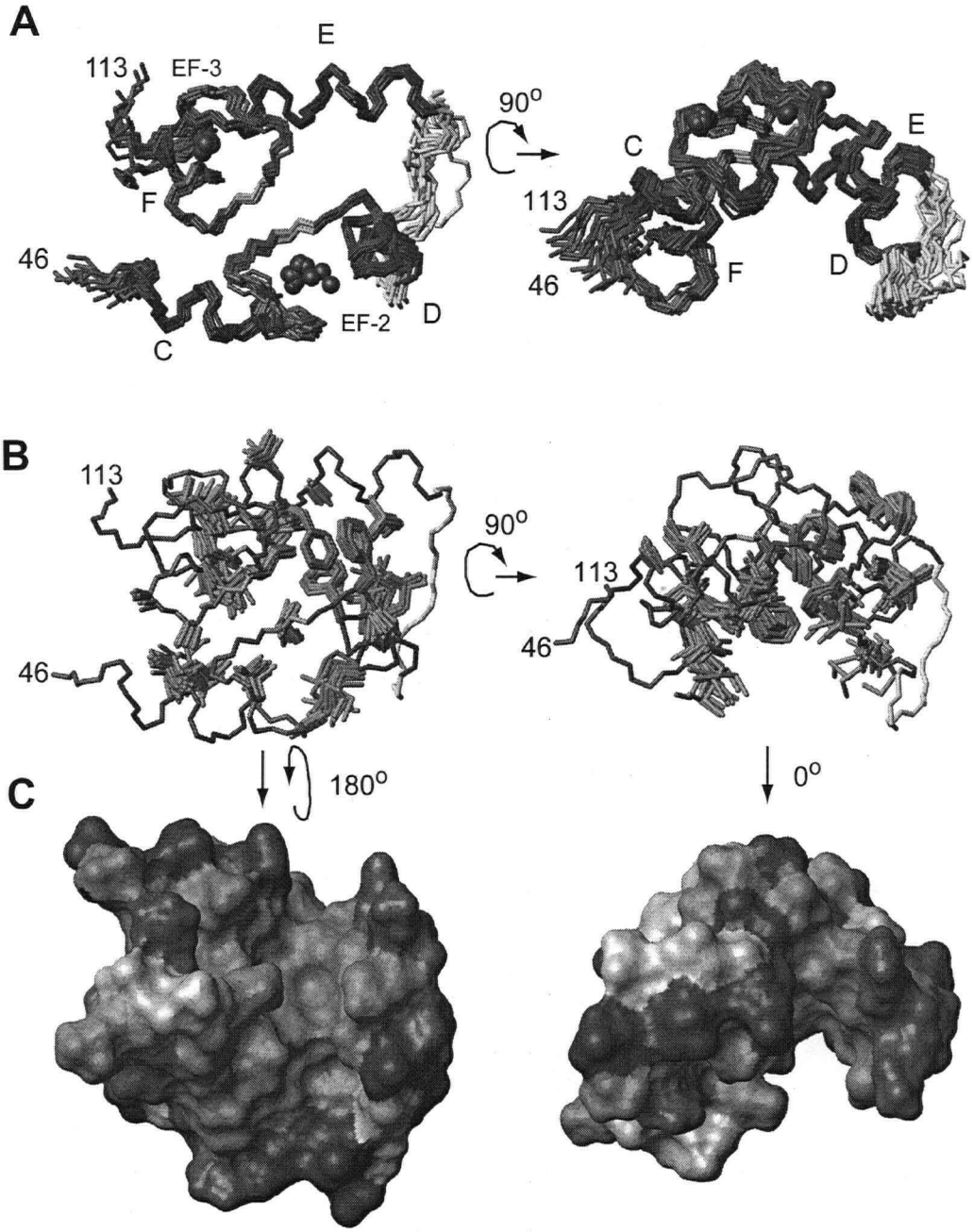

Figure 16. The NMR-derived structural ensemble of Ca^{2+}-ligated CaM2/3. For panels A and B the right-hand side of the diagram is the same as the left-hand except that the figures are rotated by 90° around the indicated axis. (**A**) The 20 lowest energy structures for CaM2/3 superimposed on to each other using the backbone heavy atoms ($^{13}C^{\alpha}$, $^{13}C'$ and ^{15}N) within the α-helical regions. Following the nomenclature for native CaM, the α-helices are labeled C through F (residues 48-55, 65-73, 82-92, 102-109), the Ca^{2+} ions are represented as spheres, and the Ca^{2+}-binding sites labeled EF-2 and EF-3. The disordered regions at the N- and C- termini (residues 46 to 47 and 110 to 113) are labeled 46 and 113, respectively. The structures are similar to both the N- and C-terminal domains of CaM. (**B**) The hydrophobic side chains within the CaM2/3 structural

ensemble. The backbone displayed is lowest energy structure orientated the same as in panel A. (**C**) The surface representation of CaM2/3. The surface figures are rotated according to the given angles with respect to the figures in panel B. The positions of the hydrophobic residues and the angles between the α-helices reveal a hydrophobic binding pocket that is similar to that seen in both domains of CaM. All structures were rendered using MOLMOL (Koradi et al. 1996).

The close contacts between the Ca^{2+}-binding segments of EF-hands 2 and 3 in CaM2/3, are mediated through residues I63 and I100 (Figure 16). These residues form the short anti-parallel β-sheet. This structure is similar to anti-parallel β-sheet structures observed between the EF-hands in both the N- and C-terminal domains of CaM (Babu et al. 1988). Evidence for this β-sheet structure lies with the downfield $^1H^N$ and ^{15}N chemical shifts of I63 and I100. Based on NMR spectroscopic studies of several EF-hand domains these shifts can be attributed to hydrogen bonds between I63 $^1H^N$ and I100 C=O, as well as I100 $^1H^N$ and I63 C=O (Ikura et al. 1985). Additional evidence for this anti-parallel β-sheet is found in NOE's detected between I63 $^1H^N$ and I100 $^1H^N$, Y99 H^α and F65 $^1H^N$, and between S101 H^β and T62 H^γ.

Figures 16B and C show that the hydrophobic residues of CaM2/3 form a well-defined hydrophobic core. A key aspect of the hydrophobic core of EF-hand proteins is the presence of stacked aromatic residues (Chapter 1 page 14). In CaM2/3, the average distances between the aromatic ring centroids of residues F65 to F89, F89 to F68, and F68 to F92 are 4.1 ± 0.1 Å, 5.4 ± 0.2 Å, and 5.9 ± 0.4 Å, respectively. These distances are within the normal range between the centroids of aromatic residues that form stacking interactions (McGaughey et al. 1998). These distances are derived partly, from NOE's detected between F65 $^1H^\alpha$ and F89 $^1H^\varepsilon$, F89 $^1H^\beta$ and F65 $^1H^\varepsilon$, and F89 $^1H^N$ and F92 $^1H^\delta$.

Figure 16A reveals that the hinge region in CaM2/3 exhibits flexibility that is similar to that observed in the same region of CaM. It is this flexibility, in CaM2/3, that allows for interactions between EF-hands 2 and 3 that are not observed between the same EF-hands in CaM. In the case of CaM2/3 the hinge region plays a similar role as the loops between EF-hands 1 and 2 and between EF-hands 3 and 4 in the N- and C- terminal domains of CaM.

Using the criteria of dihedral angles and C^{α} and C^{β} chemical shifts established by Gronenborn *et al.*, three helical N-cap structures are found at the N-terminal ends of α-helices D, E, and F in CaM2/3 (Gronenborn and Clore 1994). However, some of the CaM2/3 structures do not show side chain conformations consistent with the hydrogen-bonding pattern observed by Harper *et al.* in typical N-cap structures (Harper and Rose 1993)

The CaM2/3 ensemble includes Ca^{2+} ions chelated by EF-hand 2 and EF-hand 3 (black spheres Figure 16). Although not directly observable by NMR spectroscopic methods, experimental evidence for Ca^{2+} chelation at these EF-hands included the following. First, in the presence of saturating Ca^{2+}, the $^{1}H^{N}$ resonances of G61 and G98 are shifted dramatically downfield to 10.63 and 10.58 ppm, respectively (Figure 15C). These chemical shifts, which are diagnostic of Ca^{2+}-binding to EF-hand motifs, reflect the formation of hydrogen bonds to the carboxylates of D56 and D93 in native CaM. Second, the large difference in chemical shifts (0.32 to 0.96 ppm) between chelating residues $^{1}H^{\beta}/^{1}H^{\beta'}$ (or $^{1}H^{\gamma}/^{1}H^{\gamma'}$ in the case of glutamate) for residues D58, N60, D64, E67, D93, D95, N97, and S101 also suggests that these residues are involved in chelating Ca^{2+} (Shaw et al. 1992). Third, the downfield $^{1}H^{N}$ and ^{15}N chemical shifts for I63 and I100,

are indicative of both β-sheet formation and Ca^{2+}-chelating (Figure 15B and 15C) (Biekofsky et al. 1998). Fourth, key NOE restraints were identified between chelating residues D56, T62, and G59 in EF-hand 2, as well as between D93 and G96, K94 and E104, and D95 and D98 in EF-hand 3. These NOE restraints positioned the chelating residues close enough to justify the added Ca^{2+}-restraints. Fifth, the conformational arrangement of the EF-hand motifs in CaM2/3 are similar to that observed in crystal structures of Ca^{2+}-ligated CaM, yet distinct from those found in Ca^{2+}-free CaM (Figures 16 and 17) (Chattopadhyaya et al. 1992; Kuboniwa et al. 1995). This is seen in terms of the inter-helical angles of CaM2/3 compared to both the Ca^{2+}-free and ligated forms of CaM (Table 7). This is also reflected in the lower backbone r.m.s. deviations of EF-hand 2 and EF-hand 3 of CaM2/3 when compared with Ca^{2+}-ligated CaM versus Ca^{2+}-free CaM (Figures 17, 18 and Table 8).

Table 7. Inter-helical angles for Ca^{2+}-ligated CaM2/3

Structure	Ca^{2+} state	PDB ID	Helical pairing and resulting angles			
			C/D	E/F	D/E	C/F
CaM2/3	$+Ca^{2+}$	2HF5	82 (4.1)	91 (3.3)	102 (3.8)	108 (3.5)
CaM	$+Ca^{2+}$	1CLL	A/B	C/D	B/C	A/D
			89	88	109	106
			E/F	G/H	F/G	E/H
			102	95	112	115
CaM	$-Ca^{2+}$	1CFD	A/B	C/D	B/C	A/D
			134	129	128	128
			E/F	G/H	F/G	E/H
			135	136	139	139

Comparison of the α-helical angles (in degrees) of CaM2/3 with two representative structures of Ca^{2+} free (-Ca2+) and ligated ($+Ca^{2+}$) CaM. The α-helical parings (shaded gray) are aligned in the columns based on the order in which they appear in each domain. For CaM2/3 the order of α-helices is C, D, E, and F. For the N-terminal domain of CaM the order of α-helices is A, B, C, D and for the C-terminal domain the order is E, F, G, and H. All α-helical angles were calculated using the program interhlx. In the case of CaM2/3 the angles are given as mean and sd in parenthesis for the ensemble of 20 structures.

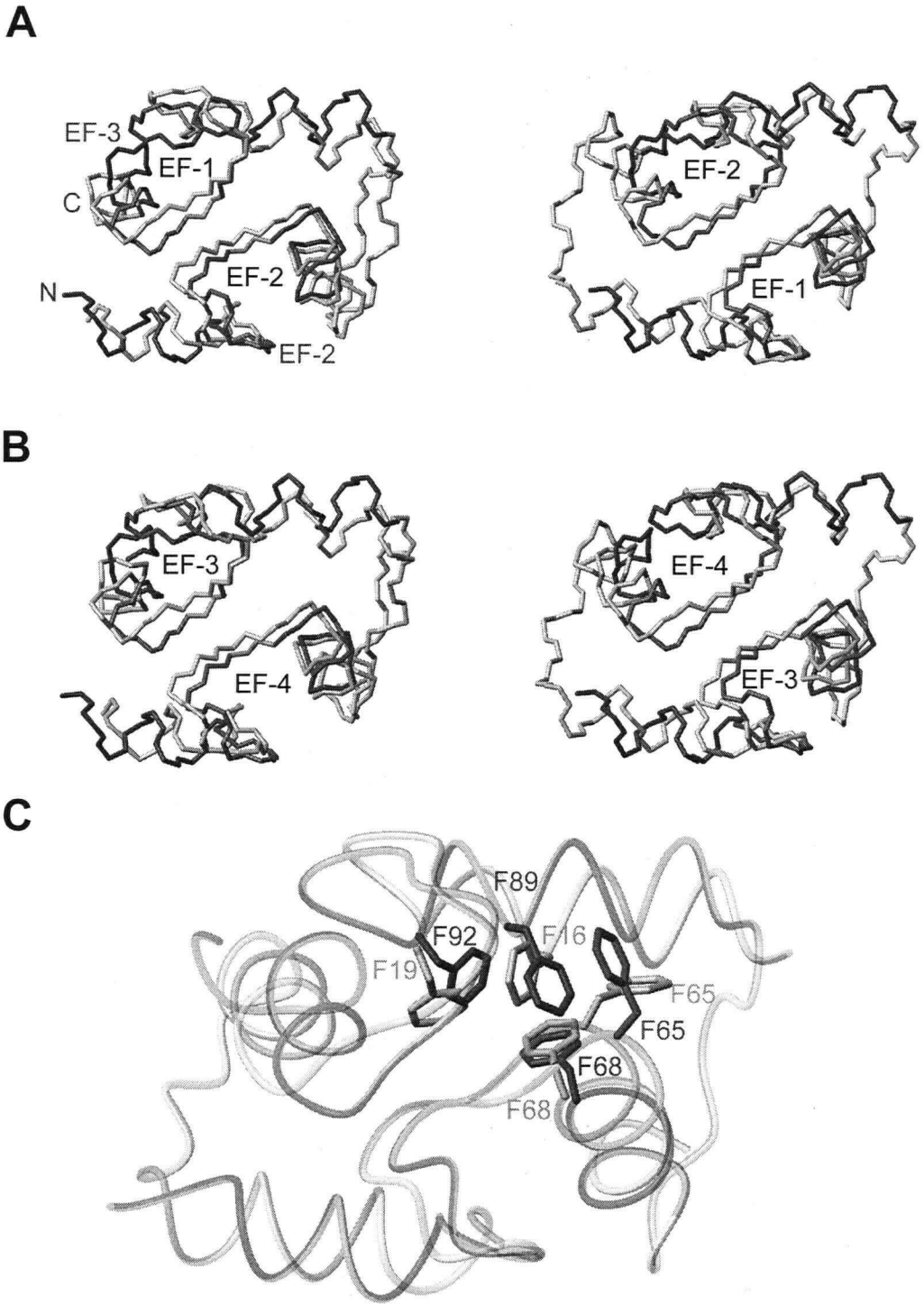

Figure 17. CaM2/3 superimposed onto Ca^{2+}-ligated CaM. The backbone of the lowest energy structure of CaM2/3 orientated according to Figure 16A and superimposed on Ca^{2+}-ligated CaM (gray) (PDB ID 1CLL). In this figure, the view of CaM2/3 is held approximately constant, and that of CaM varied, with the EF-hands of CaM labeled in black, and the EF-hands as well as the N- and C-terminals of CaM2/3 labeled (gray) in panel A for reference. (**A**) Left: the superimposition of EF-hands 2 and 3 of CaM2/3 on the N-domain EF-hands 1 and 2 of Ca^{2+}-ligated CaM, respectively. The resulting

superimposition positions the hinge of CaM2/3 over the loop between EF-hands 1 and 2 in CaM. Right: the opposite superimposition (i.e. EF-hands 2 and 3 of CaM2/3 on EF-hands 2 and 1 of CaM, respectively). (**B**) Left: the superimposition of EF-hands 2 and 3 of CaM2/3 on the C-domain EF-hands 3 and 4 of Ca^{2+}-ligated CaM, respectively. Right: the opposite superimposition. The disordered regions at the N- and C- terminals (residues 45 to 47 and 110 to 113) and Ca^{2+} are removed for clarity. (**C**) The superimposition from (A) right displayed as transparent schematic C^{α} tubes. The residues forming aromatic stacking interactions are displayed and labeled in gray for Ca^{2+}-ligated CaM and in black for CaM2/3. There is substantial overlap of the hydrophobic residues except for F65, which is displaced with respect to the equivalent residue in CaM. All superimpositions are made using backbone atoms C^{α}, C' and N over the Ca^{2+}-binding segments and eight residues of the flanking α-helical regions. See Table 8 rows 9 through 12 for the r.m.s deviations of the above superimpositions. All structures were rendered using MOLMOL (Koradi et al. 1996).

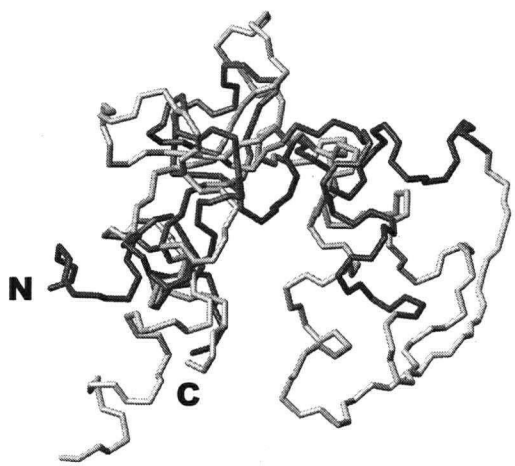

Figure 18. Ca^{2+}-ligated CaM2/3 superimposed on Ca^{2+}-free CaM. The structure of CaM2/3, is superimposed onto the N-terminal domain of Ca^{2+}-free CaM (gray) (1CDF). The structures are arranged such that EF-hand 3 of Ca^{2+}-free CaM is superimposed on EF-hand 2 of CaM2/3 while EF-hand 4 of Ca^{2+}-free CaM is superimposed on EF-and 3 of CaM2/3. Similar to CaM structures, the angles between α-helices of CaM2/3 are nearly perpendicular while the Ca^{2+}-free CaM angles are large and the α-helices nearly anti-parallel. The disordered regions at the N- and C- termini of CaM2/3 (residues 45 to 47 and 110 to 113) and Ca^{2+} were removed for clarity. This structure was rendered using MOLMOL (Koradi et al. 1996).

Table 8. List of pair wise r.m.s. deviations between Ca^{2+}-ligated CaM2/3 and CaM in the Ca^{2+}-ligated and free states

CaM2/3 EF-hand(s)	CaM EF-hand(s)	r.m.s.d. (Å) CaM +Ca^{2+}	r.m.s.d. (Å) CaM -Ca^{2+}
2	1	1.3	3.4
2	2	1.2	2.8
2	3	1.4	3.4
2	4	1.5	4.3
3	1	1.5	3.2
3	2	1.4	3.1
3	3	1.6	3.3
3	4	1.5	4.3
2\3	1\2	2.2	3.9
2\3	2\1	2.2	3.9
2\3	3\4	2.2	4.5
2\3	4\3	2.2	4.5

The backbone r.m.s. deviations (Å) of the lowest energy structure of Ca^{2+}-ligated CaM2/3 superimposed onto Ca^{2+}-free (PDB ID 1CFD) and Ca^{2+}-ligated (PDB ID 1CLL) vertebrate CaM via the indicated EF-hands. Where two EF-hands are indicated the order of numbering indicates the order of EF-hand superimposition. The indicated EF-hands were superimposed using backbone atoms C^{α}, C' and N over the Ca^{2+}-binding segments and eight residues of the flanking α-helical regions. Backbone r.m.s. deviations were calculated using the coordinates for C^{α}, C' and N with MolMol (Koradi et al. 1996). The last 4 rows (shaded) contain the r.m.s. deviations of the superimpositions described in Figure 17.

The overall structure of CaM2/3 is remarkably similar to both the N- and C-terminal domains of native CaM. Table 8 shows that the individual EF-hands of CaM2/3 superimpose well onto each of the individual EF-hands of Ca^{2+}-ligated CaM. Similar superimpositions using both EF-hands of CaM2/3 fit well onto either domain of Ca^{2+}-ligated CaM (Figure 17A and B). This is true regardless of the EF-hands superimposed. For example, if EF-hand 3 from CaM2/3 is superimposed on EF-hand 3 of CaM, while EF-hand 2 from CaM2/3 is superimposed on EF-hand 4 of CaM the r.m.s. deviation is similar if the opposite superimposition is done.

There is substantial overlap between the core hydrophobic residues of CaM2/3 and both the N- and C- (not shown) terminal domain of Ca^{2+}-ligated CaM (Figure 17C). This suggests that CaM2/3 has a hydrophobic binding pocket (Figure 16C) that is similar to the hydrophobic binding pockets observed in both domains of CaM.

A notable difference in the packing of aromatic residues in CaM2/3 is F65 (Figure 17C), which is displaced with respect to the equivalent residue in CaM. In contrast to CaM, F65 of CaM2/3 appears to form parallel-displaced aromatic stacking interactions with F89.

2.3.4 CaM2/3 backbone dynamics from amide ^{15}N relaxation

The global and local dynamic properties of CaM2/3 were probed by ^{15}N T_1, T_2, and heteronuclear ^{1}H-{^{15}N}NOE measurements (Figures 19 A, B, and C). Excluding residues exhibiting anomalous T_1/T_2 or heteronuclear ^{1}H-{^{15}N}NOE ratios indicative of conformational exchange or a high degree of internal mobility, the relaxation data yielded a fully anisotropic rotational diffusion tensor of $D_{xx} = 2.5 \pm 0.2 \times 10^7\ s^{-1}$, $D_{yy} = 3.4 \pm 0.2 \times 10^7\ s^{-1}$, and $D_{zz} = 3.9 \pm 0.2 \times 10^7\ s^{-1}$ for CaM2/3. These values correspond to an effective correlation time of 5.1 ± 0.2 ns for the global tumbling of CaM2/3. This correlation time is close to that of ~5 ns expected for a monomeric 68 residue protein (Daragan and Mayo 1997).

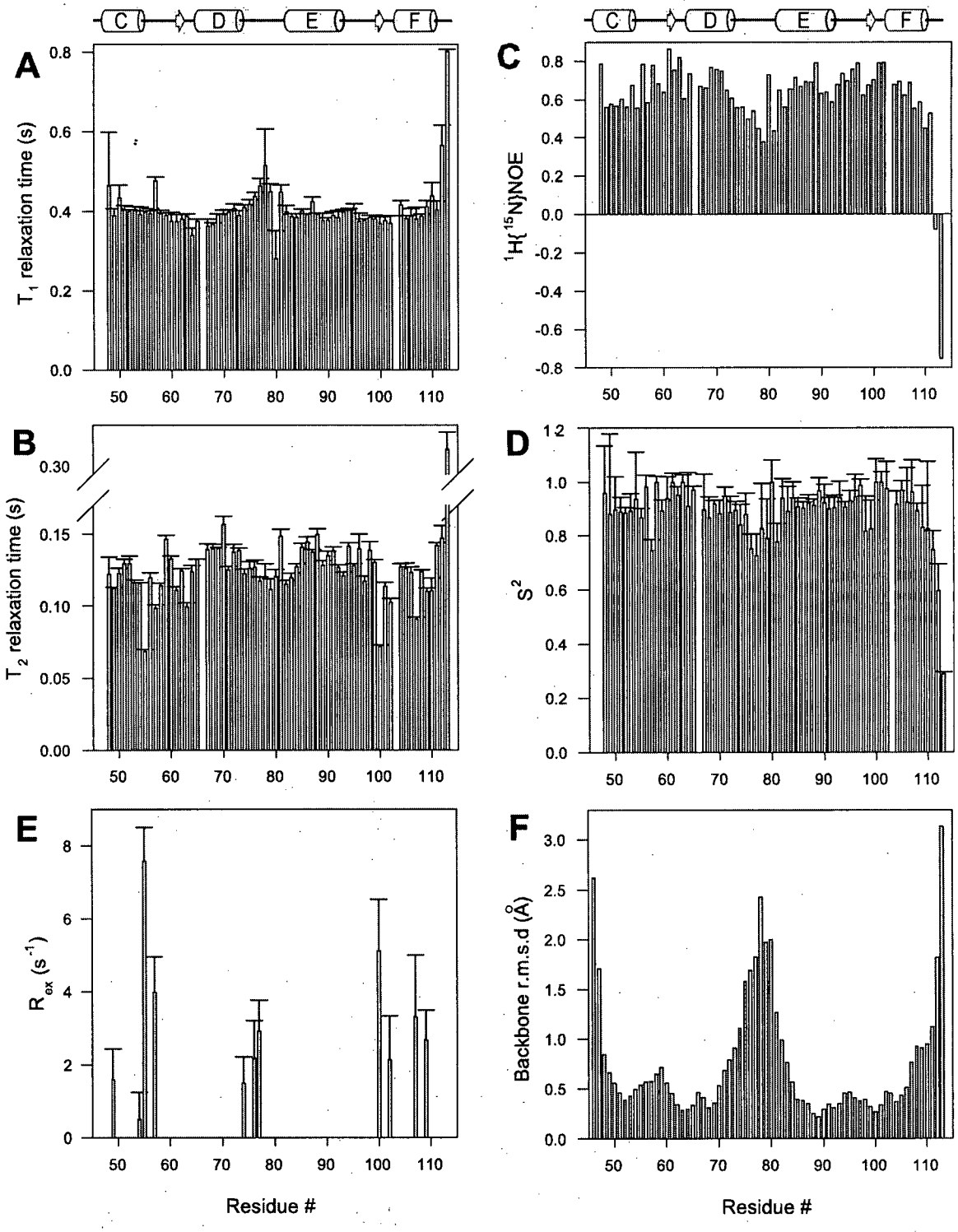

Figure 19. Backbone ^{15}N relaxation data for Ca^{2+}-saturated CaM2/3. Shown are the (**A**) longitudinal (T_1) and (**B**) transverse (T_2) relaxation times (and standard errors), the (**C**) heteronuclear $^1H\{^{15}N\}NOE$ ratios, the (**D**) fit anisotropic model free order parameters (S^2), the (**E**) conformational exchange broadening (R_{ex}) parameter and the (**F**) per-residue r.m.s. deviations of backbone heavy atoms ($^{13}C^{\alpha}$, $^{13}C'$ and ^{15}N). Missing data corresponds to P66 and residues with overlapping or very weak signals. The reduced S^2

values and $^{1}H\{^{15}N\}$NOE ratios, and the elevated r.m.s. deviations for residues near the N- and C-termini of CaM2/3, as well as hinge between α-helices D and E (corresponding to the hinge region in native CaM) indicate that these regions are more comformationally dynamic, and less well structurally defined than the remainder of the protein. A schematic of the secondary structure of CaM2/3 as determined by PROMOTIF is displayed above panels A and C.

With consideration of anisotropic diffusion, the internal dynamic properties of CaM2/3 can be described by the Lipari-Szabo model free formalism in terms of a generalized order parameter, S^2, that decreases from 1 to 0 with increasing mobility of the NH bond vector (Figure 19D). With the exception of its disordered N- and C-terminals, CaM2/3 exhibits relatively uniform average S^2 values of 0.91±0.07. This is consistent with a well-folded, globular structure. However, upon closer inspection, a decrease in S^2 (average 0.80±0.6) and ^{1}H-$\{^{15}N\}$NOE values is observed for residues 74-81, indicative of enhanced mobility on the sub-nsec timescale. These residues also exhibit high r.m.s. deviations in the CaM2/3 structural ensemble (Figures 16 and 19F). Thus, reduced structural precision, which is directly attributable to a limited number of measurable restraints, may also arise in part from local conformational dynamics. In native CaM, these residues form the flexible hinge region between the N- and C-terminal domains. In CaM2/3, the flexibility of the hinge regions allows it to act like the loops between the EF-hands in the N- and C- terminal domains of native CaM. Thus in CaM2/3, EF-hands 2 and 3 pair with one another in a manner similar to that of EF-hands 1 and 2 or EF-hands 3 and 4 in native CaM.

The values of the S^2 and ^{1}H-^{15}N-NOE ratios, corresponding to the Ca^{2+}-binding segments (residues 56-67, average S^2 0.93±0.08, residues 93-104, average S^2 0.93±0.06), are slightly higher than in the rest of CaM2/3 (residues 48-109 average S^2 0.91±0.07).

The backbone r.m.s. deviations of the Ca^{2+}-binding segments, however, are slightly higher than the adjacent α-helices. This suggests that the relative backbone stability in the Ca^{2+}-binding loop regions is not reflected in the per-reside r.m.s.d. (Figure 19F). This reduced structural precision in the Ca^{2+}-binding segments may be attributable to the low number of restraints in these regions.

The amides of the last 3 residues, N111 to G113, exhibit significantly longer T_2 relaxation times, smaller heteronuclear NOEs, and reduced S^2 values (0.54 ± 0.23), when compared with rest of CaM2/3. These data indicate that the C-terminal end of CaM2/3 exhibits fast backbone motions on the nsec-psec time scale. Not surprisingly this region also exhibits higher relative backbone per-residue r.m.s. deviations than the rest of CaM2/3 (Figure 19F). Some T_2 lifetimes for the residues on helices C and D as well as the hinge region are short. This relaxation behavior is usually the result of conformational exchange broadening (R_{ex}), which suggests that these regions undergo intermediate time scale (msec to μsec) motions (Figure 19E).

2.4 Discussion

2.4.1 Structure and Ca^{2+}-binding of CaM1/2 and CaM3/4

The CD spectra for both CaM1/2 and CaM3/4 indicate that the secondary structures of these peptides are predominantly α-helical in both the Ca^{2+}-free and ligated forms. This is consistent with the known secondary structures of TR1C and TR2C (Finn et al. 1995; Bentrop et al. 1997; Olsson and Sjolin 2001). This is not surprising as the sequences of CaM1/2 and CaM3/4 differ from those of TR1C and TR2C by only 3 residues. These data show that it is likely that the structures of CaM1/2 and CaM3/4 are similar to those of TR1C and TR2C (or the N- and C-terminal domains of CaM), respectively.

The CaM1/2 peptide exhibits a relatively small change in molar ellipticity upon Ca^{2+}-binding ($[\theta]_{222+Ca}{}^{2+}/([\theta]_{222-Ca}{}^{2+}$ = 1.06), while the CaM3/4 peptide shows a larger change in molar ellipticity upon Ca^{2+}-binding ($[\theta]_{222+Ca}{}^{2+}/[\theta]_{222-Ca}{}^{2+}$ = 1.25) (Table 4). These data are consistent with repeated studies on the N- and C-terminal tryptic fragments of CaM: TR1C ($[\theta]_{222+Ca}{}^{2+}/[\theta]_{222-Ca}{}^{2+}$ = 1.09) and TR2C ($[\theta]_{222+Ca}{}^{2+}/([\theta]_{222-Ca}{}^{2+}$ = 1.29) (Maune et al. 1992a). Differences in the spectroscopic properties between the N- and C-terminal domains of CaM have been attributed to the lack of tyrosine residues in the N-terminal domain of CaM (VanScyoc and Shea 2001; VanScyoc et al. 2002).

We observed that the global Ca^{2+}-binding affinity (as measured by ΔG_{tot}) of the C-terminal peptide CaM3/4 (ΔG_{tot} = -65.1 kJ/mol) is slightly greater than that of the N-terminal peptide CaM1/2 (ΔG_{tot} = -61.7 kJ/mol) (Table 5). These results are also in agreement with previous studies on the TR2C (ΔG_{tot} = -68.9 kJ/mol) and TR1C (ΔG_{tot} = -58.5 kJ/mol) peptides under similar conditions (Linse et al. 1991). However, the CaM1/2

and CaM3/4 peptides do not show as large a difference in global Ca^{2+}-binding affinity as the TR1C and TR2C peptides. It is possible that the small difference in Ca^{2+} affinity is a result of the lack of a difference in net charge between the CaM1/2 and CaM3/4 peptides. The estimated net charge of the TR1C and TR2C peptides are –10 and –14 respectively, but the estimated net charge of both the CaM1/2 and CaM3/4 peptides is –12 (at pH 7). However, it is also possible that the small difference in binding affinity between the CaM1/2 and CaM3/4 peptides is due to a lack of Mg^{2+} in the titration buffer which has been shown to mask differences in Ca^{2+}-affinity between the domains of CaM (Klee et al. 1986; Linse et al. 1991). Both the CaM1/2 and CaM3/4 peptides show strong positive cooperativity in Ca^{2+}-binding. This is also in agreement with previous studies on the tryptic fragments of CaM under similar conditions (Linse et al. 1991).

2.4.2 Structure and Ca^{2+}-binding of CaM2/3

2.4.2.1 The coupling of Ca^{2+}-binding and folding in CaM2/3

In the absence of Ca^{2+}, CaM2/3 shows no discernable tertiary structure. This is reflected by the random coil pattern of amide chemical shifts in the ^{15}N-HSQC spectra of CaM2/3 (Figure 15A). However, CD spectropolarimetry reveals that Ca^{2+}-free CaM2/3 contains at least transiently formed α-helices (Figure 14B). In contrast, upon the binding of one Ca^{2+} by EF-hand 3 (K_{d1}= 30 ± 5μM), CaM2/3 folds co-operatively to an intermediate, albeit nearly complete, globular structure. In this state, the signal of G61 is not observed in the ^{15}N-HSQC spectra, whereas those of neighboring residues are weak, indicating that the Ca^{2+}-binding segment of EF-hand 2 may undergo msec timescale motions leading to conformational exchange broadening. This broadening propagates to the amide of I100, which although in EF-hand 3, is involved in hydrogen-bonding to I63

of EF-hand 2 to form the short anti-parallel β-sheet between these EF-hands. The binding of a second Ca^{2+} to EF-hand 2 (K_{d2}= 1800 ± 400μM) stabilizes the local conformation of the Ca^{2+}-binding segment of EF-hand 2 so that it adopts a well-defined structure. The stabilization of the local conformation of the Ca^{2+}-binding segment of EF-hand 2 causes the line widths of the peaks corresponding to the residues neighboring G61 to sharpen, but their chemical shifts do not change. This suggests that although conformationally dynamic, Ca^{2+}-free EF-hand 2 is native-like when a Ca^{2+} ion is ligated to EF-hand 3. Thus, Ca^{2+}-binding by EF-hand 3 and the folding of EF-hand 2 and 3 are tightly coupled in a thermodynamic and structural sense. This coupling of both folding and Ca^{2+}-binding is similar to the mechanism of dimerization of single EF-hand Ca^{2+}-binding models of TnC3 (Shaw et al. 1991). In this mechanism it was found that a single TnC3 monomer binds Ca^{2+} coupled to dimerization with a Ca^{2+}-free TnC3 monomer to yield a homodimer, which then weakly binds a second Ca^{2+} (Shaw et al. 1991) (scheme 3).

2.4.2.2 Cooperative interactions in CaM2/3

We have noted that there is stepwise binding of Ca^{2+} to CaM2/3 (i.e. Ca^{2+} binds to EF-hand 3 and then to 2). This is supported by the wide difference between the dissociation constants of Ca^{2+}-binding sites 2 and 3, and by the appearance of a peak, in the ^{15}N-HSQC spectra, corresponding to G61 of Ca^{2+}-binding site 2 at high Ca^{2+} concentrations. This is similar to the stepwise Ca^{2+}-binding that has been observed in the N-terminal tryptic fragment of troponin C except that both of the Ca^{2+}-binding dissociation constants were within the micromolar range (Li et al. 1995). However, the wide difference between the dissociation constants of CaM2/3 makes it nearly impossible

to determine if cooperativity is present. This determination would require the measurement of the Ca^{2+}-affinity of the high-affinity Ca^{2+}-binding site 3 while site 2 is occupied, and that of the low-affinity site 2 while site 3 is Ca^{2+}-free (Linse and Forsen 1995). This is difficult to do since the Ca^{2+}-affinity for site 3 is roughly sixty-times higher than for site 2.

2.4.2.3 The association of EF-hands 2 and 3 in CaM2/3

The Ca^{2+}-saturated CaM2/3 peptide adopts a structure that is similar to the N- or C-terminal domains of native CaM. The flexibility of the hinge region of CaM2/3 likely allows for the interaction of EF-hands 2 and 3 and for the formation of a short anti-parallel β-sheet between the Ca^{2+}-binding segments. As with the N- and C-terminal domains of CaM, this short anti-parallel β-sheet is composed of only two direct hydrogen-bonds between the Ca^{2+}-chelating position 8 residues (in the case of CaM2/3, I63 and I100) (Chapter 1) (Babu et al. 1988; Olsson and Sjolin 2001). The present structure provides additional evidence for the adaptability of the flexible hinge region of CaM, and it confirms that this region extends from residues 74 to 81 in solution (Fiorin et al. 2005). In the case of CaM2/3, the hinge region plays the same role that the loop regions between EF-hands (linking helix B to C and helix F to G) play in CaM. This suggests the possibility that the flexible hinge region in CaM evolved out of a loop between EF-hands in a progenitor EF-hand Ca^{2+} binding protein.

Despite the structural similarities between CaM2/3 and both the N- and C-terminal domains of CaM, the 2/3 EF-hand pairing is never observed in CaM. A possible explanation for this is that the EF-hands in the N- and C-terminal domains of CaM are always linked together via the short β-sheet region between the Ca^{2+}-binding sites. This

holds true for Ca^{2+}-free structures of CaM (Kuboniwa et al. 1995; Zhang et al. 1995), and for the Ca^{2+}-free TR2C fragment of CaM (which has at least one hydrogen bond between EF-hands 3 and 4 via residues I100 and I136) (Ikura et al. 1985). In addition, the paring of EF-hands 2 and 3 in CaM would leave EF-hands 1 and 4 unfolded or require the pairing of EF-hands 1 and 4. This would be thermodynamically unfavorable and structurally unfeasible.

In native CaM, EF-hand 2 is the C-terminal EF-hand of the N-terminal domain, while EF-hand 3 is the N-terminal EF-hand of the C-terminal domain. In contrast, for CaM2/3 EF-hand 2 is the N-terminal EF-hand, and EF-hand 3 is the C-terminal EF-hand. Given the hypothesis that a progenitor EF-hand gave rise to an EF-hand domain, that in turn evolved into a two-domain progenitor EF-hand protein, then EF-hands 1 and 3 and EF-hands 2 and 4 of CaM are closely related to each other (Goodman et al. 1979; Moncrief et al. 1990; Nakayama et al. 1992). Thus, with respect to CaM, EF-hand 1 has evolved to associate with EF-hand 2, and EF-hand 3 has evolved to associate with EF-hand 4. Therefore, in both a structural and evolutionary sense, the EF-hands in CaM2/3 are packed in reverse order with respect to CaM. The poor Ca^{2+}-affinity of CaM2/3 is likely a consequence of this reversed arrangement of EF-hands suggesting that there is a structural motivation behind the evolutionary mandated paring of EF-hands 1 and 2, and EF-hands 3 and 4 in CaM.

2.4.2.4 Ca^{2+}-affinity and the position of the "aromatic zipper"

Ca^{2+}-binding site 2 of CaM2/3 has a high dissociation constant (on a millimolar scale), whereas site 3 has a low dissociation constant on a micromolar scale. Similar divergent Ca^{2+}-dissociation constants have been observed with dimers of single EF-hand peptide models of some EF-hand proteins (Reid 1987a; Kay et al. 1991; Shaw et al. 1991; Franchini and Reid 1999a). A peptide homodimer of EF-hand 3 of TnC exhibits a high dissociation constant at the second Ca^{2+}-binding site, where K_d > 1mM, whereas the dissociation constant of the first site is in the micromolar range (Shaw et al. 1991). A peptide homodimer of EF-hand 4 of TnC has a global Ca^{2+}-binding dissociation constant K_d > 1 mM (Kay et al. 1991). Additionally, a peptide model of CaM3 forms homodimers and has an estimated global dissociation constant of 878 μM (Reid 1987a; Franchini and Reid 1999a). Heterodimers of TnC EF-hands 3 and 4 and calbindin D_{9k} EF hands 1 and 2 do not show wide variation in their Ca^{2+}-binding sites and seem to have improved Ca^{2+}-binding when compared to homodimers (Finn et al. 1992; Shaw and Sykes 1996). However, the dissociation constants of these heterodimers are still higher than in their respective native proteins (Leavis et al. 1978; Finn et al. 1992; Shaw and Sykes 1996). Clearly the particular pairing of EF-hands has an important effect on Ca^{2+}-affinity in EF-hand proteins. In the case of EF-hand homodimers and CaM2/3, Ca^{2+}-affinity of at least one Ca^{2+}-binding site is compromised without any mutations to specific Ca^{2+}-chelating residues.

It is thought that the most important determinant of EF-hand domain stability is the association of hydrophobic residues on neighboring α-helices to form a hydrophobic core (Sekharudu and Sundaralingam 1988; Shaw and Sykes 1996). Aromatic stacking

interactions between the first and fourth α-helices in each domain are formed from four aromatic residues each stacked nearly perpendicularly to its neighbor. The first aromatic residue is found four residues before the termination of the first α-helix. The second aromatic residue is the terminating residue of the first α-helix. The third and fourth aromatic residues are located at Ca^{2+}-chelating position 10 and just after position 12 of the second Ca^{2+}-binding segment, respectively (Babu et al. 1988; Chattopadhyaya et al. 1992; Wilson and Brunger 2000) (Appendix F). Theoretical calculations indicate that the energy change due to such aromatic stacking interactions depends on the inter-centroid distance and the orientation of the aromatic rings with respect to each other, and can approach values as favorable as -1.9 to -2.8 kcal/mol for T-shaped and displaced parallel alignments, respectively (McGaughey et al. 1998). Therefore, we postulate that this conserved arrangement of aromatic side chains acts as an "aromatic zipper" holding the first and fourth α-helices of an EF-hand domain together. Note that in native EF-hand proteins, this "aromatic zipper" holds the EF-hand domain closed, because it is opposite the loop between EF-hands (Figure 20A). The "aromatic zipper" exists in the correct position in EF-hand heterodimers resulting in higher Ca^{2+}-affinity than the homodimers. However, the loop between EF-hands is absent, which may result in lower Ca^{2+}-affinity than in their native domains. In EF-hand homodimers, the "aromatic zipper" interaction cannot form because the aromatic residues in each monomer do not associate with each other due to the anti-parallel pairing of the EF-hands, and this may result in lower Ca^{2+}-affinity (Figure 20B) (Kay et al. 1991; Shaw et al. 1992). In CaM2/3, the residues forming the aromatic stacking arrangement are on the same side as the hinge between the EF-hands, and in CaM2/3 the hinge plays the same role as the loop between EF-hands in

the N- or C-terminal domains of native CaM. This positions the aromatic residues of CaM2/3 on the second and third α-helices (D and E) rather than the first and fourth α-helices. In effect, there is no "aromatic zipper" opposite the hinge between EF-hands to hold helices C and F together (Figure 20C). Rather, the "aromatic zipper" is adjacent to the hinge between EF-hands and as such is redundant as far as its ability to stabilize the CaM2/3 domain (Figure 20D). This could alter the stability of the CaM2/3 peptide, leading to the lower Ca^{2+} affinity observed at site 2. Both CaM1/2 and CaM3/4 retain the residues in the right positions for aromatic stacking interactions (i.e. on helices A and D for CaM1/2 and E and H for CaM3/4), similar to the position of the aromatic residues in the structures of the TR1C and TR2C tryptic fragments of CaM (Finn et al. 1995; Bentrop et al. 1997; Olsson and Sjolin 2001). As a result the high affinity Ca^{2+}-binding and positive cooperative interactions observed in native CaM are also observed in CaM1/2 and CaM3/4.

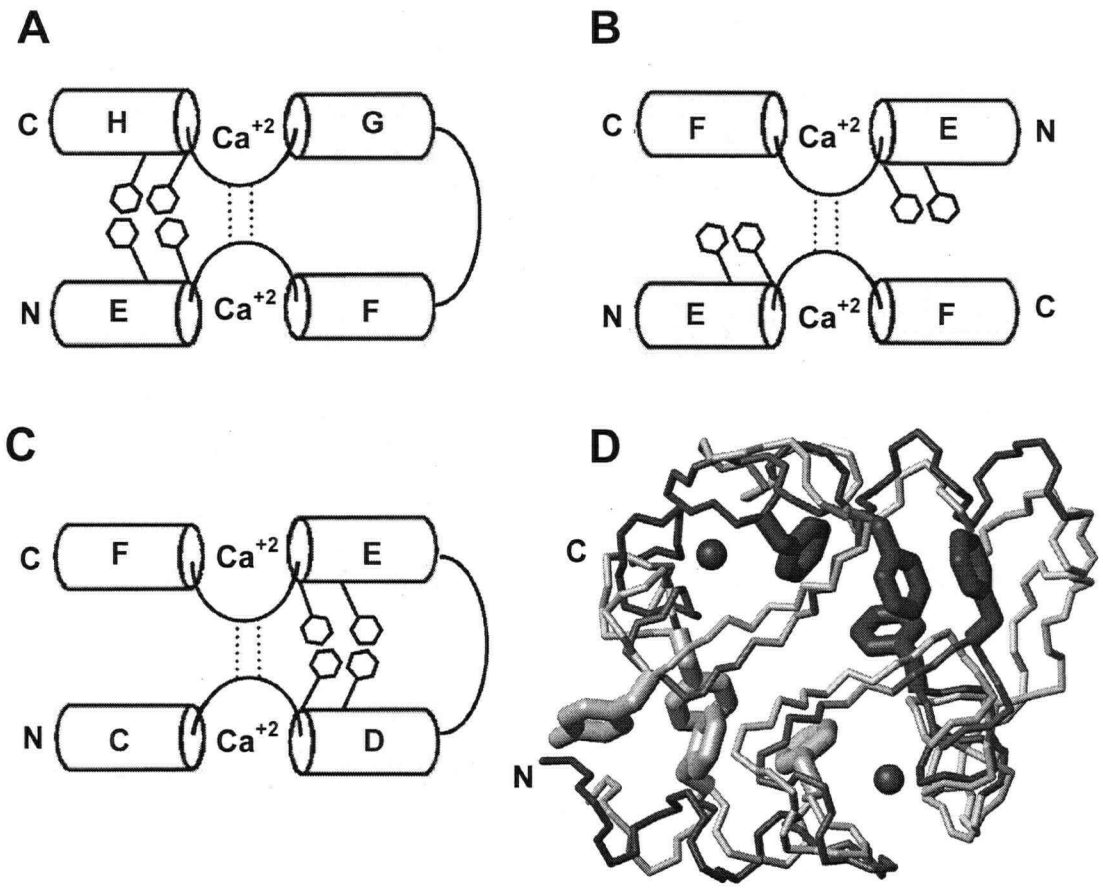

Figure 20. Aromatic stacking in CaM2/3 and CaM. Schematic structures of (**A**) the C-terminal domain of CaM, (**B**) an EF-hand homodimer (such as TnC3), and (**C**) CaM2/3. The helices are labeled alphabetically in light gray. The positions of key aromatic residues forming the "aromatic zipper" are represented as hexagons. In the CaM domain, this "aromatic zipper" structure is positioned opposite the loop between EF-hands and this helps to stabilize the domain by holding it tightly closed. An EF-hand heterodimer would look like A but without the loop between EF-hands. With the EF-hand homodimer the "aromatic zipper" structure cannot form. With CaM2/3 the "aromatic zipper" structure forms but is positioned adjacent to the hinge between EF-hands. Therefore, there is no interaction stabilizing the contacts between helices C and F. (**D**) The superimposition of CaM2/3 onto the C-terminal domain of Ca^{2+}-ligated CaM. The structures are arranged such that EF-hand 3 of CaM is superimposed on EF-hand 2 of CaM2/3 while EF-hand 4 of CaM is superimposed on EF-hand 3 of CaM2/3. As a result the hinge region of CaM2/3 overlaps the loop between EF-hands 3 and 4 of CaM. CaM2/3 is orientated as in Figure 16 and CaM is colored gray. The aromatic residues involved in the aromatic stacking arrangement are displayed as thickened bonds that are black for CaM2/3 and gray for CaM. The Ca^{2+} ions of CaM2/3 are represented as spheres. Figure 20D was rendered with MOLMOL (Koradi et al. 1996).

The aromatic residues F65 and F89 in CaM2/3 appear to be stacked on top of each other in a parallel fashion rather than in the T-shaped pattern observed in CaM (Figures 16A and 20D) (Babu et al. 1988). Residue F65 in CaM2/3 is clearly displaced with respect to its equivalent position in CaM (Figures 17C and 20D). As this residue occupies position 10 of Ca^{2+}-chelating loop 2, the unfavorable interactions may cause a reduction of Ca^{2+}-affinity at that site. Since this residue is involved in the "aromatic zipper" interaction, it is possible that it represents a conduit for the transmission of cooperativity from one EF-hand to the other. This suggests that the position of F65 somehow disrupts cooperative interactions between EF-hands 2 and 3 in CaM2/3.

2.4.2.5 Position 8 Ca^{2+}-chelating, β-sheet forming residues

Within the β-sheet structure of CaM2/3, the hydrogen-bond between I63 C=O and I100 $^1H^N$ is unusually long (average 2.5 ± 0.2Å). This distance seems large when compared to the typical $^1H^N$ to C=O hydrogen-bond distances in the β-sheet region of other CaM structures where the distance varies between 1.98 and 1.80Å (Chattopadhyaya et al. 1992; Wilson and Brunger 2000; Fallon and Quiocho 2003). It is possible that instability at the interface between EF-hands may result in unfavorable interactions between Ca^{2+}-binding sites 2 and 3, leading to the unusually long hydrogen-bond. This may also result in the high Ca^{2+}-dissociation constant observed at site 2 of CaM2/3.

Studies of EF-hand proteins have revealed a Ca^{2+}-dependent preference for the H^{α}-C^{α}-C^{β}-H^{β} dihedral angles at the β-sheet forming position 8 residue of the Ca^{2+}-binding segment (Biekofsky et al. 1998). Typically, in each EF-hand domain, one H^{α}-C^{α}-C^{β}-H^{β} dihedral angle at Ca^{2+} chelating position 8 rotates from 60° in the Ca^{2+}-free state to 180° in the Ca^{2+}-ligated state, while the other H^{α}-C^{α}-C^{β}-H^{β} dihedral angle stays at 180°

regardless of the presence of Ca^{2+} (Biekofsky et al. 1998). Thus, in the Ca^{2+}-ligated state, the H^{β}s from each of the Ca^{2+} chelating position 8 residues are pointing at each other across the β-sheet between EF-hands. This conformation is thought polarize the Ca^{2+} chelating position 7 backbone carbonyl, making it a better Ca^{2+} chelator (Biekofsky et al. 1998). As expected, the average H^{α}-C^{α}-C^{β}-H^{β} dihedral angle (178 ± 2) for I100 in CaM2/3 is similar to those observed in Ca^{2+}-ligated structures of CaM. However, the average H^{α}-C^{α}-C^{β}-H^{β} dihedral angle for I63 is 121 ± 14°. This angle, defined indirectly through NMR restraints that pack the core of CaM2/3, is midway between those expected for the Ca^{2+}-free and Ca^{2+}-ligated states. This unusual H^{α}-C^{α}-C^{β}-H^{β} dihedral angle may adversely affect Ca^{2+} chelation at EF-2. It is also possible that it may contribute unfavorable contacts between EF-hands in CaM2/3 because the $C^{\gamma 2}$ methyl group of I63 is rotated between the EF-hands.

Chapter 3

Interaction of fragments of calmodulin with selected targets [2]

3.1 Introduction

Previous studies have shown that the N- (TR1C) and C-terminal (TR2C) fragments of CaM can bind to CaM-target enzymes (Kuznicki et al. 1981; Guerini et al. 1984; Newton et al. 1984; Wolff et al. 1986). These studies have shown that fragments of CaM can act as agonists, antagonists, and partial agonists of the activity of specific CaM stimulated enzymes (Kuznicki et al. 1981; Guerini et al. 1984; Newton et al. 1984; Wolff et al. 1986). In addition, previous studies have shown that fragments of CaM can bind to peptides representing the CaM-binding sites of CaM-target proteins (Klee 1988; Bayley et al. 1996; Onions et al. 2000). The similarity of the CaM1/2 and CaM3/4 peptides to the characterized TR1C and TR2C tryptic fragments of CaM suggest that these peptides will likely bind to CaM target peptides.

The finding that the CaM2/3 peptide folds into a domain structure that is strikingly similar to both the N- and C-terminal domains of CaM prompted the question as to whether this novel EF-hand peptide can bind to CaM-targets. The structure of CaM2/3 suggest that a hydrophobic binding pocket may be present on the surface of the peptide that is similar to both the N- and C-terminal domains of CaM (Chapter 2 Figure 16B and C).

---

[2] A version of this chapter will be submitted for publication. Lakowski, T. M., Lee, G. M., Lelj-Garolla, B., Okon, M., Reid, R. E., and McIntosh, L. P., 2006. Peptide Binding by a Fragment of Calmodulin Composed of EF-Hands 2 and 3

In this study, we measured the ability of the CaM fragments CaM1/2, CaM2/3 and CaM3/4 to bind to the CaM-binding peptides M13 and bHLHW using fluorescence monitored titrations and cross-linking reactions. We found that the CaM3/4 (C-terminal CaM fragment) has higher affinity for both the M13 and bHLHW peptides than the CaM1/2 (N-terminal CaM fragment). Although both CaM1/2 and CaM3/4 have higher affinity for M13 than CaM2/3, the CaM2/3 peptide has higher affinity than CaM1/2 for bHLHW.

We studied the binding of CaM2/3 to M13 in depth, and partially assigned the CaM2/3-M13 complex using NMR spectroscopy. We found that the CaM2/3-M13 complex produced a "double" set of signals in the ^{15}N-HSQC spectra, and this prevented the determination of the structure of this complex. Regardless, the presence of these equal intensity peaks suggested the presence of two equally populated binding conformations. Cross-linking, and analytical ultracentrifugation (AUC) experiments suggest the presence of both 1:1 and 2:2 CaM2/3 : M13 stoichiometries. Thus, we proposed that in the 1:1 CaM2/3 : M13 complex, the M13 peptide binds in two orientations through the same hydrophobic residue or residues of M13. These stoichiometries may exist in equilibrium with a 2:2 CaM2/3 : M13 asymmetrical dimer.

The ability of all CaM fragments to stimulate calcineurin activity was measured using an enzyme assay. Confirming previous studies with CaM fragments, CaM1/2 and CaM3/4 have little or no ability to stimulate the activity of calcineurin (Newton et al. 1984). However, CaM2/3 has a limited ability to stimulate calcineurin, and can inhibit the stimulatory effect of CaM on calcineurin thus reducing its activity.

3.2 Materials and Methods

3.2.1 Peptide synthesis

The 26-residue peptide corresponding to the CaM-binding sequence of skeletal muscle myosin light chain kinase (M13) was synthesized via total sequential solid phase peptide synthesis on an Applied Biosystems 433A peptide synthesizer. The peptide was composed of the following sequence KRRWKKNFIAVSAANRFKKISSSGAL. The peptide had a free N-terminal and was amidated at the C-terminal. All amino acids were 9-fluorenylmethoxycarbonyl (N-Fmoc) protected (Carpino and Han 1972; Fields and Noble 1990). The C-terminal amino acid was linked to the Rink amide resin as the solid phase support, and the peptide was synthesized to the N-terminal in N-methylpyrrolidone (NMP) (Advanced ChemTech) as the reaction solvent (Rink 1987). The addition of each amino acid (cycle) was performed in three steps: de-protection, active ester formation, and coupling. N-Fmoc amino acids were deprotected using 20% piperidine in NMP. Active ester formation was achieved using 0.45 M 1-hydroxybenzotriazole (HOBt), (Advanced Chemtech), 2(1H-benzotriazol-1-yl)-1,1,3,3-tetramethyluronium hexafluorophosphate (HBTU) (Advanced Chemtech), dissolved in N,N-dimethylformamide (Sigma) and NMP (Dourtoglou et al. 1984; Knorr et al. 1989). The previous deprotected amino acid was coupled to the next activated HOBt ester amino acid using 2 M N,N-diisopropylethylamine (Sigma) in NMP. After each coupling cycle the growing peptide chain was treated with 0.5 M acetic anhydride (Sigma) in NMP to acetylate unreacted amines and prevent the occurrence of peptides with deletions. Each cycle of the reaction was monitored by measuring the conductivity induced by the formation of the piperidine carbamate salt after the deprotection step. After synthesis

was completed the resin was washed with dicholormethane (Fisher) and dried in a vacuum desiccator overnight. After drying, the resin was cooled on ice for 30 min and then cleaved at room temperature for 3 h under nitrogen with a mixture of 82.5% trifluroacetic acid (TFA) (Fisher), 5% phenol (Sigma), 5% de-ionized H_2O, 5% thioanisole (Sigma), and 2.5% 1,2-ethanedithiol (EDT) (Sigma) (King et al. 1990). The cleavage reaction was stopped by filtering the mixture directly into ice-cold methyl tertiary butyl ether (MTBE) (Sigma), and the precipitated peptide was centrifuged, washed with additional MTBE, dialyzed for 3 h against 50 mM NH_4HCO_3, and then lyophilized. The crude peptide was purified using RP-HPLC according to the protocol described in Chapter 2 (section 2.2.3.5).

The 21-residue peptide corresponding to the CaM-binding sequence of the bHLH transcription factor TCF4 (also known as E2-2) was synthesized as described above. The peptide had the following sequence: KERRMANNARERLRVRGGCGW. Previous studies determined that the monomer peptide of the TCF4 CaM-binding sequence had low affinity for CaM, but high affinity binding was attained if the peptide was dimerized (Corneliussen et al. 1994; Onions et al. 1997). We dimerized the TCF4 CaM-binding sequence monomer peptides via disulfide bond formation between cysteine residues in the peptides. The purified TCF4 CaM-binding sequence monomer peptide was dissolved in 50 mM Tris HCl and 50 mM NaCl and dimerized using 1 mM 1,1-azobis-(N,N-dimethylformamide) (Aldrich) at 0 °C for 30 min (Nestle and Roberts 1969; Bisaccia et al. 1996). The resulting TCF4 CaM-binding sequence dimer peptide (bHLHW) was purified using HPLC as described in Chapter 2, except that the gradient was formed over 50 min.

After purification all peptides were lyophilized and stored at –80 °C. The peptides were characterized by LCMS and amino acid analysis, according to the protocols described in Chapter 2 (section 2.2.4) (Appendix C).

The construction of the genes for CaM1/2, CaM2/3, CaM3/4 and CaM is described in Chapter 2 (sections 2.2.1 and 2.2.2). The expression, purification, and characterization of natural abundance CaM1/2, CaM2/3, CaM3/4, and CaM as well as ^{15}N-CaM2/3, and ^{13}C/^{15}N-CaM2/3 are also described in Chapter 2 (section 2.2.3).

3.2.2 Fluorescence monitored CaM binding peptide studies.

Equilibrium binding studies were performed by titrating either the M13 or bHLHW peptides with each of the CaM fragments CaM1/2, CaM2/3 and CaM3/4. Both the M13 and bHLHW peptides had a tryptophan residue that was used as a fluorescent reporter group to measure binding. The M13 and bHLHW peptides were titrated with increasing concentrations of the CaM fragment peptides at 25 °C and the change in fluorescence was monitored using a Shimadzu RF-540 spectrofluorophotometer. The excitation wavelength and slit width were 280 nm and 5 nm, respectively, and the emission wavelength and slit width were 350 nm and 2 nm, respectively. Matched, 10 mm path-length, Hellma QS 104F 1.4 mL quartz cells were used. The binding buffer was composed of 20 mM Tris HCl, 50 mM KCl, and 10 mM $CaCl_2$ at pH 7.4. A 1 mL solution of 5 μM bHLHW peptide in binding buffer was titrated with 2.5 to 5 μL aliquots of a 250 μM solution of CaM fragment, in binding buffer, and at the end of the titration a 2.55 : 1 molar ratio of CaM fragment : bHLHW peptide was attained. The same increments of CaM peptide were added to the matched cuvette containing only the above binding buffer as a control.

A similar procedure was used for the titration of M13 with the CaM fragment peptides except that at the end of the titration a 1.8 : 1 molar ratio of CaM fragment : M13 peptide was attained.

3.2.3 Cross-linked CaM fragments and CaM binding peptides

For the cross-linking of the M13 peptide to the CaM fragments and CaM, a 1:1 molar ratio of M13 : CaM fragment or CaM was used. The cross-linking reactions were performed in 200 μL volumes with 10 μM M13 and each of the CaM fragment peptides in a buffer containing 20 mM MES (Sigma) and 50 mM KCl at pH 6.8. Initially the CaM fragment peptides were incubated in the buffer with either 10 mM $CaCl_2$ or 20 mM EGTA for 30 min at room temperature. The M13 peptide was added to the mixture and the peptide complexes were cross-linked using 0.01% glutaraldehyde (final concentration) (Sigma) for 60 min. Control reactions were performed with each of the CaM fragments and the M13 peptide separately with the above buffer, and 10 mM $CaCl_2$. Samples were taken at regular intervals and the reaction quenched using a mixture of 1 M Tris/glycine pH 6.8. The same procedure was used for the cross-linking of the CaM fragments to bHLHW except a 4 : 1 molar ratio of CaM fragment : bHLHW was used. The CaM fragment peptides were also cross-linked to M13 and bHLHW using the same protocol as above except a combination of both N-hydroxysulfosuccinimide (sulfo-NHS) (Fluka) and 1-Ethyl-3-[3-dimethylaminopropyl]carbodiimide hydrochloride (EDC) (Sigma) at a final concentration of 5 mM and 20 mM, respectively were used as the cross-linking reagents (Kalkhof et al. 2005). This reaction was quenched using 20 mM dithiothreitol (DTT) (Sigma). The cross-linking and quenching reagents were removed by filtration through Microcon YM-3 centrifugal filters. The cross-linked samples were

also washed on the centrifugal filters with an equal volume of dH_2O and centrifuged again to concentrate the samples to a final volume of approximately 15 µL. The mass of the M13 peptide was below the molecular weight cut off of the centrifugal filters. Therefore, the control samples of M13 were precipitated in acetone (Fisher) at –20 °C overnight. The next day the M13 control samples were centrifuged at 12000 xg for 20 min, the acetone aspirated, and the samples air-dried.

3.2.4 Tris-Tricine gel electrophoresis

The concentrated cross-linked protein samples and standards were diluted such that the final volume was 48 µL. Half of this sample was mixed with 6 µL 5X Tris-Tricine sample dilution buffer containing 50 mM Tris HCl pH 6.8, 70% glycerol (Sigma), 4% SDS, and 0.05% Brilliant Blue G-250 (BioRad). In the case of the samples cross-linked with M13, 2% mercaptoethanol (Sigma) was also included to the loading buffer. The samples were boiled, for 2 min, and loaded onto a 16.5% Tris Tricine gel (Schagger and von Jagow 1987). The gel was run using the BioRad Mini-Protean II electorphoresis apparatus and a BioRad model 1000/500 power supply. A 0.75 mm thick 16.5%T, 3%C (from a 46.5% acrylamide (Fisher), 3% bis-acrylamide (Fisher) stock) separating gel was prepared with 1 M Tris HCl pH 8.45, 0.1% SDS, 10% glycerol, ammonium persulfate (Fisher), and N,N,N,N -tetramethyl-ethylenediamine (TEMED) (Fisher). A 4%T, 3%C (from a 48% acrylamide, 1.5% bis-acrylamide stock) stacking gel was prepared as above except no glycerol was added. The anode buffer was composed of 0.2 M Tris at pH 8.9, and the cathode buffer was composed of 0.1 M Tris-Tricine, and 0.1% SDS at pH 8.25. The gel was run at 35 V for 1 h through the stacking gel then at 105 V for 6 h through the separating gel. After electrophoresis the gels were fixed using 8% phosphoric acid in

50% ethanol for 30min. The gels were stained in colloidal Brilliant Blue stain containing 16% NH_4SO_4, 0.29 M phosphoric acid, 0.1% Brilliant Blue G-250, and 20% methanol overnight (Neuhoff et al. 1988). Following staining, the gels were rinsed in water and photographed using a Kodak DC120 digital camera.

3.2.5 Analytical ultracentrifugation of the CaM2/3-M13 complex

Sedimentation velocity experiments were conducted at 20°C with a Beckman Optima XL-I analytical ultracentrifuge equipped with both absorbance and interference optics. Standard aluminum double-sector centerpieces (12 mm) were filled with protein solution (400-450 mL), in a buffer composed of 20 mM Tris HCl, 50 mM KCl, and 10 mM $CaCl_2$ at pH 7.4. Buffer was also placed in the reference cell. Prior to each run, the loaded cells were thermally equilibrated in the centrifuge for at least 1 h after the instrument had reached 20 °C under vacuum. Sedimentation equilibrium experiments were performed at 20 °C in a 6-channel epon centerpiece and interference optics. 4-hole (AnTi60) and 8-hole (AnTi50) rotors were used. Sapphire and quartz windows were used with interference and absorbance optics, respectively. During sedimentation velocity experiments, radial scans were acquired with 0.003 cm radial steps in continuous mode without averaging and the rotor speed was set at 50,000 rpm. During sedimentation equilibrium experiments, radial scans were acquired with 0.001 cm radial steps by averaging 5 scans. The rotor speed was set at 20,000, 30,000 and 50,000 rpm and the sample equilibration was tested with the program WinMatch (Jeffrey and Yphantis). Velocity experiments were analyzed with a c(s) distribution of the Lamm equation solutions calculated with the program SEDFIT (Schuck et al. 2002), assuming the regularization parameter p to be 0.95. Sedimentation coefficient increments of 200

were used in the appropriate range for each sample. Sedimentation velocity experiments were performed on separate samples of both CaM2/3 and M13 at concentrations of 75 μM. Additional sedimentation velocity experiments were performed on the CaM2/3-M13 complex at concentrations of 150 and 300 μM, total protein, in a 1:1 Cam2/3 : M13 ratio. Sedimentation equilibrium experiments were performed at concentrations of 20, 40 and 75 μM for either CaM2/3 or M13 and at concentrations of 75, 150 and 300 μM total protein for the complex at a 1:1 ratio. The solution densities and partial specific volumes were calculated with the program SEDNTERP (Laue et al. 1992). The program SEDPHAT (Schuck 2003) was used for the analysis of the equilibrium experiments.

3.2.6 NMR spectroscopy of the CaM2/3-M13 complex

3.2.6.1 NMR monitored titration of CaM2/3 with M13

We measured the binding of CaM2/3 to M13 by titrating a sample of ^{15}N-CaM2/3 with natural abundance M13 peptide and monitoring changes using a series of ^{15}N HSQC spectra run on a Varian Inova 600 MHz spectrometer. The initial concentration of ^{15}N-CaM2/3 was 0.18 mM in 0.48 mL of NMR buffer (Chapter 2 page 64) at pH 7.4. A total volume of 85 μL of 1.8 mM M13 peptide in NMR buffer, was added in 5 or 10 μL aliquots. At the end of the titration there was a 1.8:1 molar ratio of M13 : ^{15}N-CaM2/3. The results were analyzed by plotting peak intensity for backbone amides for specific regions of CaM2/3 including the α-helices and hinge region from the ^{15}N HSQC spectra, versus M13 concentration normalized by the ^{15}N-CaM2/3 concentration. The data were fit to a single site binding model using the program CaLigator (Andre and Linse 2002).

3.2.6.2 Partial assignment of the CaM2/3–M13 complex

The CaM2/3-M13 complex was partially assigned using NMR experiments performed on Varian Unity 500 MHz and Inova 600 MHz spectrometers. The data were processed using NMRpipe (Delaglio et al. 1995) and analyzed using Sparky (Goddard and Kneeler 1999). Spectra were acquired at 25 °C on a 0.5 mM sample of $^{13}C/^{15}N$-CaM2/3 with 0.5 mM natural abundance M13 in the NMR buffer. The protein backbone connectivity was established using ^{15}N-HSQC, HNCACB, and CBCA(CO)NH spectra recorded on the 500 MHz NMR spectrometer (Grzesiek and Bax 1992; 1993; Wittekind and Mueller 1993). The assignment of resonances from some of the main chain and aliphatic side chain ^{1}H and ^{15}N nuclei were obtained using sensitivity enhanced gradient ^{15}N-HSQC and H(CCO)TOCSY-NH spectra recorded on the 500 MHz NMR spectrometer (Logan et al. 1992; Montelione et al. 1992). The resonances from aromatic side chains in the CaM2/3-M13 complex were obtained using ^{13}C-HSQC, CβHδ and CβHε experiments recorded on the 600MHz NMR (Yamazaki et al. 1993). An additional spectrum, a ^{1}H-^{15}N-^{1}H NOESY-HSQC (τ_m = 150 msec), was recorded on the 500 MHz NMR spectrometer (Jahnke et al. 1995).

Weighted secondary chemical shifts were calculated using the program CSI (Yap and Tomomori 1999) with the $^{13}C^{\alpha}$ and $^{13}C^{\beta}$ chemical shifts from both CaM2/3 and the CaM2/3-M13 complex. The program calculates the secondary chemical shift according to the following method. The average random coil chemical shift for the $^{13}C^{\alpha}$ ($\delta C^{\alpha}_{(coil)}$) and $^{13}C^{\beta}$ ($\delta C^{\beta}_{(coil)}$) for each residue is subtracted from the same chemical shifts for each residue in the respective proteins. These differences in the $^{13}C^{\beta}$ chemical shift are then subtracted from the differences in $^{13}C^{\alpha}$ chemical shift according to the following equation

$\Delta_{C\alpha\beta(i)}=(\delta C^{\alpha}_{(i)}-\delta C^{\alpha}_{(coil)})-(\delta C^{\beta}_{(i)}-\delta C^{\beta}_{(coil)})$. The calculation is weighted for each residue according to the following equation $CSI=(\Delta_{C\alpha\beta(i-1)}2+\Delta_{C\alpha\beta(i)}+\Delta_{C\alpha\beta(i+1)})/4$ (Wishart et al. 1991; 1992; Yap and Tomomori 1999).

Differences in chemical shift between CaM2/3 and the CaM2/3-M13 complex were calculated using the chemical shift data from the ^{15}N-HSQC, the aromatic ^{13}C-HSQC, the CβHδ and CβHε experiments as well as the $^{13}C^{\beta}$ and $^{1}H^{\beta}$ alanine methyl chemical shifts. The differences in chemical shifts between CaM2/3 and the CaM2/3-M13 complex ($\Delta\delta$) were calculated according to the following equations: $\Delta\delta=[(\Delta\delta^{1}H)^{2}+(\Delta\delta^{15}N(\gamma^{15}N/\gamma^{1}H))^{2}]^{0.5}$ for the ^{15}N-HSQC spectra and $\Delta\delta=[(\Delta\delta^{1}H)^{2}+(\Delta\delta^{13}C(\gamma^{13}C/\gamma^{1}H))^{2}]^{0.5}$ for the ^{13}C-HSQC, CβHδ and CβHε spectra, and the alanine methyl groups. The $\Delta\delta^{1}H$, $\Delta\delta^{15}N$ and $\Delta\delta^{13}C$ are the differences for chemical shifts at the indicated nuclei between CaM2/3 and the CaM2/3-M13 complex. The gyromagnetic ratios (γ) for the ^{1}H, ^{15}N, and ^{13}C nuclei are 26.75, -2.71, and 6.73 x10^{7} rad $T^{-1}s^{-1}$ respectively.

3.2.6.3 Backbone ^{15}N relaxation of the CaM2/3-M13 complex.

The backbone amide ^{15}N relaxation parameters were acquired for $^{13}C/^{15}N$-CaM2/3 at 25 °C using a Varian Unity 500 MHz NMR spectrometer (Farrow et al. 1994; Farrow et al. 1995). Data points for the T_1 (10, 150.2, 301.1, 451.6, 602.2, 752.7, 903.2, and 1053.5 msec) and T_2 (16.7, 33.4, 50, 66.8, 83.5, 100, 116.9, 133, 150, and 166.0 msec) experiments were collected in random order. Steady-state heteronuclear $^{1}H\{^{15}N\}$-NOE spectra were acquired using the method described in Chapter 2 (section 2.2.7.3), and errors were estimated using previously described methods (Farrow et al. 1994). All data were processed using the method described in Chapter 2 (section 2.2.7.3). Isotropic

diffusion and model-free order parameters (S^2) were calculated with the program Tensor 2.0 using the lowest energy structural model of CaM2/3 (Dosset et al. 2000). Criteria for exclusion of residues from calculations can be found in Chapter 2 (section 2.2.7.3).

3.2.7 Calcineurin stimulation assay

The ability of the CaM fragments and CaM to stimulate calcineurin (protein phosphatase-2B (PP-2B)) was assessed by measuring phosphatase activity of calcineurin against para-nitrophenol (pNPP) (BDH). An assay for the appearance of nitrophenol was performed at 37°C in a 96 well plate and measurements were made with a Labsystems Multiskan Ascant plate reader at 405 nm (Klee et al. 1983; Mondragon et al. 1997). The reaction buffer was composed of 50 mM Tris pH 7.0, 1 mM $CaCl_2$, 1 mM $NiCl_2$ (BDH), and 0.125 mg/mL BSA (Sigma). Samples with calcineurin alone, as well as calcineurin with each CaM fragment or CaM, were pre-incubated at 37°C for 30 min under low light conditions. The reaction was initiated by the addition of 0.9 mg/mL pNPP (final concentration) in the reaction buffer. Initial maximal rates were measured from the slopes of progress curves constructed over 80-120 min from reactions with 50 nM (0.70-0.74 μg) calcineurin, and CaM or CaM fragments at concentrations of 0, 5, 10, 25, 50, 100, and 300 nM per reaction. Samples were performed with 8 replicates and standards of nitrophenol (Sigma) were measured with 4 replicates. An inhibition assay was also performed with the above protocol for CaM including 10, 50, and 100 nM CaM2/3 and a control without CaM2/3. This was done in an attempt to see if CaM2/3 could compete with CaM for the CaM-binding site on calcineurin.

3.3 Results

3.3.1 Binding of CaM fragments to bHLHW

The binding of CaM fragments CaM1/2, CaM2/3, and CaM3/4 to bHLHW was measured using fluorescence monitored titrations. The results of the titrations are presented in Table 9 and Figure 21. The data were fit to a one site binding model using the program CaLigator (Andre and Linse 2002). The resulting apparent dissociation constants are presented in Table 9. The results show that the C-terminal fragment CaM3/4 appears to have a higher apparent affinity for the bHLHW peptide than the N-terminal, CaM1/2 or the middle CaM2/3 fragments. However the CaM2/3 peptide has higher affinity for bHLHW than CaM1/2. Figure 21 shows that the apparent stoichiometry of the bHLHW peptide for the CaM1/2 and CaM3/4 fragments is approximately 1:1. The nature of the stoichiometry of the CaM2/3-bHLHW complex is not clear from this titration.

Table 9. The dissociation constants for the binding of Ca^{2+}-loaded CaM fragments and the M13 and bHLHW peptides

CaM-binding peptide	Apparent dissociation constants K_{1d} (nM) ± SE		
	CaM1/2	CaM2/3	CaM3/4
M13	63±20	520±100	11±4
bHLHW	320±50	190±50	100±10

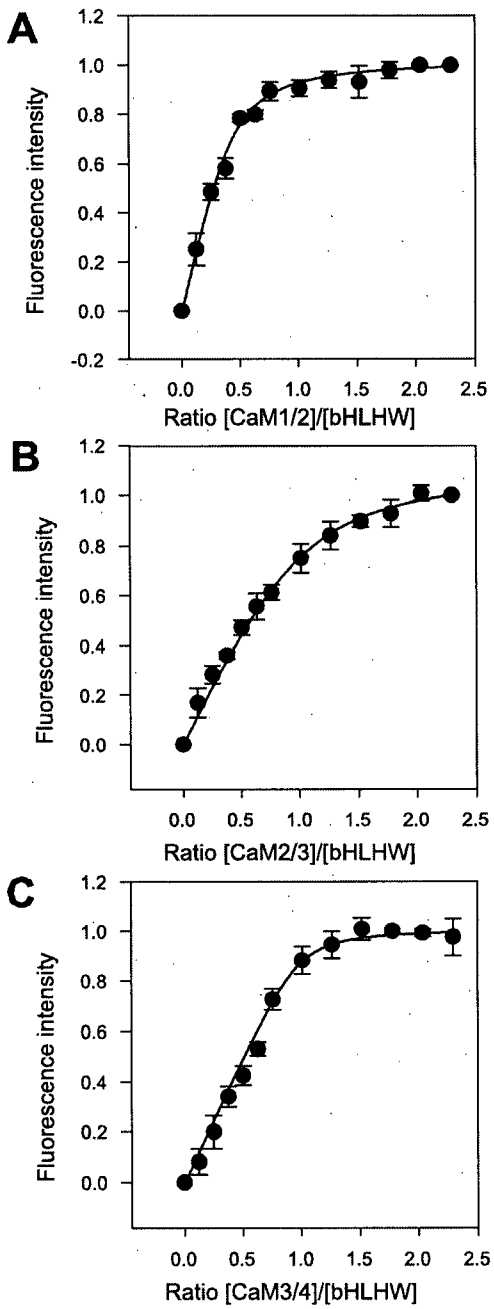

Figure 21. The titration of bHLHW with CaM1/2, CaM2/3 and CaM3/4. The titration curves of bHLHW with (**A**) CaM1/2, (**B**) CaM2/3 and (**C**) CaM3/4. The data were fit to a one site binding model using the program CaLigator (Andre and Linse 2002). The titrations of CaM1/2 and CaM3/4 appear to saturate at an approximate molar ratio of 1:1 CaM fragment : bHLHW. From the titration the stoichiometry of the CaM2/3-bHLHW complex is not clear. The black circles represent the mean and the error bars standard error for 3 replicates.

The binding of the CaM and the CaM fragments to bHLHW was also evaluated using cross-linking reactions. Figure 22A shows a 16.5% Tris-Tricine gel with lanes containing cross-linked samples of CaM or CaM1/2 with bHLHW in the presence of either EGTA or Ca^{2+}. Figure 22B shows a 16.5% Tris-Tricine gel with lanes containing cross-linked samples of CaM2/3 or CaM3/4 with bHLHW in the presence of either EGTA or Ca^{2+}. Some degree of cross-linking is visible in each of the groups, although there seems to be less cross-linking in the CaM1/2 group and significantly less in the CaM2/3 group. All groups exhibit little or no interaction in the EGTA treated lanes.

Previous studies have shown that the expected stoichiometry of the CaM-bHLHW complex is 2 : 1 (Onions et al. 1997), and the predicted molecular weight of this complex is 38kDa. However, the Ca^{2+} treated CaM lane in Figure 22A shows that the weight of the predominant CaM-bHLHW complex is closer to 21.5kDa. This is more consistent with a 1:1 CaM-bHLHW complex (predicted weight 22kDa). All of the CaM fragments in Figure 22A and 22B show that the molecular weights in the Ca^{2+} treated complex lanes are consistent with a 1:1 stoichiometry.

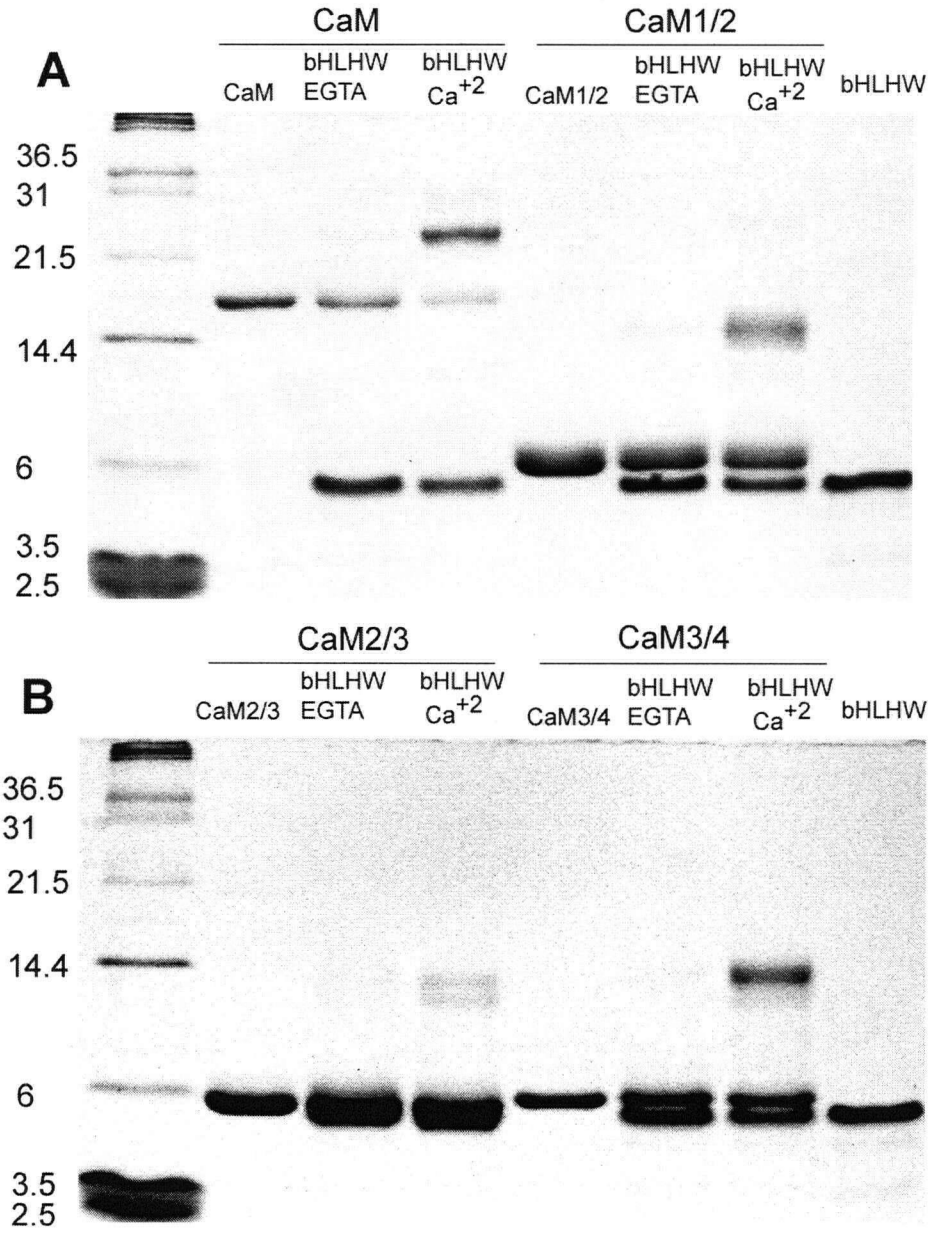

Figure 22. Non-reducing Tris-Tricine gels for bHLHW cross-linked with CaM1/2, CaM2/3, CaM3/4, and CaM. **(A)** The Tris-Tircine gel of CaM or CaM1/2 with bHLHW cross-linked using 0.01% glutaraldehyde. **(B)** The Tris-Tircine gel of CaM2/3 or CaM3/4 with bHLHW cross-linked using 0.01% glutaraldehyde. The lanes labeled Ca^{2+} represent reactions incubated with Ca^{2+}, lanes labeled EGTA represent reactions incubated with EGTA. The lanes labeled with CaM or CaM fragment represent CaM or the indicated CaM fragment controls. The lane labeled bHLHW contains bHLHW as a control. Both CaM and all of the CaM fragments appear to have bands in the Ca^{2+} treated complex lanes with molecular weights that are consistent with a 1:1 stoichiometry.

3.3.2 Binding of CaM fragments to M13

The binding of the CaM fragments to M13 was measured using fluorescence monitored titrations. The results of the titrations are presented in Figure 23. The data were fit to a one site binding model, using the program CaLigator, and the resulting apparent dissociation constants are presented in Table 9 (Andre and Linse 2002). The results show that the C-terminal fragment, CaM3/4 appears to have a higher apparent affinity for the M13 peptide than the N-terminal fragment CaM1/2. Both CaM1/2 and CaM3/4 have higher affinity for the M13 peptide than CaM2/3. Although the CaM1/2 and CaM3/4 fragments have higher affinity for M13 than bHLHW, it appears that the reverse is true for the CaM2/3 peptide.

The binding of CaM and the CaM fragments to M13 was also evaluated using cross-linking reactions. Figure 24A shows a 16.5% Tris-Tricine gel with lanes containing cross-linked samples of CaM or CaM1/2 with M13 in the presence of either EGTA or Ca^{2+}. Figure 24B shows a 16.5% Tris-Tricine gel with lanes containing cross-linked samples of CaM2/3 or CaM3/4 with M13 in the presence of either EGTA or Ca^{2+}. Some degree of cross-linking is visible in each of the groups, although there seems to be significantly less in the CaM2/3 group. All groups show some cross-linked complexes in the EGTA treated lanes, though less than in the Ca^{2+} treated lanes. The Ca^{2+} treated lanes for all CaM fragments show additional high molecular weight bands when cross-linked with M13. The molecular weights of these bands suggest the presence of a 2:2 and n:n CaM fragment : M13 peptide stoichiometries, along with the expected 1:1 complex.

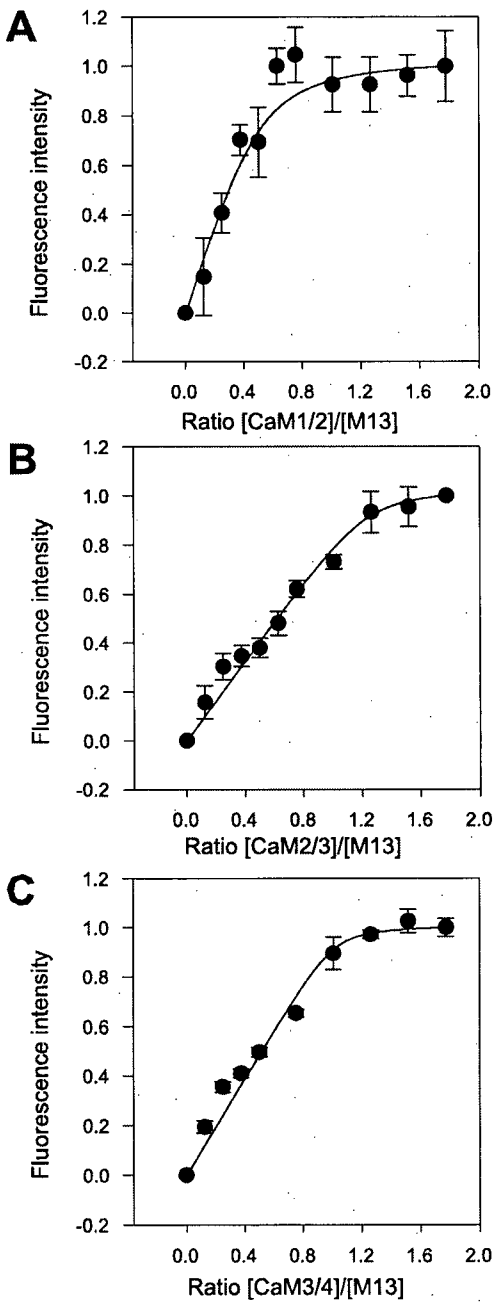

Figure 23. The titration of M13 with CaM1/2, CaM2/3 and CaM3/4. The titration curves of M13 with (**A**) CaM1/2, (**B**) CaM2/3 and (**C**) CaM3/4. The data were fit to one site binding model using the using the program CaLigator (Andre and Linse 2002). All of the titrations saturate at an approximate 1:1 molar ratio of CaM fragment : M13. All of the binding interactions are relatively tight.

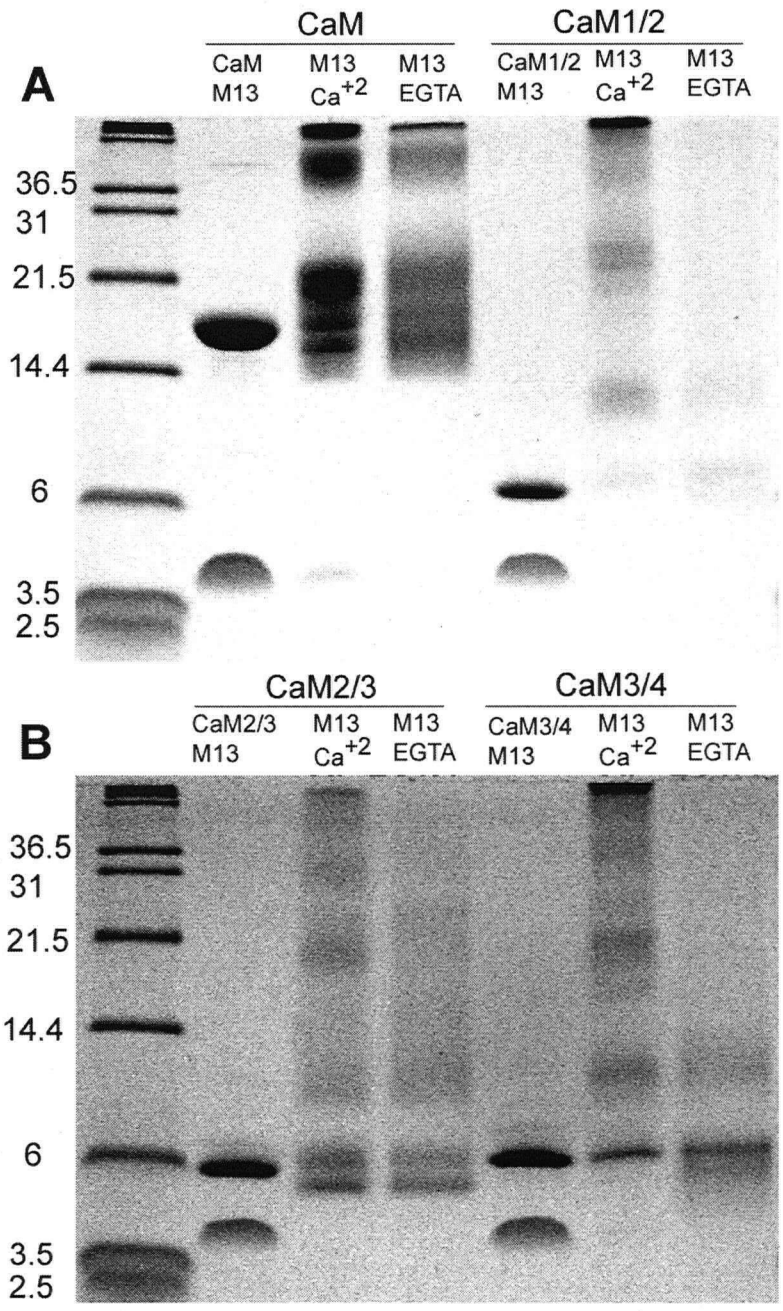

Figure 24. Tris-Tricine gels for M13 cross-linked with CaM1/2, CaM2/3, CaM3/4, and CaM. (**A**) The Tris-Tircine gel of CaM or CaM1/2 with M13 cross-linked using 0.01% glutaraldehyde. (**B**) The Tris-Tircine gel of CaM2/3 or CaM3/4 with M13 cross-linked using 0.01% glutaraldehyde. The lanes labeled Ca^{2+} represent reactions incubated with Ca^{2+} and lanes labeled EGTA represent reactions incubated with EGTA. The lanes labeled with CaM or CaM fragment and M13 represent CaM or the indicated CaM fragment and M13 controls. Both CaM and all of the CaM fragments appear to have bands in the Ca^{2+} treated complex lanes with molecular weights that are consistent with a 1:1, 2:2 and higher order n:n stoichiometries.

3.3.3 Analytical ultracentrifugation of the CaM2/3-M13 complex

The results of cross-linking studies suggested that 1:1, 2:2 and higher order n:n stoichiometries were present for the CaM2/3-M13 complex. In order to ascertain the stoichiometry of the CaM2/3-M13 complex in solution, we performed analytical ultracentrifugation (AUC). Sedimentation velocity data were obtained for CaM2/3, M13 and the CaM2/3-M13 complex at 20 °C and analyzed with the program SEDFIT (Gill and von Hippel 1989) to obtain *c(s)* distribution plots. Figure 25 shows that the M13 peptide (75 μM) sediments as a single peak with a sedimentation coefficient of 0.48 S, and sedimentation equilibrium experiments confirm that this peptide is monomeric in solution. Sedimentation velocity experiments show that CaM2/3 (75 μM) is mainly monomeric with a sedimentation coefficient of 1.34 S. Sedimentation equilibrium analysis indicates that CaM2/3 has a very low tendency to dimerize ($K_d \sim 4$ mM). This confirms the light scattering experiment that shows that CaM2/3 is essentially monomeric in solution (Appendix E).

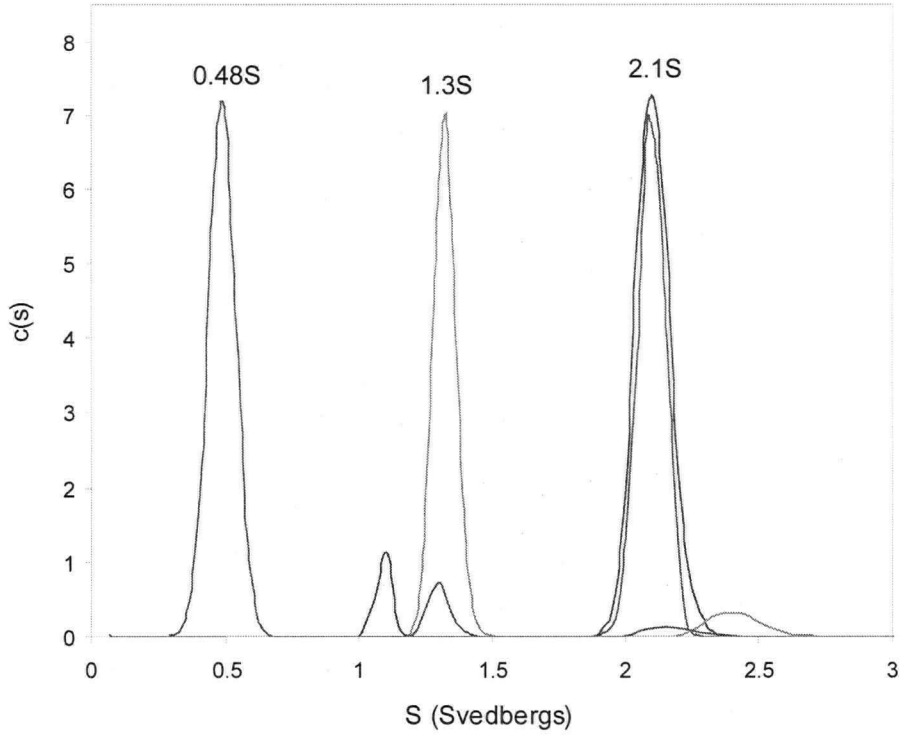

Figure 25. Analytical ultracentrifugation of the CaM2/3-M13 complex. Sedimentation velocity experiments obtained separately for, CaM2/3 (1.3S), M13 (0.48S), the CaM2/3-M13 complex (at both 150μM and 300μM total protein (2.1S)) at 20 °C, analyzed with the program SEDFIT (Gill and von Hippel 1989), and plotted as *c(s)* distribution plots. The M13 peptide sediments as a single peak with 0.48 S. CaM2/3 sediments as a single peak and is essentially monomeric with a sedimentation coefficient of 1.34 S. CaM2/3 and M13 in a 1:1 ratio at 150 and 300 μM total protein concentration show the presence of a single peak that sediments at approximately 2.1 S. This sedimentation coefficient is larger than what would be expected for a 1:1 CaM-M13 complex (S = 1.74) but smaller than what would be expected for a 2:2 CaM2/3-M13 complex (S = 2.76). This suggests that in solution the CaM2/3-M13 complex exists in an equilibrium between a 1:1 and 2:2 complex.

Sedimentation velocity experiments performed on CaM2/3 and M13 mixed in a 1:1 ratio at 150 and 300 μM total protein concentration show the presence of a single peak that sediments at ~ 2.1 S. This sedimentation coefficient is larger than what would be expected for a 1:1 CaM-M13 complex (S = 1.74) but smaller than what would be expected if a 2:2 CaM2/3-M13 complex was present (S = 2.76). These experiments

indicate that in solution there is a mixture of 1:1 and 2:2 CaM2/3:M13 complexes in equilibrium. Table 10 shows that at higher rotor speeds the apparent molecular weight of the CaM2/3-M13 is lower than at lower rotor speeds. The lowest apparent molecular weight (13.7 kDa) is closer to the expected molecular weight of a 1:1 CaM2/3-M13 complex (10.6 kDa). The highest apparent molecular weight (20.1 kDa) is closer to the expected molecular weight of a 2:2 CaM2/3-M13 complex (21.3 kDa). The apparent molecular mass of the complex varies directly with protein concentration (Table 10), reflecting the reversibility of the association. This behavior suggests that the higher apparent molecular weight species are due to the self association of a 1:1 CaM2/3-M13 complex to a 2:2 CaM2/3-M13 complex rather than the formation of higher molecular weight nonspecific aggregates.

Table 10. The apparent molecular weights of the CaM2/3-M13 complex

Concentration of CaM2/3-M13 (μM)	Apparent molecular weight (kDa) for given rotor speed (rpm) 20000	30000	50000
300	20.1	18.0	14.5
150	17.9	17.7	14.5
75	16.7	16.7	13.7

3.3.4 Binding of CaM2/3 to M13 measured by an NMR monitored tritation

The interaction between Ca^{+2}-ligated CaM2/3 and M13 was investigated by a titration of ^{15}N-CaM2/3 with M13 monitored by ^{15}N-HSQC spectroscopy. The chemical shifts and relaxation properties of an amide are highly sensitive to even subtle conformational changes, such as those occurring at interaction surfaces. Thus, shift perturbations in NMR-monitored titrations can be used to qualitatively identify binding interfaces and to quantitatively measure binding affinities. Upon the incremental addition

of M13, a progressive disappearance of the amide $^{1}H^{N}$ signals from unbound CaM2/3 was observed, along with concomitant appearance of a new set of signals (Figure 26). These signals, which arise from a CaM2/3-M13 complex, clearly indicate that M13 binds CaM2/3 in the slow exchange limit on the chemical shift timescale (i.e. the rate of exchange between free and bound states is less than the observed chemical shift differences). In addition, the titration spectrum exhibits additional peaks when compared with the spectrum of unbound CaM2/3. The HNCACB and CBCA(CO)NH spectra, that establish backbone connectivity, reveal that many of the residues of CaM2/3 in the CaM2/3-M13 complex give rise to two amide peaks in the ^{15}N-HSQC rather than one. Thus many residues, but not all, that give rise to a single amide peak in the unbound CaM2/3 ^{15}N-HSQC spectrum give rise to two near equal intensity amide peaks in the CaM2/3-M13 complex ^{15}N-HSQC spectrum. This behavior suggests that there are two, equally populated conformations for the CaM2/3-M13 complex.

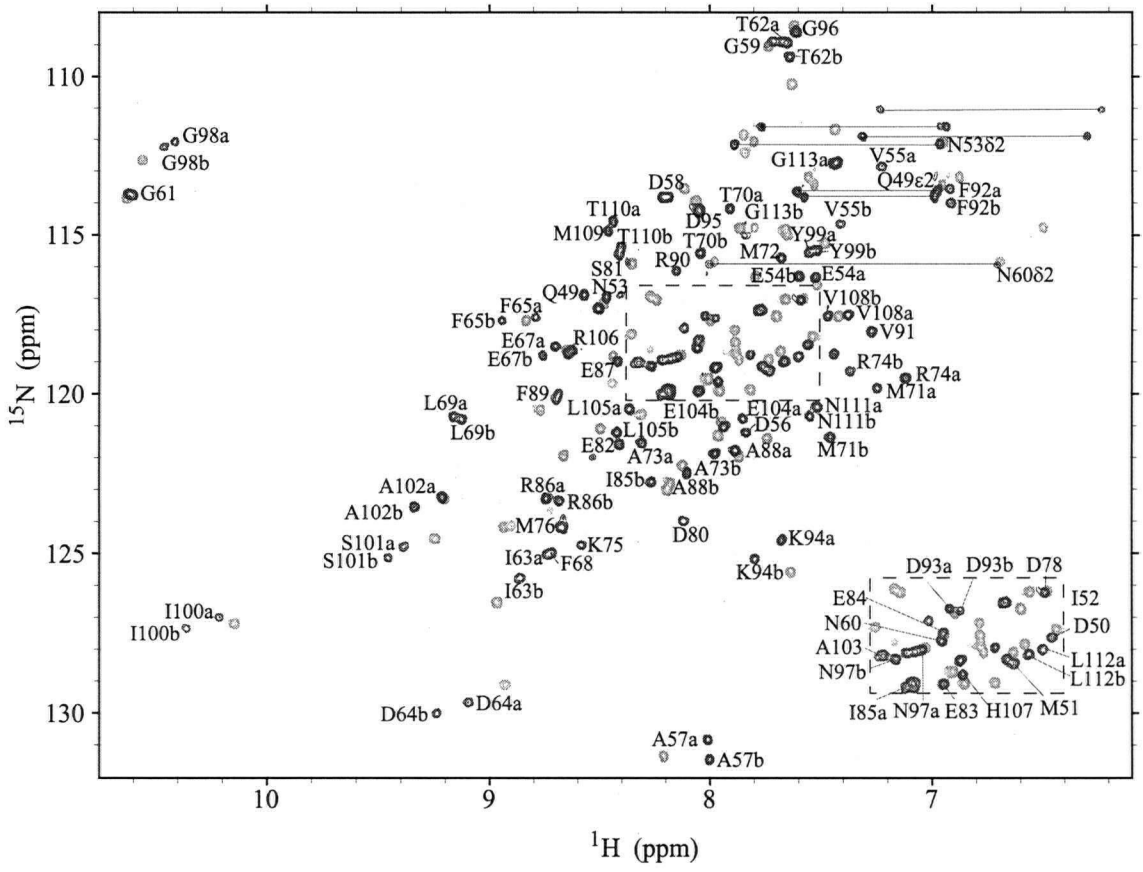

Figure 26. ^{15}N-HSQC spectrum of CaM2/3 superimposed onto the ^{15}N-HSQC spectrum of the CaM2/3-M13 complex. The ^{15}N-HSQC spectrum of the final point of the titration of ^{15}N-CaM2/3 with M13 is presented in black with the residues labeled with the one letter amino acid code and the numbering as it in CaM. Several amides give rise to two peaks (confirmed with backbone connectivity experiments HNCACB, HBCBCACONH) and are arbitrarily labeled a and b to differentiate them. Horizontal lines connect resonances from glutamine or asparagine side chain $^{15}NH_2$ groups. There are four unlabeled peaks (that are not side chain $^{15}NH_2$ groups) in black that could not be assigned. The original the ^{15}N HSQC spectrum of Ca^{2+}-ligated CaM2/3 without M13 is presented as gray peaks without labels (compare with Figure 15).

Figure 27A shows the results of the ^{15}N-HSQC monitored titration of ^{15}N-CaM2/3 with M13. The average normalized peak intensity from the ^{15}N HSQC spectra for residues 48-55, 65-92, and 102-113 is plotted versus the M13 concentration normalized by the ^{15}N-CaM2/3 concentration. For construction of the curve in Figure 27A the intensity of the double peaks were added together for each residue that results in double peaks. The data in Figure 27A were fit to a single site binding model using the program CaLigator (Andre and Linse 2002). The interaction produced an apparent $K_d = 400 \pm 50$ nM, (mean and sd) which is the similar to the dissociation constant derived from the fluorescence monitored titration of M13 with CaM2/3 (Table 9). Also, similar to the fluorescence monitored titration, the NMR monitored titration of CaM2/3 with M13 saturates at a ratio of 1:1 CaM2/3 : M13; ruling out 1:2 or 2:1 stoichiometry species. Viewing this data alone it is unclear if the stoichiometry of the CaM2/3-M13 complex is 1:1, 2:2 or an even higher order multimeric complex (i.e. n:n). However, the AUC data and the cross-linking studies confirm that both a 1:1 and 2:2 CaM2/3-M13 stoichiometry species exist in an equilibrium (Figures 24, 25 and Table 10). Figure 27B shows a plot of the double peaks from I100 (I100a and b) and L105 (L105a and b) versus the M13 concentration normalized by the ^{15}N-CaM2/3 concentration. This plot demonstrates that the double peaks are of nearly equal intensity over any ratio of M13 : CaM2/3 concentrations

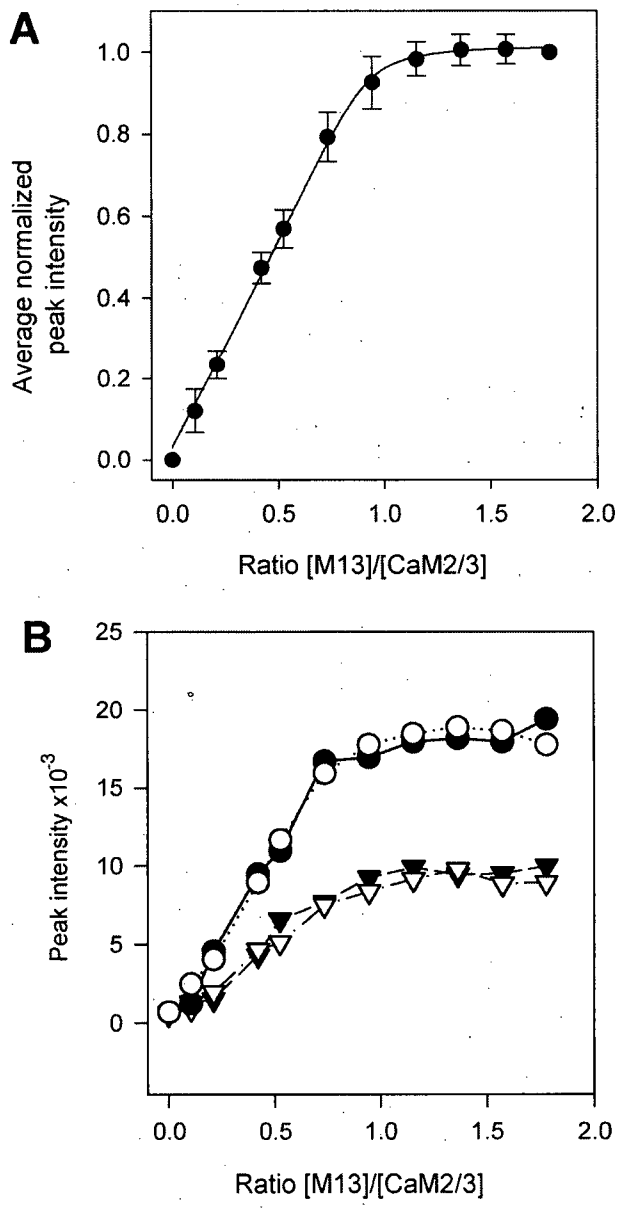

Figure 27. The fit curve from the ^{15}N-HSQC monitored titration of ^{15}N-CaM2/3 with unlabeled M13. (**A**) The black circles represent the average normalized peak intensity for amides from residues 48-55, 65-92, and 102-113 plotted versus the increasing ratio of M13 : CaM2/3 concentrations. The error bars represent the standard deviation, the curve is fit using the program CaLigator (Andre and Linse 2002) and the K_d = 400 ± 50 nM (mean and standard error). The curve appears to saturate at an M13 : CaM2/3 ratio of 1:1, ruling out 1:2 or 2:1 stoichiometry species. (**B**) Plots of ^{15}N-HSQC peak intensity vs. ratio of M13 to CaM2/3. The peak intensities for residues exhibiting double peaks I100a(▼) and I100b(▽), L105a(●) L105b(○), show that the double peaks are of nearly equal intensity at every point.

3.3.5 Secondary structure of the CaM2/3-M13 complex

The overall secondary structure of the CaM2/3-M13 complex, as measured by $^{13}C^{\alpha}$-$^{13}C^{\beta}$ secondary chemical shifts, is essentially the same as that of unbound CaM2/3. For example, Figure 28 shows that there are prominent negative peaks for the residues surrounding I63 and I100 in the CaM2/3-M13 complex that are also observed in unbound CaM2/3. This suggests that these residues adopt a β-sheet structure in both unbound CaM2/3 and the CaM2/3-M13 complex. In addition, NOE peaks were detected between I63 $^{1}H^{N}$ and I100 $^{1}H^{N}$ for both of the double peaks (I63a and b, and I100a and b) in the CaM2/3-M13 complex that were also detected in unbound CaM2/3. Together these data suggest that the anti-parallel β-sheet observed in unbound CaM2/3 is retained in the CaM2/3-M13 complex.

The only major difference in secondary structure between the CaM2/3-M13 complex and CaM2/3 is a cluster of large positive values in the hinge region between helices D and E (Figure 28A and 27B). This suggests that these residues (75-79) now adopt a helical conformation rather than the flexible conformation found in both CaM and CaM2/3. These data suggest that with the exception of the hinge region between helix D and E, the structure of CaM2/3 in the CaM2/3-M13 complex is relatively unchanged from that of unbound CaM2/3.

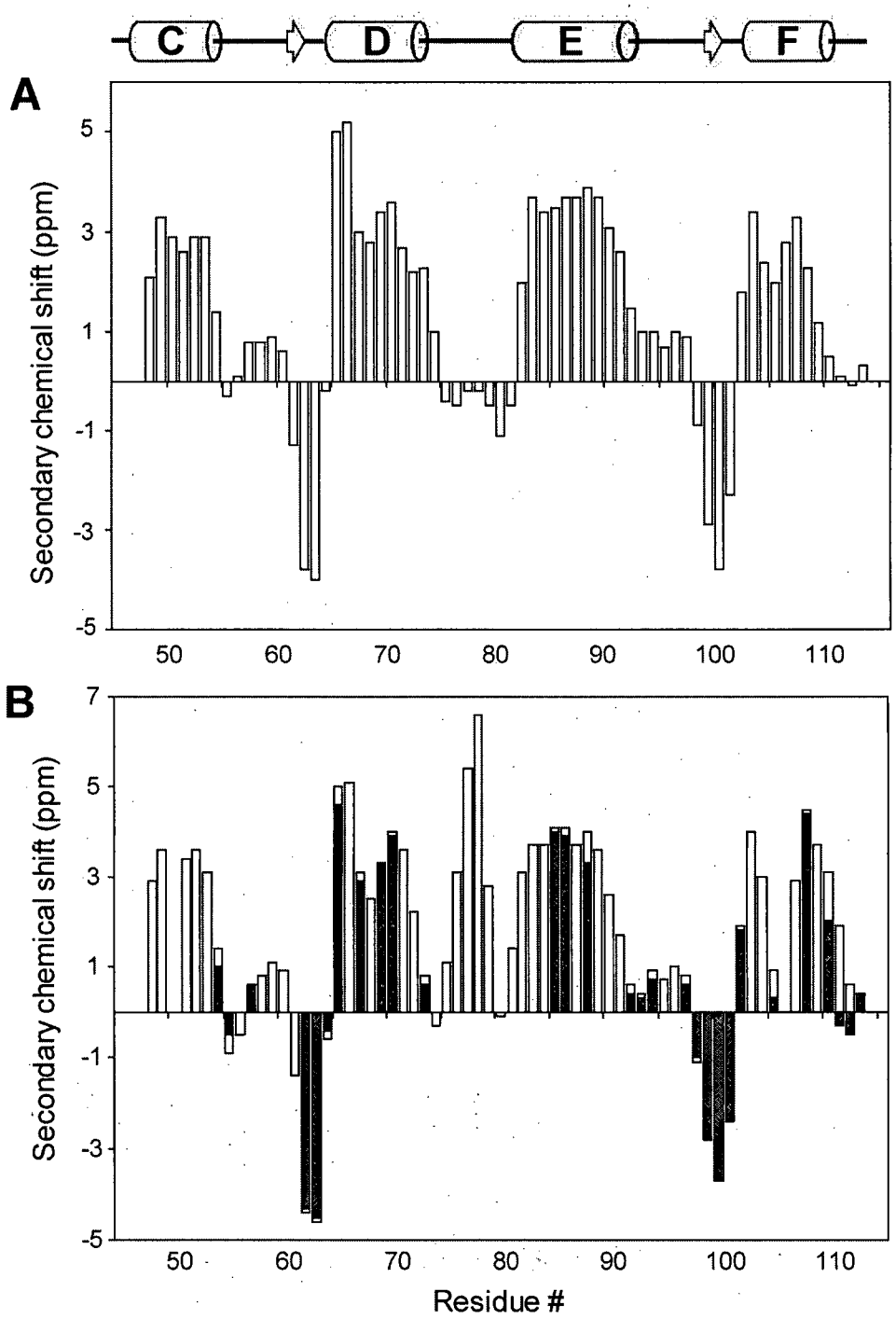

Figure 28. The secondary chemical shifts of CaM2/3 and the CaM2/3-M13 complex. **(A)** The weighted secondary chemical shift calculated $=(\Delta_{C\alpha\beta(i-1)}2+\Delta_{C\alpha\beta(i)}+\Delta_{C\alpha\beta(i+1)})/4$ where $\Delta_{C\alpha\beta(i)}=(\ \delta C^{\alpha}_{(i)}-\delta C^{\alpha}_{(coil)})-(\ \delta C^{\beta}_{(i)}-\ \delta C^{\beta}_{(coil)})$, by the program CSI for CaM2/3. Residues with positive chemical shifts are consistent with α-helix while residues with negative chemical shifts are consistent with β-sheet structure, and residues close to zero are considered random coil. The calculated secondary structure corresponds with the secondary structure of CaM2/3 as determined with PROMOTIF (schematic above panel

A). (**B**) The weighted secondary chemical shifts for CaM2/3 in the CaM2/3-M13 complex. The secondary structure of CaM2/3 in the CaM2/3-M13 complex is essentially the same as that of CaM2/3, except that there is a cluster of large positive values centered on the hinge region between helices D and E. This is consistent with this region adopting a short helical segment. The secondary chemical shifts of the double peaks are plotted together as black (lower value) and, white (higher value) bars on the graph for each residue where double peaks are observed.

3.3.6 Difference in chemical shifts between CaM2/3 and CaM2/3-M13

The differences in chemical shifts between nuclei in unbound CaM2/3 and the CaM2/3-M13 complex can provide a qualitative identification of the residues involved in forming this complex. The differences in chemical shifts between CaM2/3 and the CaM2/3-M13 complex were calculated for the ^{1}H and ^{15}N chemical shifts. This produced an average difference of 0.27±0.23 ppm (mean and sd). Residues with chemical shifts that show the most perturbation (i.e. those greater than twice the sd or 0.5ppm) included M71, M72, R74, K75, M76, D78, E82, E83, F92, R106, M109, T110, and N111. As with the secondary chemical shift, the most drastic changes in chemical shifts appear around the hinge region between helices D and E and the final helix F (Figure 29A). When viewed as a whole, the most substantial changes in chemical shifts are seen in the C-terminal portion of the molecule and the hinge region (Figure 29A).

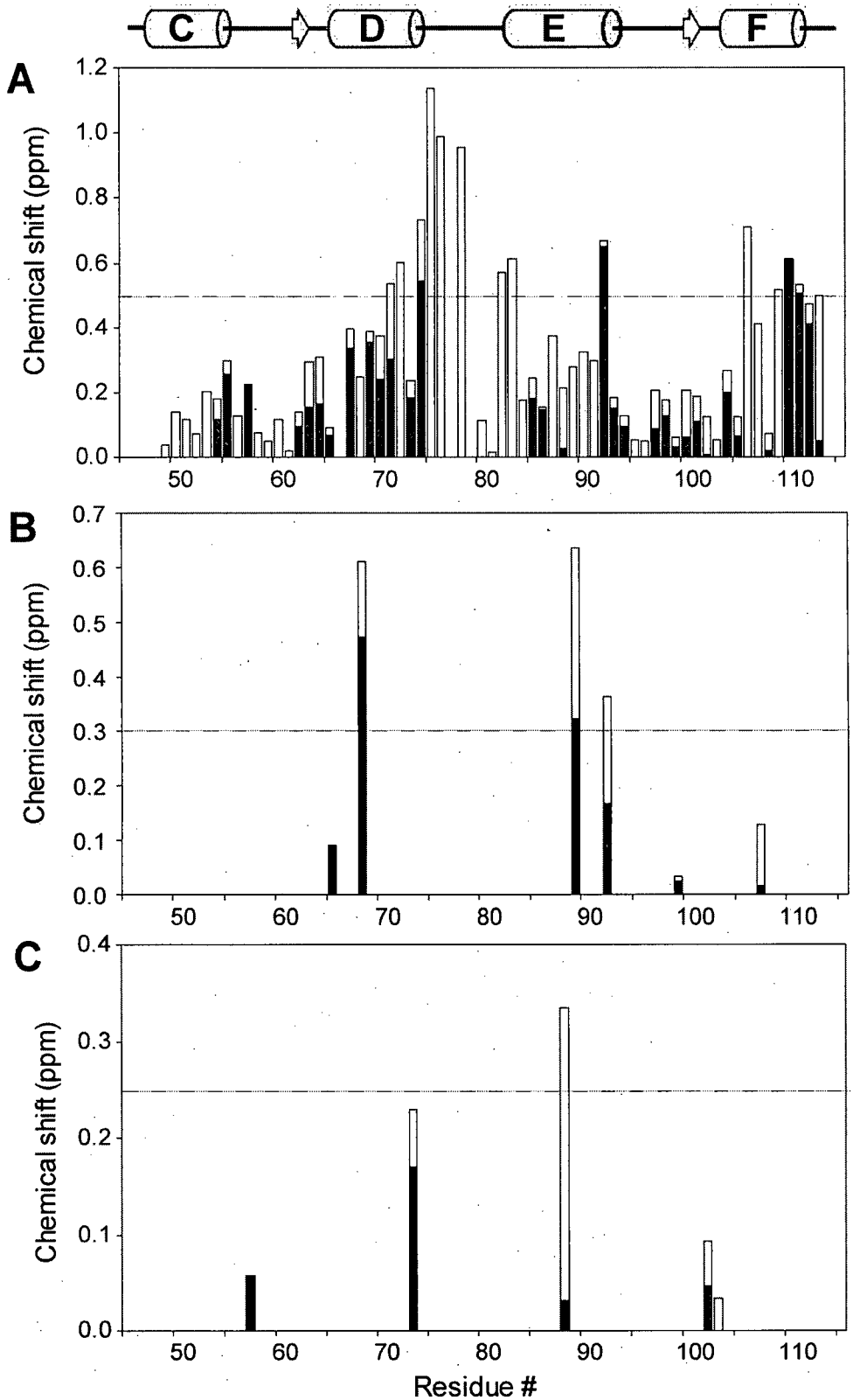

Figure 29. The difference in chemical shifts between CaM2/3 and the CaM2/3-M13 complex. Calculated as $\Delta\delta=[(\Delta\delta^{1}H)^{2} +(\Delta\delta I(\gamma I/\gamma^{1}H))^{2}]^{0.5}$ where $\Delta\delta$ is the difference between the indicated chemical shifts (calculated δCaM2/3- δCaM2/3-M13), I is either

^{13}C or ^{15}N and γ is the gyromagnetic ratio for the appropriate nuclei. (**A**) The chemical shift differences between CaM2/3 and the CaM2/3-M13 complex for the $^{1}H^{N}$ and ^{15}N nuclei from the respective ^{15}N-HSQC spectra. Residues with $\Delta\delta > 0.5$ ppm (gray dashed line) were considered significantly perturbed (M71 M72, R74, K75, M76, D78, E82, E83, F92, R106 and M109) (**B**) The chemical shift differences between CaM2/3 and the CaM2/3-M13 complex for the ^{1}H and ^{13}C aromatic Cε-Hε (black bars) and for the Cδ-Hδ (white bars). Residues with $\Delta\delta > 0.3$ ppm (gray dashed line) were considered significantly perturbed (F68, F89, and F92) (**C**) The chemical shift differences between CaM2/3 and the CaM2/3-M13 complex for the ^{1}H and ^{13}C of the alanine methyl groups. Alanine methyls with $\Delta\delta > 0.25$ ppm (gray dashed line) were considered significantly perturbed, (A88). For panels A and C the residues with double peaks are plotted together as white (higher value) and black (lower value) bars where double peaks occur. A schematic of the secondary structure of CaM2/3 as determined by PROMOTIF is displayed above panel A. The most prominent changes in chemical shift occur around the hinge between helices D and E, as well as helix F.

The spectral differences between CaM2/3 and the CaM2/3-M13 complex were also calculated for the ^{1}H and ^{13}C shifts from aromatic residues, as well as the alanine methyls. An examination of aromatic spectra of the CaM2/3-M13 complex shows that the H^{δ}, C^{δ}, H^{ε}, and C^{ε} chemical shifts for F65, Y99, and H107 are very similar to those of the unbound CaM2/3 structure, however, residues F68, F89, and F92 show substantial changes (i.e. chemical shift differences greater than 0.3ppm) (Figure 29B). In addition, examination of the HNCACB, CBCA(CO)NH, and H(CCO)TOCSY-NH spectra of the CaM2/3-M13 complex show that the H^{β}, and C^{β} chemical shifts for most alanine methyls are very similar to those of the unbound CaM2/3 structure, with the exception of the methyl group of A88 which is different from the unbound CaM2/3 (i.e. chemical shift difference is greater than 0.25ppm) (Figure 29C).

Many of the residues cited above as showing the greatest changes in chemical shift also help to form the hydrophobic binding pocket seen in the unbound CaM2/3 structure (Figure 16 B and C). These results suggests that the proposed hydrophobic

binding pocket of CaM2/3 may bind to the hydrophobic residues of the M13 peptide. This is analogous to the behavior of both domains of CaM.

3.3.7 CaM2/3-M13 complex backbone dynamics from amide ^{15}N relaxation

The global and local dynamic properties of the CaM2/3-M13 complex were measured with the ^{15}N T_1, T_2, and heteronuclear ^{1}H-{^{15}N}NOE ratios shown in Figures 30 A, B, and C, respectively. Consistent with its larger size, the CaM2/3-M13 complex exhibits longer average T_1 (0.53 ± 0.07) and shorter average T_2 (0.085 ± 0.02) values than unbound CaM2/3 (average T_1= 0.41 ± 0.07 and T_2= 0.13 ± 0.03)

Excluding residues exhibiting T_1/T_2 or heteronuclear ^{1}H-{^{15}N}NOE ratios indicative of conformational exchange or a high degree of internal mobility, the relaxation data were fit to an isotropic rotational diffusion tensor for the CaM2/3-M13 complex. This produced an effective correlation time of 7.7 ± 0.1 ns for the global tumbling of the CaM2/3-M13 complex. This is slightly larger than the ~7 ns expected for a 94 residue protein corresponding to the 1:1 CaM2/3-M13 complex but much smaller than the ~13 ns expected for a 188 residue protein corresponding to the 2:2 CaM2/3-M13 complex (Daragan and Mayo 1997). However, as expected the global tumbling time for the CaM2/3-M13 complex is larger than unbound CaM2/3 (5.1 ± 0.2 ns).

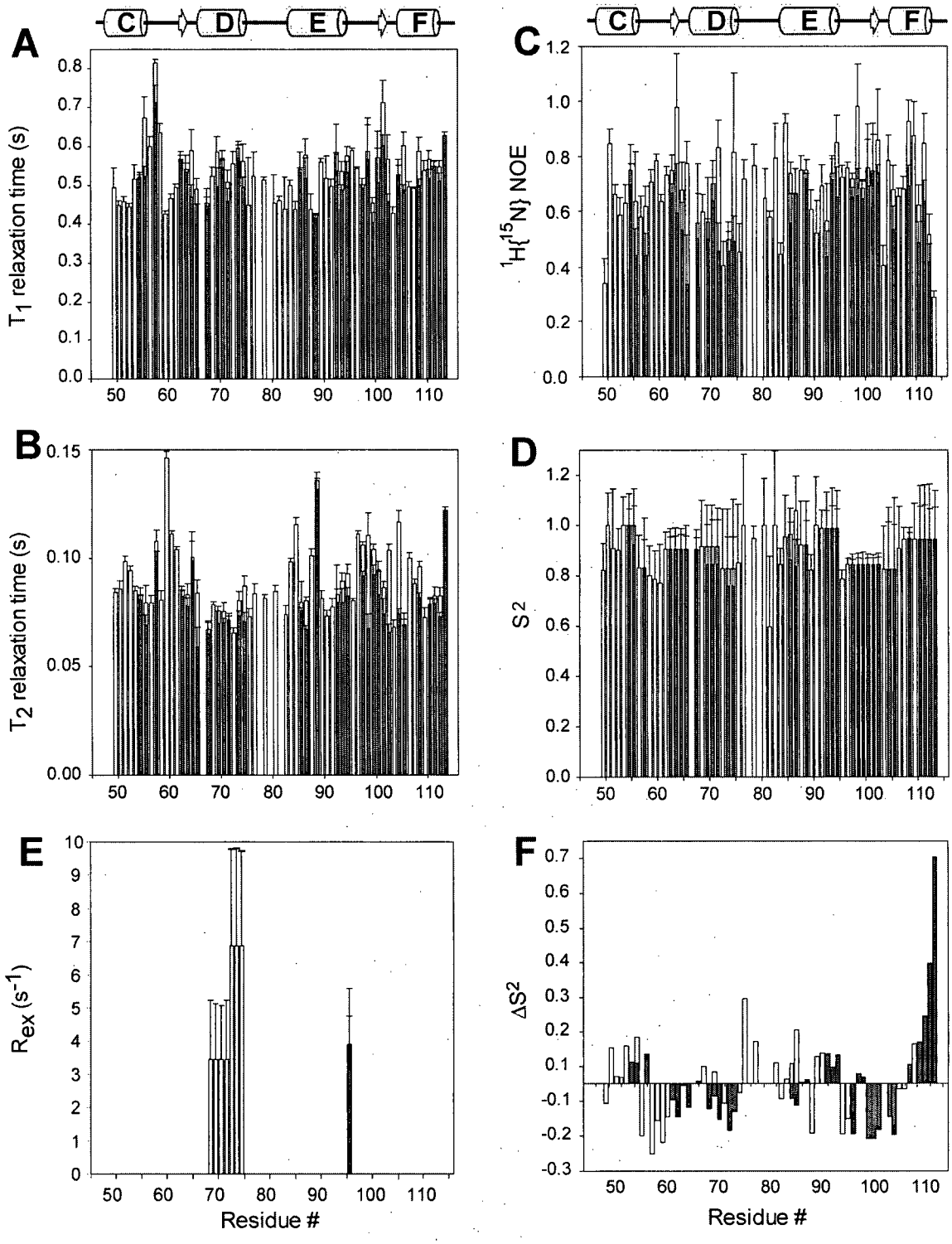

Figure 30. Backbone ^{15}N relaxation data for the CaM2/3-M13 complex. Displayed are the (**A**) longitudinal (T_1) and (**B**) transverse (T_2) relaxation times, the (**C**) heteronuclear $^1H\{^{15}N\}$NOE ratios (and standard errors), the (**D**) fit isotropic model free order parameter (S^2) (using the structure of CaM2/3), the (**E**) conformational exchange broadening (R_{ex}) parameter, and the (**F**) the change in S^2 (ΔS^2) calculated $S^2_{CaM2/3\text{-}M13}$ –

$S^2_{CaM2/3}$. Missing data corresponds to P66 and residues with overlapping or very weak signals. The reduced S^2 values and $^1H\{^{15}N\}$NOE ratios in the hinge region between α-helices D and E observed with unbound CaM2/3 are not observed with the CaM2/3-M13 complex. This may indicate that this region is less comformationally dynamic, and better defined structurally than the same region in unbound CaM2/3. For the residues with double peaks the parameters are plotted together as white (higher value) and, black (lower value) overlapping bars. A schematic of the secondary structure of CaM2/3 as determined by PROMOTIF is displayed above panels A and C.

With respect to the isotropic diffusion, the internal dynamic properties of the CaM2/3-M13 complex were described using Lipari-Szabo model free formalism in terms of the generalized order parameter S^2 with the structure of unbound CaM2/3 as a model (Figure 30D). The CaM2/3-M13 complex exhibits relatively uniform S^2 values of 0.87 ± 0.09. This is consistent with the CaM2/3-M13 complex having a folded, globular structure. However, unlike the unbound CaM2/3 structure, residues 74-81 in the CaM2/3-M13 complex do not show a decrease in S^2 (average 0.85±0.10) and $^1H\{^{15}N\}$NOE ratio values (Figures 19 and 30). The difference in the order parameters (ΔS^2) between CaM2/3 and the CaM2/3-M13 complex (calculated $S^2_{CaM2/3\text{-}M13} - S^2_{CaM2/3}$) are presented in Figure 30F. Figure 30F shows that there are increases in the S^2 of the CaM2/3-M13 complex (with respect to unbound CaM2/3) at the end of the C-terminal helix F, parts of the hinge region and surrounding helices D and E, specifically residues R74, M76, D78, E82, I85 and R86. These relaxation studies are consistent with the secondary chemical shift and chemical shift difference results (Figures 28B and 29) in as much as they show that there is a significant change in the structure and backbone dynamics for residues in the hinge region when comparing the CaM2/3-M13 complex to CaM2/3.

The T_2 lifetimes for residues 68 to 74 of CaM2/3 in the CaM2/3-M13 complex are anomalously short. This relaxation behavior is usually the result of conformational exchange broadening (R_{ex}) (Figure 30E). It suggests that these residues undergo intermediate time scale (msec-μsec) motions. Most of the resides exhibiting R_{ex} parameters have been identified as a being involved in the binding of CaM2/3 to M13. Therefore, it is possible that this motion entropically stabilizes the binding of CaM2/3 to M13.

3.3.8 Calcineurin activity assay

The M13 binding activity displayed by CaM2/3 suggests that it may retain some of the function of native CaM, such as the stimulation of calcineurin phosphatase activity. To test this, we used a calcineurin phosphatase assay to determine if CaM2/3 can stimulate calcineurin activity (Klee et al. 1983). Previous studies have shown that the C- and N-terminal fragments of CaM do not stimulate calcineurin (Newton et al. 1984). Consistent with this result, both CaM1/2 and CaM3/4 did not significantly stimulate the activity of calcineurin (Figure 31). However, the results of calcineurin activity assays confirm that CaM2/3 produces a small, but significant, increase in the phosphatase activity of calcineurin (Figures 31 and 32A). This low-level stimulation of calcineurin by CaM2/3 led to the speculation that CaM2/3 could compete with CaM for the CaM-binding site on calcineurin. An inhibition assay was performed via a series of CaM/calcineurin stimulation assays with increasing concentrations of CaM2/3. Figure 32B shows that CaM2/3 inhibits the stimulatory effect of CaM on calcineurin. The apparent maximal rate of calcineurin phosphatase activity, stimulated by CaM, appears to decrease with increasing CaM2/3. This is in contrast to the N- and C- terminal tryptic

fragments TR1C and TR2C, which do not effect the stimulation of calcineurin by CaM (Newton et al. 1984).

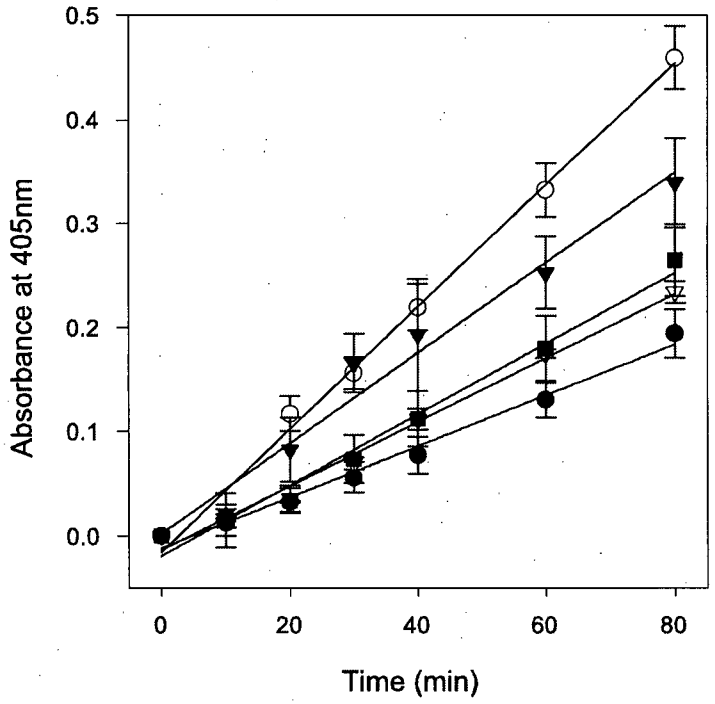

Figure 31. Progress curves for CaM fragments, CaM and calcineurin. The progress curves for the stimulation of calcineurin by (○) CaM, (▼) CaM2/3, (▽) CaM1/2, and (■) CaM3/4. Calcineurin (●) is included as a control since it has some activity on its own. The concentration of CaM and the CaM fragments was 300nM. The absorbance at 405nm was corrected by subtraction of the measurement at time 0.

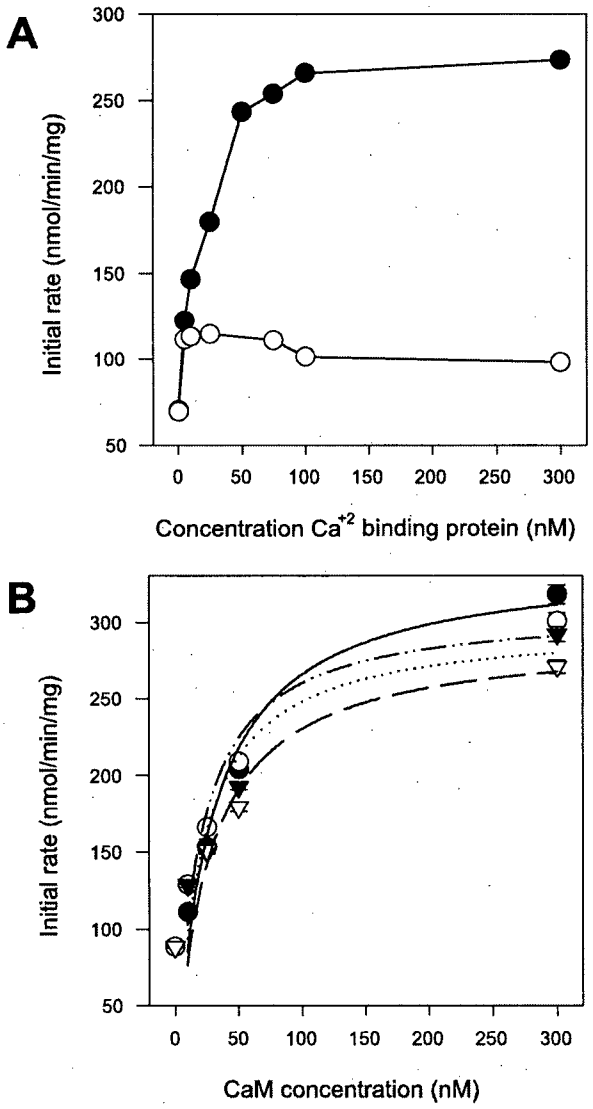

Figure 32. Calcineurin stimulation experiments. **(A)** Enzyme stimulation curve showing increasing initial rate of calcineurin phosphatase activity (nmol/min/mg) with increasing concentrations of (●) CaM and (○) CaM2/3. CaM2/3 promotes a small but significant increase in calcineurin activity. **(B)** A CaM competition experiment performed with CaM2/3. Each experimental group consists of a calcineurin stimulation study with 0, 10, 50 and 300 nM CaM in the presence of either (●) (—) 0, (○) (-..-) 10, (▼) (....) 50 and (▽) (----) 100 nM of CaM2/3. The results show that there is a decrease in the maximum rate of calcineurin phosphatase activity in the presence of CaM2/3.

3.4 Discussion

3.4.1 The interaction of the CaM fragments and CaM-binding peptides

The present binding studies revealed that CaM fragments associate with the bHLHW peptide in a 1:1 bHLHW : CaM fragment stoichiometry. Both fluorescence titrations and cross-linked complex studies confirm this stoichiometry. However, it has been shown previously that the interaction of native CaM and bHLHW produces a 2:1 CaM : bHLHW stoichiometry (Onions et al. 1997). Using an NMR monitored titration of $^{13}C/^{15}N$-CaM with bHLHW we were able to subsequently confirm this 2:1 CaM : bHLHW stoichiometry (Appendix F). Therefore, the interaction between the CaM fragments and bHLHW is significantly different from the proposed interaction of native CaM and bHLHW (Larsson et al. 2001). Our results confirm previous studies that show that the C-terminal (CaM3/4) domain has a higher affinity for the bHLHW peptide than the N-terminal (CaM1/2) domain (Onions et al. 2000). However, the CaM2/3 peptide has intermediate affinity between that of the CaM3/4 and CaM1/2 peptides.

The binding of CaM fragments to M13, as measured by cross-linking reactions, revealed the presence of complexes with molecular weights consistent with 1:1, 2:2 and higher order n:n CaM fragment : M13 stoichiometries. Fluorescence titrations confirm the presence of a 1:1 CaM fragment : M13 stoichiometry, but cannot rule out the presence of 2:2 or higher order stoichiometry species. All CaM fragments exhibit relatively high affinity for M13 as measured by fluorescence titrations. As with the bHLHW binding studies, the C-terminal fragment (CaM3/4) has higher affinity for the M13 peptide than the N-terminal (CaM1/2) peptide. However, CaM2/3 has significantly lower affinity for M13 than either the CaM1/2 or CaM3/4.

3.4.2 The interaction of CaM2/3 and M13 as measured by NMR

NMR spectroscopy confirms that CaM2/3 binds to the M13 peptide. In particular, the greatest chemical shift changes occur in the hinge region between helices D and E and in helix F including residues M71 M72, F68, R74, K75, M76, D78, E82, E83, A88, F89, F92, R106, M109, T110, and N111. In many CaM-target peptide complexes, all of the methionine residues in CaM are involved in hydrophobic binding interactions (Ikura et al. 1992; Meador et al. 1992). The chemical shift data suggest that all methionines in CaM2/3 with the exception of M51 appear to be involved in the interaction with M13. Additional hydrophobic residues involved in the binding of CaM2/3 to M13 include aromatic residues F68, F89 and F92, as well as the β-methyl group from A88.

Figure 33 shows the residues in CaM2/3 with the greatest chemical shift perturbation from Figure 29 (and listed above) mapped on to the surface of the structure of unbound CaM2/3. The hydrophobic residues seem to delineate a hydrophobic binding pocket that is similar to that of Ca^{2+}-ligated CaM in complex with the M13 peptide (Ikura et al. 1992). These data suggests that the hydrophobic binding pocket observed in the structure of CaM2/3 (Chapter 2 Figure 16B and C) appears to be the principal site of interaction with the M13 peptide.

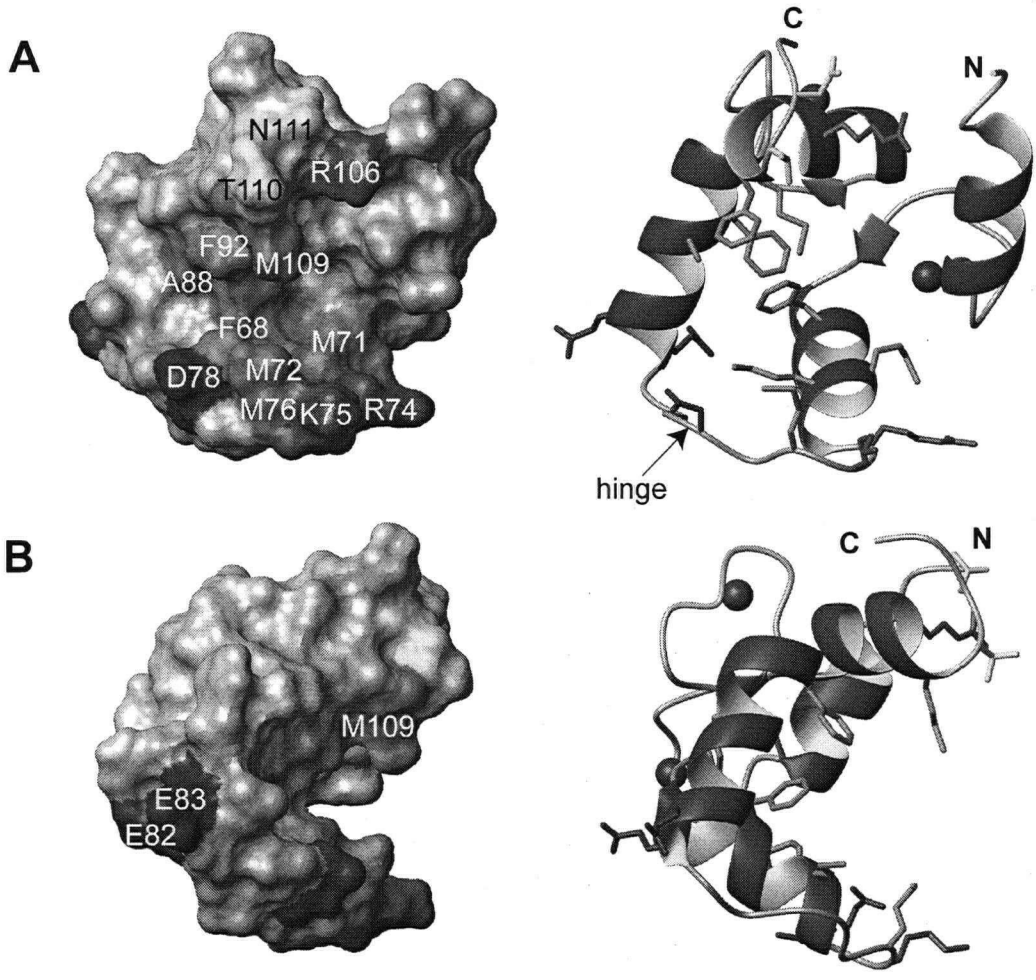

Figure 33. Residues involved in the CaM2/3-M13 complex mapped on to the surface of CaM2/3 (**A**) The residues of CaM2/3 involved in binding to M13 are shaded on the surface (left-hand side) according to amino acid properties. Hydrophobic residues F68, M71, M72, M76, A88, F92, and M109, acidic residues D78, E82, and E83, basic residues R74, K75, and R106, and polar residues T110, and N111 are labeled. F89 is not labeled because it is obscured by both F65 and F92. A ribbon structure with the same residues and in the same orientation as on the left-hand side is shown on the right-hand side. The spheres represent Ca^{2+} and the C- and N- termini are labeled. (**B**) Same as A, except the models are rotated 90° to the right. A hydrophobic binding pocket is formed showing a possible surface for interaction with the hydrophobic residues of the M13 peptide. The models were rendered using MOLMOL (Koradi et al. 1996).

The secondary chemical shift data (Figure 28) suggests that it is possible that residues 75-79 of CaM2/3 adopt a helical secondary structure in the CaM2/3-M13 complex, rather than the flexible hinge seen in CaM2/3. This is not without precedent as it has been observed that the hinge region of Ca^{2+}-free unbound CaM may transiently adopt an α-helical conformation in solution (Kuboniwa et al. 1995). In addition, many of the crystal structures of Ca^{2+}-ligated CaM show that this sequence can form an α-helix (Babu et al. 1988; Chattopadhyaya et al. 1992; Wilson and Brunger 2000). However, the presence of this helical structure would suggest an extended conformation that would not allow interaction of EF-hand 2 with EF-hand 3 seen in unbound CaM2/3 (Figure 16).

3.4.3 Two equally populated binding conformations

3.4.3.1 M13 binds in two orientations to CaM2/3

CaM2/3 shows high affinity for the M13 peptide but with two equally populated binding conformations. One explanation is that M13 and CaM2/3 bind to each other in two orientations. With respect to CaM, the charge distribution across the so-called channel outlets of the protein determine the binding orientation of CaM-binding peptides (pages 30-31). The α-helices B, C, D and E make up channel outlet 1 (CO1) with a net charge of –3, while α-helices A, F, G and H make up channel outlet 2 (CO2) with a net charge of –8. In addition, most CaM-target sequences are more positively charged or basic at one end of the target sequence (Yap et al. 2000). The basic part of a CaM-target peptide has preference for the more negatively charged CO2 and this determines binding orientation in CaM-target peptide complexes (Osawa et al. 1999). CaM2/3 is similar to CO1, being composed of helices C, D, E and F and having a net charge of –4. It is

possible that the small net charge in the regions forming the channel outlet of CaM2/3 makes it unable to selectively bind to the M13 peptide in a single orientation.

The M13 peptide is grouped into the 1-5-8-14 class of CaM-binding sequences (Table 3) based on the position of hydrophobic residues involved in binding to the hydrophobic binding pockets of CaM. The M13 peptide has two hydrophobic "anchors" tryptophan at position 1 and phenylalanine at position 14, and additional hydrophobic residues include phenylalanine at position 5 and valine at position 8 (Ikura et al. 1992). It is likely that these hydrophobic residues are the principal source of interaction between M13 and the hydrophobic binding pocket on CaM2/3. The two binding conformations detected by NMR spectroscopy may be explained by the possibility that M13 and CaM2/3 bind in two orientations with respect to each other. The similarity of the chemical shifts exhibiting double peaks in the NMR spectra suggest that the hydrophobic residues involved in this binding model are the same regardless of orientation. However, the near equal signal intensity of the double peaks, mean both orientations are isoenergetic. A possible schematic of this type of interaction is shown in Figure 34A. In one orientation the C-terminal EF-hand of CaM2/3 is next to the N-terminal of the M13 peptide (left hand side Figure 34A), and in the other orientation, the N-terminal EF-hand of CaM2/3 is next to the N-terminal of the M13 peptide (right hand side Figure 34A).

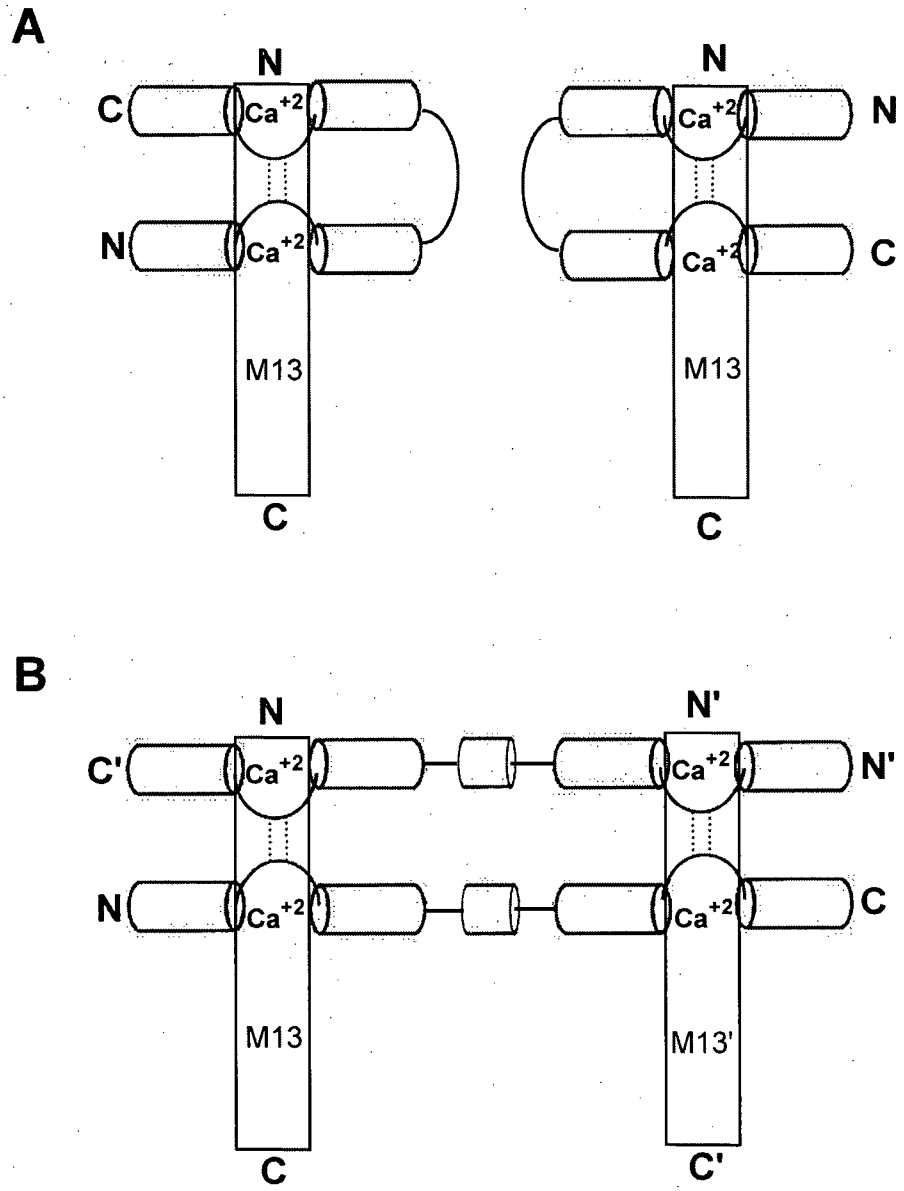

Figure 34. The schematic representations of the CaM2/3-M13 complexes (**A**) The 1:1 CaM2/3:M13 schematic structures. The M13 peptide is represented as a rectangle. CaM2/3 is represented as a schematic where the cylinders are helices, the curved lines between them are the Ca^{2+}-binding segments (labeled "Ca^{2+}"), and the dashed lines are the hydrogen-bonds between I00 and I63. The schematic of CaM2/3 is in two orientations: (left) where the N-terminal of M13 is adjacent to the C-terminal EF-hand of CaM2/3, and (right) where the N-terminal of M13 is adjacent to the N-terminal EF-hand of CaM2/3. (**B**) The 2:2 CaM2/3 : M13 asymmetrical dimer structure. The schematic shows two M13 peptides and two CaM2/3 peptides forming the complex. Both structural scenarios produce the same set of two peaks in the NMR spectra. The right half of the 2:2 dimer complex in B gives rise to the same peaks in an ^{15}N-HSQC spectra as the right hand structure in A. Similarly the left half of the 2:2 dimer complex in B gives rise to the same peaks in an ^{15}N-HSQC spectra as the left hand structure in A.

There is precedent for a single domain of CaM binding to a target peptide. An NMR solution structure of a complex of CaM with a binding peptide (C20W) from a Ca^{2+} pump reveals that only the C-terminal domain of CaM is involved in binding to the C20W peptide. This peptide is unique among CaM-binding sequences in that it has only one of the usual two hydrophobic "anchor" residues (Elshorst et al. 1999). However, this structure differs from the proposed 1:1 CaM2/3-M13 complex because the C20W peptide binds to the C-terminal domain of CaM in only one orientation (Elshorst et al. 1999).

3.4.3.2 The asymmetrical CaM2/3-M13 dimer complex

The proposed structures in Figure 34A are not the only possible explanation of why the double peaks from the titration of CaM2/3 with M13 have similar intensities (Figure 27B). Another possible cause of this behavior is that the CaM2/3-M13 complex exists as a 2:2 asymmetrical dimer (Figure 34B). This model is also supported by the AUC and the cross-linking experiments, which show that the CaM2/3-M13 complex exists as an equilibrium between a 1:1 and 2:2 complex (Figure 25 and Table 10). In such a structure, two CaM2/3 molecules swap EF-hands in an anti-parallel fashion, and the hinge region (loop between helices D and E) would have to twist 180° to form an extended structure. Each swapped pair of EF-hands would form a separate domain that retains the same 2/3 EF-hand pairing seen in the unbound CaM2/3 structure (Figure 34B). As the domain structure of unbound CaM2/3 is retained in this model, it is expected that the hydrophobic binding pocket observed in CaM2/3 is also still present. Thus, making it possible that each of these dimer-domains might accommodate the same hydrophobic residues from two separate M13 molecules, thus forming a 2:2 dimer. A possible

schematic model structure of the 2:2 dimer is proposed in Figure 34B. This model would explain the presence of the short helical structure within the hinge region of CaM2/3 (as predicted with the secondary chemical shift data (Figure 28)). Since the model predicts an extended structure in this region it could accommodate the formation of a helix. The large number of charged residues in the hinge region that appear to be involved in this interaction may be forming salt bridges from one CaM2/3 monomer to the other. For example, residues R74 and K75 are positively charged, whereas D78 is negatively charged and because the monomers run anti-parallel to each other these residues may interact. The presence of α-helical structure and possible salt bridges in this region would lead to increased stability in the normally flexible hinge region and this would explain the decrease in mobility of these residues observed in the ^{15}N backbone relaxation studies (Figure 30F). In addition, this model would also explain the presence of the proposed short anti-parallel β-sheet in the 2:2 CaM2/3-M13 complex because the 2/3 EF-hand paring is expected to be retained.

The studies of single EF-hand Ca^{2+}-binding site models have shown that EF-hand pairs can homodimerize, but preferentially heterodimerize with the appropriate partner EF-hand (Finn et al. 1992; Shaw and Sykes 1996). These studies support the proposed anti-parallel arrangement of CaM2/3 monomers in the 2:2 CaM2/3-M13 complex model, rather than a parallel formation with 2/2 and 3/3 EF-hand parings (Figure 34B). The recent discovery of domain-swapped EF-hand parings in Ca^{2+}-free CaM also show that the EF-hand swapping proposed in the 2:2 CaM2/3-M13 complex model is possible (Schumacher et al. 2004).

We have outlined two structural scenarios to explain the presence of nearly equal intensity split peaks on the ^{15}N-HSQC spectra for the titration of CaM2/3 with M13 (Figures 26 and 27B). The AUC and cross-linking data suggest the presence of an equilibrium between a 2:2 dimer and a 1:1 CaM2/3 : M13 complex. These data would suggest that both complexes are involved in the binding of CaM2/3 with M13. A close examination of Figure 34 shows that both schematic scenarios could give rise to the same double peak pattern observed in the ^{15}N-HSQC spectra for the titration of CaM2/3 with M13. If one compares the scenario with the two populations of 1:1 CaM2/3 : M13 complexes in Figure 34A with the 2:2 asymmetrical dimer complex in Figure 34B, one can see that other than the hinge region between the EF-hands of CaM2/3 the structures have significant similarities. We would expect that the right half of the 2:2 dimer complex in Figure 34B would give rise to the same peaks in an ^{15}N-HSQC spectrum as the right hand structure in Figure 34A. Similarly, the left half of the 2:2 dimer complex in Figure 34B could give rise to the same peaks in an ^{15}N-HSQC spectra as the left hand structure in Figure 34A. This explains how both sets of structures can exist at the same time and give rise to only two peaks. This mechanism also explains why the phenomena of double peaks seems to occur only in the EF-hands of CaM2/3 and the amides in hinge region between EF-hands yield single peaks.

3.4.4 CaM2/3 inhibits the stimulation of calcineurin by CaM

Confirming previous studies with CaM fragments, the N-terminal (CaM1/2) and C-terminal (CaM3/4) domains have little or no ability to stimulate the activity of calcineurin (Newton et al. 1984). However, CaM2/3 has a limited ability to stimulate calcineurin. CaM2/3 also appears to be able to inhibit the stimulation of calcineurin by CaM. At higher concentrations of CaM2/3, this leads to a reduction in the maximum phosphatase activity of calcineurin (Figure 32B). In this way, CaM2/3 appears to possess a "partial agonist" like activity with respect to calcineurin.

The CaM-binding sequence of calcineurin is similar to the M13 peptide and they are both classified as the 1-14 class (1-5-8-14) of CaM-binding sequences (Chapter 1 Table 3). The finding that CaM2/3 binds to M13 suggests that it may also bind to the CaM-binding sequence of calcineurin. This would explain the small increase in the phoshatase activity of calcineurin in the presence of CaM2/3 (Figure 32A). As a possible mechanism, CaM2/3 may bind to the CaM-binding sequence of calcineurin but is unable to efficiently remove the adjacent auto-inhibitory domain from the active site of calcineurin. This results in only a small increase in the activity of calcineurin in the presence of CaM2/3.

CaM2/3 inhibits the stimulation of calcineurin by CaM. Given the modest stimulation of calcineurin by CaM2/3 it is reasonable to assume that CaM2/3 may compete with CaM for the CaM-binding sequence of calcineurin producing a competitive inhibition. In contrast, Figure 32B shows that the maximum initial rate of CaM stimulated phosphatase activity of calcineurin decreases with increasing CaM2/3 suggesting an apparent non-competitive inhibition. However, it is unclear if sufficient

CaM was present to compete with CaM2/3 and reveal a competitive inhibition. Ultimately we were unable to carry out calcineurin stimulation experiments at higher CaM concentrations because high CaM concentrations (> 300 nM) alone appeared to inhibit the activity of calcineurin. This phenomena of decreased calcineurin activity at high CaM concentrations has been observed before and has been attributed to the effect of CaM on the phosphorylation of calcineurin (Hashimoto et al. 1988). Thus, it appears clear that CaM2/3 inhibits the stimulation of calcineurin by CaM, but the mechanism of inhibition and the location of the binding site for CaM2/3 on calcineurin are unclear.

Conclusion

In this study, we examined the typical EF-hand parings of CaM1/2 and CaM3/4 as well as the structure of a novel EF-hand pairing using CaM2/3 as a model. We tested for the presence of cooperative interactions between the second and third EF-hand Ca^{2+}-binding sites of CaM, and explored the effect of novel EF-hand pairings on Ca^{2+}-affinity using CaM2/3. We used NMR to solve the structure of the CaM2/3 fragment of CaM and found that its structure is very similar to both the N- and C-terminal domains of CaM. We also found that CaM2/3 binds Ca^{2+} in a stepwise manner (i.e. Ca^{2+} binds to binding site 3 first, and then to binding site 2). Cooperativity between binding sites 2 and 3 could not be determined because of the large dissociation constant disparity between the Ca^{2+}-binding sites 2 and 3.

Our results stress the importance of stacking interactions between aromatic residues in EF-hand proteins. These residues, when located opposite the loop between EF-hands, act as an "aromatic zipper" to hold the first and fourth helices of an EF-hand domain together, and thereby confer structural stability on the domain by acting as a structural counterbalance to the loop between EF-hands. In effect, the EF-hands associate through hydrophobic interactions between neighboring α-helices, the loop between EF-hands holds one side of the domain together and the "aromatic zipper" holds the other side together. The low Ca^{2+}-affinity observed with EF-hand homodimers is explained by the anti-parallel pairing of EF-hands that prevents aromatic stacking interactions (Reid 1987b; Kay et al. 1991; Shaw et al. 1992; Franchini and Reid 1999a). This also explains the partial restoration of Ca^{2+}-affinity with EF-hand heterodimers because the aromatic stacking interactions are restored, but the loop between EF-hands is

still broken (Finn et al. 1992; Shaw and Sykes 1996). In the case of the novel CaM2/3 peptide, we found that the "aromatic zipper" is in a structurally redundant position adjacent to the hinge region, and in the case of CaM2/3 the hinge region acts as the loop between EF-hands 2 and 3. The lack of an "aromatic zipper" holding the first (C) and fourth (F) helices together in CaM2/3 may lead to reduced Ca^{2+}-affinity at EF-hand 2 and the disruption of cooperativity.

These results lead us to conclude that the unique relationship between the EF-hands that associate to form an EF-hand domain and the Ca^{2+}-affinity and cooperativity within that EF-hand domain is dependant upon the position of the "aromatic zipper" with respect to the loop between EF-hands. This relationship extends to the evolutionary mandated paring of EF-hands; with EF-hand 1 having evolved to pair with EF-hand 2, and EF-hand 3 with EF-hand 4 (Moncrief et al. 1990; Nakayama et al. 1992). We conclude that these EF-hand pairings have evolved to position the "aromatic zipper" opposite the loop between EF-hands in an EF-hand domain (Appendix F).

Furthermore, we have also shown that EF-hand pairing in CaM may have as much of an effect on structural stability and Ca^{2+}-binding affinity as the particular residues directly involved in Ca^{2+}-chelation.

In this study we also measured the ability of CaM fragments to bind to the CaM binding peptides M13 and bHLHW using fluorescence monitored titrations and cross-linking reactions. We found that the CaM3/4 has higher affinity for both the M13 and bHLHW peptides than the CaM1/2. Both CaM1/2 and CaM3/4 have higher affinity for M13 than CaM2/3, and CaM2/3 has higher affinity than the CaM1/2 peptide for bHLHW.

We studied in depth the binding of CaM2/3 and M13 using NMR spectroscopy. The finding that many amides in the CaM2/3-M13 complex yielded two peaks in the ^{15}N-HSQC spectra prevented the determination of the structure of this complex. However, the presence of equal intensity peaks for these residues suggested the presence of two equally populated complex conformations. We found the residues showing the most change in chemical shift in CaM2/3 upon M13 binding were clustered around the hinge region between helices D and E as well as in helix F. When these residues were mapped onto the surface of CaM2/3, they were found to coincide with the previously identified hydrophobic binding pocket of CaM2/3. This finding confirmed that the CaM2/3 peptide behaves like both the N- and C-terminal domains of CaM. Upon further investigation using secondary chemical shifts we were able to determine that the region of CaM2/3 showing the greatest change in secondary structure upon M13 binding was the hinge between helices D and E.

The results of cross-linking experiments suggest the presence of 1:1, 2:2 and higher order CaM2/3: M13 stoichiometries. Additionally, the AUC experiments revealed that the CaM2/3-M13 exists as an equilibrium between a 1:1 and a 2:2 CaM2/3 : M13 complex. These findings lead to the proposal of two possible complexes. In one complex the stoichiometry is 1:1 CaM2/3 : M13, but M13 and CaM2/3 peptides bind in two orientations with respect to each other. The other proposed complex. is a 2:2 asymmetrical dimer. In this structure two CaM2/3 molecules swap EF-hands in an anti-parallel fashion, and the hinge between helices D and E forms an extended structure. Each swapped pair of EF-hands forms a separate dimer-domain that retains the 2/3 pairing seen in the CaM2/3 structure. The difference is that each EF-hand is contributed

by a different CaM2/3 monomer. This structure predicts that the domain structure of CaM2/3 is retained and that the hydrophobic binding pocket observed in CaM2/3 would still be present, making it possible that each of these domains might accommodate the same hydrophobic residue or residues from two separate M13 molecules thus forming a 2:2 dimer.

CaM1/2 and CaM3/4 have little or no ability to stimulate the activity of calcineurin. However, CaM2/3 was found to have a limited ability to stimulate calcineurin. It was found that CaM2/3 inhibited the stimulation of calcineurin by CaM, but the mechanism of inhibition and the location of the binding site for CaM2/3 on calcineurin are unclear.

We have shown that we can affect the ability of CaM fragments to bind to CaM targets and regulate CaM-stimulated enzymes by changing the associating EF-hands in a domain. CaM2/3 is an example of this because it has differing abilities to bind to both the M13 and bHLHW peptides, as well as unique behavior regarding calcineurin regulation when compared to the CaM1/2 and CaM3/4 fragments of CaM.

Future Studies

In relation to future studies, our findings confirm that single EF-hand peptides should not be used as models for testing the effects of mutations to the Ca^{2+} chelating residues on Ca^{2+}-binding affinity because the effect of homodimeric EF-hand pairing may have a confounding effect on Ca^{2+}-binding affinity.

Our results imply that it should be possible to restore high Ca^{2+}-binding affinity in both EF-hand Ca^{2+} binding sites of CaM2/3 by changing the position of the aromatic residues with respect to the hinge between EF-hands 2 and 3. This rearrangement of aromatic residues would reposition the "aromatic zipper" on helices C and F (rather than D and E) opposite the hinge between EF-hands 2 and 3. The aromatic residues forming the "aromatic zipper" could also be repositioned opposite the loop between EF-hands by rearranging the EF-hands so that EF-hand 3 is the N-terminal EF-hand and EF-hand 2 is the C-terminal EF-hand. This peptide (CaM3/2) would have a helical arrangement of E, F, C, D and aromatic residues forming the "aromatic zipper" would be on the first (E) and fourth (D) helices. It should also be possible to make another novel association of two EF-hands by fusing EF-hands 1 and 4 together. This peptide (CaM1/4) would have a helical arrangement of A, B, G, H, and aromatic residues forming the "aromatic zipper" would be on the first (A) and fourth (H) helices. We expect that all of these two EF-hand fragments of CaM would have two high affinity Ca^{2+}-binding sites with cooperative interactions between them. Another simple test could also be performed using a single Ca^{2+}-binding EF-hand fragment like CaM3. This EF-hand fragment would be mutated such that the aromatic residues capable of forming an "aromatic zipper" positioned one and four residues before the Ca^{2+} chelating segment as well as occupying Ca^{2+} chelating

position 10 and just after the Ca^{2+} chelating segment. We would expect that such a mutant single EF-hand peptide would dimerize in an anti-parallel fashion thus producing an "aromatic zipper" holding together helices from each monomer peptide. It is possible that such an EF-hand dimer peptide would have two high affinity Ca^{2+}-binding sites. All of these proposed studies would allow us to better understand how EF-hand association affects the structure, Ca^{2+}-affinity, and cooperativity of CaM and EF-hand proteins in general.

In addition to the above studies all of the proposed Ca^{2+}-binding peptides should be tested for the ability to bind to CaM-binding peptides. If enough EF-hand combinations are tested, it may be possible to develop a structure/activity relationship between the associating EF-hands and the differential activation or inhibition of CaM-target enzymes. Such a relationship could be used to develop EF-hand proteins that have the ability to specifically stimulate or inhibit specific CaM-target enzymes.

References

Andre, I., and Linse, S. 2002. Measurement of Ca^{2+}-binding constants of proteins and presentation of the CaLigator software. *Anal Biochem* **305:** 195-205.

Babu, Y.S., Bugg, C.E., and Cook, W.J. 1988. Structure of calmodulin refined at 2.2 Å resolution. *J Mol Biol* **204:** 191-204.

Barbato, G., Ikura, M., Kay, L.E., Pastor, R.W., and Bax, A. 1992. Backbone dynamics of calmodulin studied by ^{15}N relaxation using inverse detected two-dimensional NMR spectroscopy: the central helix is flexible. *Biochemistry* **31:** 5269-5278.

Bayley, P.M., Findlay, W.A., and Martin, S.R. 1996. Target recognition by calmodulin: dissecting the kinetics and affinity of interaction using short peptide sequences. *Protein Sci* **5:** 1215-1228.

Bentrop, D., Bertini, I., Cremonini, M.A., Forsen, S., Luchinat, C., and Malmendal, A. 1997. Solution structure of the paramagnetic complex of the N-terminal domain of calmodulin with two Ce^{3+} ions by 1H NMR. *Biochemistry* **36:** 11605-11618.

Biekofsky, R.R., Martin, S.R., Browne, J.P., Bayley, P.M., and Feeney, J. 1998. Ca2+ coordination to backbone carbonyl oxygen atoms in calmodulin and other EF-hand proteins: ^{15}N chemical shifts as probes for monitoring individual-site Ca2+ coordination. *Biochemistry* **37:** 7617-7629.

Bisaccia, F., Zara, V., Capobianco, L., Iacobazzi, V., Mazzeo, M., and Palmieri, F. 1996. The formation of a disulfide cross-link between the two subunits demonstrates the dimeric structure of the mitochondrial oxoglutarate carrier. *Biochim Biophys Acta* **1292:** 281-288.

Black, D.J., Tikunova, S.B., Johnson, J.D., and Davis, J.P. 2000. Acid pairs increase the N-terminal Ca^{2+} affinity of CaM by increasing the rate of Ca^{2+} association. *Biochemistry* **39:** 13831-13837.

Brunger, A.T., Adams, P.D., Clore, G.M., DeLano, W.L., Gros, P., Grosse-Kunstleve, R.W., Jiang, J.S., Kuszewski, J., Nilges, M., Pannu, N.S., et al. 1998. Crystallography & NMR system: A new software suite for macromolecular structure determination. *Acta Crystallogr D Biol Crystallogr* **54:** 905-921.

Carpino, L.A., and Han, G.Y. 1972. The 9-fluorenylmethoxycarbonyl amino-protecting group. *J. Org. Chem*: 3404-3409.

Chattopadhyaya, R., Meador, W.E., Means, A.R., and Quiocho, F.A. 1992. Calmodulin structure refined at 1.7 Å resolution. *J Mol Biol* **228:** 1177-1192.

Chou, J.J., Gaemers, S., Howder, B., Louis, J.M., and Bax, A. 2001a. A simple apparatus for generating stretched polyacrylamide gels, yielding uniform alignment of proteins and detergent micelles. *J Biomol NMR* **21:** 377-382.

Chou, J.J., Li, S., Klee, C.B., and Bax, A. 2001b. Solution structure of $Ca^{(2+)}$-calmodulin reveals flexible hand-like properties of its domains. *Nat Struct Biol* **8:** 990-997.

Clore, G.M., Gronenborn, A.M., and Tjandra, N. 1998. Direct structure refinement against residual dipolar couplings in the presence of rhombicity of unknown magnitude. *J Magn Reson* **131:** 159-162.

Corneliussen, B., Holm, M., Waltersson, Y., Onions, J., Hallberg, B., Thornell, A., and Grundstrom, T. 1994. Calcium/calmodulin inhibition of basic-helix-loop-helix transcription factor domains. *Nature* **368:** 760-764.

Cornilescu, G., Delaglio, F., and Bax, A. 1999. Protein backbone angle restraints from searching a database for chemical shift and sequence homology. *J Biomol NMR* **13:** 289-302.

Crivici, A., and Ikura, M. 1995. Molecular and structural basis of target recognition by calmodulin. *Annu Rev Biophys Biomol Struct* **24:** 85-116.

Dahlquist, F.W. 1978. The meaning of Scatchard and Hill plots. *Methods Enzymol* **48:** 270-299.

Daragan, V.A., and Mayo, K.H. 1997. Motional model analyses of protein and peptide dynamics using ^{13}C and ^{15}N NMR relaxation. *Prog. Nucl. Magn. Reson. Spect.* **31:** 63-105.

Delaglio, F., Grzesiek, S., Vuister, G.W., Zhu, G., Pfeifer, J., and Bax, A. 1995. NMRPipe: a multidimensional spectral processing system based on UNIX pipes. *J Biomol NMR* **6:** 277-293.

DeLano, W.L. 2002. The PyMOL Molecular Graphics System, 0.99 ed. DeLano Scientific, San Carlos, CA, USA.

Don, R.H., Cox, P.T., Wainwright, B.J., Baker, K., and Mattick, J.S. 1991. 'Touchdown' PCR to circumvent spurious priming during gene amplification. *Nucleic Acids Res* **19:** 4008.

Dosset, P., Hus, J.C., Blackledge, M., and Marion, D. 2000. Efficient analysis of macromolecular rotational diffusion from heteronuclear relaxation data. *J Biomol NMR* **16:** 23-28.

Dourtoglou, V., Gross, B., Lambropoulou, V., and Zioudrou. 1984. O-Benzotriazolyl-N,N,N',N' tetramethyluronium hexaflurophosphate as a coupling reagent for the synthesis of peptides of biological interest. *Synthesis*: 572-574.

Drabikowski, W., Brzeska, H., and Venyaminov, S. 1982. Tryptic fragments of calmodulin. Ca^{2+}- and Mg^{2+}-induced conformational changes. *J Biol Chem* **257:** 11584-11590.

Elshorst, B., Hennig, M., Forsterling, H., Diener, A., Maurer, M., Schulte, P., Schwalbe, H., Griesinger, C., Krebs, J., Schmid, H., et al. 1999. NMR solution structure of a complex of calmodulin with a binding peptide of the Ca^{2+} pump. *Biochemistry* **38:** 12320-12332.

Falke, J.J., Drake, S.K., Hazard, A.L., and Peersen, O.B. 1994. Molecular tuning of ion binding to calcium signaling proteins. *Q Rev Biophys* **27:** 219-290.

Fallon, J.L., and Quiocho, F.A. 2003. A closed compact structure of native $Ca^{(2+)}$-calmodulin. *Structure (Camb)* **11:** 1303-1307.

Farrow, N.A., Muhandiram, R., Singer, A.U., Pascal, S.M., Kay, C.M., Gish, G., Shoelson, S.E., Pawson, T., Forman-Kay, J.D., and Kay, L.E. 1994. Backbone dynamics of a free and phosphopeptide-complexed Src homology 2 domain studied by ^{15}N NMR relaxation. *Biochemistry* **33:** 5984-6003.

Farrow, N.A., Zhang, O., Szabo, A., Torchia, D.A., and Kay, L.E. 1995. Spectral density function mapping using ^{15}N relaxation data exclusively. *J Biomol NMR* **6:** 153-162.

Fields, G.B., and Noble, R.L. 1990. Solid phase peptide synthesis utilizing 9-fluorenylmethoxycarbonyl amino acids. *Int J Pept Protein Res* **35:** 161-214.

Finn, B.E., Evenas, J., Drakenberg, T., Waltho, J.P., Thulin, E., and Forsen, S. 1995. Calcium-induced structural changes and domain autonomy in calmodulin. *Nat Struct Biol* **2:** 777-783.

Finn, B.E., Kordel, J., Thulin, E., Sellers, P., and Forsen, S. 1992. Dissection of calbindin D_9k into two $Ca^{(2+)}$-binding subdomains by a combination of mutagenesis and chemical cleavage. *FEBS Lett* **298:** 211-214.

Fiorin, G., Biekofsky, R.R., Pastore, A., and Carloni, P. 2005. Unwinding the helical linker of calcium-loaded calmodulin: A molecular dynamics study. *Proteins.* **61:** 829-839

Forsen, S., and Linse, S. 1995. Cooperativity: over the Hill. *Trends Biochem Sci* **20:** 495-497.

Franchini, P.L., and Reid, R.E. 1999a. Investigating site-specific effects of the -X glutamate in a parvalbumin CD site model peptide. *Arch Biochem Biophys* **372:** 80-88.

Franchini, P.L., and Reid, R.E. 1999b. A model for circular dichroism monitored dimerization and calcium binding in an EF-hand synthetic peptide. *J Theor Biol* **199:** 199-211.

Gill, S.C., and von Hippel, P.H. 1989. Calculation of protein extinction coefficients from amino acid sequence data. *Anal Biochem* **182:** 319-326.

Gillis, J.M. 1985. Relaxation of vertebrate skeletal muscle. A synthesis of the biochemical and physiological approaches. *Biochim Biophys Acta* **811:** 97-145.

Goddard, T.D., and Kneeler, D.G. 1999. Sparky, 3rd ed. University of California, San Francisco, San Francisco, CA.

Goodman, M., Pechere, J.F., Haiech, J., and Demaille, J.G. 1979. Evolutionary diversification of structure and function in the family of intracellular calcium-binding proteins. *J Mol Evol* **13:** 331-352.

Gronenborn, A.M., and Clore, G.M. 1994. Identification of N-terminal helix capping boxes by means of 13C chemical shifts. *J Biomol NMR* **4:** 455-458.

Grzesiek, S., and Bax, A. 1992. Correlating backbone amide and side chain resonances in larger proteins by multiple relayed triple resonance NMR. *J. Am. Chem. Soc.*: 6291–6293.

Grzesiek, S., and Bax, A. 1993. Amino acid type determination in the sequential assignment procedure of uniformly 13C/15N-enriched proteins. *J Biomol NMR* **3:** 185-204.

Guerini, D., Krebs, J., and Carafoli, E. 1984. Stimulation of the purified erythrocyte Ca^{2+}-ATPase by tryptic fragments of calmodulin. *J Biol Chem* **259:** 15172-15177.

Haiech, J., Klee, C.B., and Demaille, J.G. 1981. Effects of cations on affinity of calmodulin for calcium: ordered binding of calcium ions allows the specific activation of calmodulin-stimulated enzymes. *Biochemistry* **20:** 3890-3897.

Harper, E.T., and Rose, G.D. 1993. Helix stop signals in proteins and peptides: the capping box. *Biochemistry* **32:** 7605-7609.

Hashimoto, Y., King, M.M., and Soderling, T.R. 1988. Regulatory interactions of calmodulin-binding proteins: phosphorylation of calcineurin by autophosphorylated Ca^{2+}/calmodulin-dependent protein kinase II. *Proc Natl Acad Sci U S A* **85:** 7001-7005.

Herzberg, O., and James, M.N. 1985. Common structural framework of the two Ca^{2+}/Mg^{2+} binding loops of troponin C and other Ca2+ binding proteins. *Biochemistry* **24:** 5298-5302.

Hutchinson, E.G., and Thornton, J.M. 1996. PROMOTIF--a program to identify and analyze structural motifs in proteins. *Protein Sci* **5:** 212-220.

Ikura, M., Clore, G.M., Gronenborn, A.M., Zhu, G., Klee, C.B., and Bax, A. 1992. Solution structure of a calmodulin-target peptide complex by multidimensional NMR. *Science* **256:** 632-638.

Ikura, M., Minowa, O., and Hikichi, K. 1985. Hydrogen bonding in the carboxyl-terminal half-fragment 78-148 of calmodulin as studied by two-dimensional nuclear magnetic resonance. *Biochemistry* **24:** 4264-4269.

Jahnke, W., Baur, M., G., G., and Kessler, H. 1995. Improved Accuracy of NMR Structures by a Modified NOESY-HSQC Experiment. *J. Magn. Reson. Ser. B* **106, B:** 86-88.

Jeffrey, L., and Yphantis, D. WinMatch. National Analytical Ultracentrifugation Facility University of Connecticut, Storrs.

Johnson, W.C., Jr. 1988. Secondary structure of proteins through circular dichroism spectroscopy. *Annu Rev Biophys Biophys Chem* **17:** 145-166.

Kalkhof, S., Ihling, C., Mechtler, K., and Sinz, A. 2005. Chemical cross-linking and high-performance fourier transform ion cyclotron resonance mass spectrometry for protein interaction analysis: application to a calmodulin/target peptide complex. *Anal Chem* **77:** 495-503.

Kawasaki, H., Nakayama, S., and Kretsinger, R.H. 1998. Classification and evolution of EF-hand proteins. *Biometals* **11:** 277-295.

Kay, L.E., Forman-Kay, J.D., McCubbin, W.D., and Kay, C.M. 1991. Solution structure of a polypeptide dimer comprising the fourth $Ca^{(2+)}$-binding site of troponin C by nuclear magnetic resonance spectroscopy. *Biochemistry* **30:** 4323-4333.

King, D.S., Fields, C.G., and Fields, G.B. 1990. A cleavage method which minimizes side reactions following Fmoc solid phase peptide synthesis. *Int J Pept Protein Res* **36:** 255-266.

Klee, C.B. 1988. Interaction of calmodulin with Calcium and target proteins. In *Calmodulin: molecular aspects of cellular regulation.* (ed. P. Cohen), pp. 35-56. Elsevier Science Publishers, Amsterdam.

Klee, C.B., Krinks, M.H., Manalan, A.S., Cohen, P., and Stewart, A.A. 1983. Isolation and characterization of bovine brain calcineurin: a calmodulin-stimulated protein phosphatase. *Methods Enzymol* **102:** 227-244.

Klee, C.B., Newton, D.L., Ni, W.C., and Haiech, J. 1986. Regulation of the calcium signal by calmodulin. *Ciba Found Symp* **122:** 162-182.

Knorr, R., Trzeciak, A., Bannwarth, W., and Gillessen, D. 1989. New coupling reagents in peptide chemistry. *Tetrahedron Letters* **30:** 1927-1930.

Koradi, R., Billeter, M., and Wuthrich, K. 1996. MOLMOL: a program for display and analysis of macromolecular structures. *J Mol Graph* **14:** 51-55, 29-32.

Kretsinger, R.H., and Nockolds, C.E. 1973. Carp muscle calcium-binding protein. II. Structure determination and general description. *J Biol Chem* **248:** 3313-3326.

Kuboniwa, H., Tjandra, N., Grzesiek, S., Ren, H., Klee, C.B., and Bax, A. 1995. Solution structure of calcium-free calmodulin. *Nat Struct Biol* **2:** 768-776.

Kuznicki, J., Grabarek, Z., Brzeska, H., Drabikowski, W., and Cohen, P. 1981. Stimulation of enzyme activities by fragments of calmodulin. *FEBS Lett* **130:** 141-145.

Larsson, G., Schleucher, J., Onions, J., Hermann, S., Grundstrom, T., and Wijmenga, S.S. 2001. A novel target recognition revealed by calmodulin in complex with the basic helix--loop--helix transcription factor SEF2-1/E2-2. *Protein Sci* **10:** 169-186.

Laskowski, R.A., Rullmannn, J.A., MacArthur, M.W., Kaptein, R., and Thornton, J.M. 1996. AQUA and PROCHECK-NMR: programs for checking the quality of protein structures solved by NMR. *J Biomol NMR* **8:** 477-486.

Laue, T.M., Shah, B.D., Ridgeway, T.M., and Pelletier, S.L. 1992. *Analytical Ultracentrifugation in Biochemistry and Polymer Science*. Royal Society of Chemistry, Cambridge.

Leavis, P.C., Rosenfeld, S.S., Gergely, J., Grabarek, Z., and Drabikowski, W. 1978. Proteolytic fragments of troponin C. Localization of high and low affinity Ca2+ binding sites and interactions with troponin I and troponin T. *J Biol Chem* **253:** 5452-5459.

Lee, W., Revington, M.J., Arrowsmith, C., and Kay, L.E. 1994. A pulsed field gradient isotope-filtered 3D 13C HMQC-NOESY experiment for extracting intermolecular NOE contacts in molecular complexes. *FEBS Lett* **350:** 87-90.

Lewit-Bentley, A., and Rety, S. 2000. EF-hand calcium-binding proteins. *Curr Opin Struct Biol* **10:** 637-643.

Li, M.X., Gagne, S.M., Tsuda, S., Kay, C.M., Smillie, L.B., and Sykes, B.D. 1995. Calcium binding to the regulatory N-domain of skeletal muscle troponin C occurs in a stepwise manner. *Biochemistry* **34:** 8330-8340.

Linge, J.P., Habeck, M., Rieping, W., and Nilges, M. 2003. ARIA: automated NOE assignment and NMR structure calculation. *Bioinformatics* **19:** 315-316.

Linse, S., and Chazin, W.J. 1995. Quantitative measurements of the cooperativity in an EF-hand protein with sequential calcium binding. *Protein Sci* **4:** 1038-1044.

Linse, S., and Forsen, S. 1995. Determinants that govern high-affinity calcium binding. *Adv Second Messenger Phosphoprotein Res* **30:** 89-151.

Linse, S., Helmersson, A., and Forsen, S. 1991. Calcium binding to calmodulin and its globular domains. *J Biol Chem* **266:** 8050-8054.

Linse, S., Jonsson, B., and Chazin, W.J. 1995. The effect of protein concentration on ion binding. *Proc Natl Acad Sci U S A* **92:** 4748-4752.

Logan, T.M., Olejniczak, E.T., Xu, R.X., and Fesik, S.W. 1992. Side chain and backbone assignments in isotopically labeled proteins from two heteronuclear triple resonance experiments. *FEBS Lett* **314:** 413-418.

Mann, S. 1988. Molecular recognition in biomineralization. *Nature* **332:** 119.

Maune, J.F., Beckingham, K., Martin, S.R., and Bayley, P.M. 1992a. Circular dichroism studies on calcium binding to two series of Ca^{2+} binding site mutants of Drosophila melanogaster calmodulin. *Biochemistry* **31:** 7779-7786.

Maune, J.F., Klee, C.B., and Beckingham, K. 1992b. Ca^{2+} binding and conformational change in two series of point mutations to the individual $Ca^{(2+)}$-binding sites of calmodulin. *J Biol Chem* **267:** 5286-5295.

McGaughey, G.B., Gagne, M., and Rappe, A.K. 1998. pi-Stacking interactions. Alive and well in proteins. *J Biol Chem* **273:** 15458-15463.

McPhalen, C.A., Strynadka, N.C., and James, M.N. 1991. Calcium-binding sites in proteins: a structural perspective. *Adv Protein Chem* **42:** 77-144.

Meador, W.E., Means, A.R., and Quiocho, F.A. 1992. Target enzyme recognition by calmodulin: 2.4 Å structure of a calmodulin-peptide complex. *Science* **257:** 1251-1255.

Meador, W.E., Means, A.R., and Quiocho, F.A. 1993. Modulation of calmodulin plasticity in molecular recognition on the basis of x-ray structures. *Science* **262:** 1718-1721.

Misura, K.M., Morozov, A.V., and Baker, D. 2004. Analysis of anisotropic side-chain packing in proteins and application to high-resolution structure prediction. *J Mol Biol* **342:** 651-664.

Moncrief, N.D., Kretsinger, R.H., and Goodman, M. 1990. Evolution of EF-hand calcium-modulated proteins. I. Relationships based on amino acid sequences. *J Mol Evol* **30:** 522-562.

Mondragon, A., Griffith, E.C., Sun, L., Xiong, F., Armstrong, C., and Liu, J.O. 1997. Overexpression and purification of human calcineurin alpha from Escherichia coli and assessment of catalytic functions of residues surrounding the binuclear metal center. *Biochemistry* **36:** 4934-4942.

Montelione, G.T., Lyons, B.A., Emerson, S.D., and Tashiro, M. 1992. An efficient triple resonance experiment using carbon 13 isotropic mixing for determining sequence-specific resonance assignments of isotopically enriched proteins. *J. Am. Chem. Soc.*: 10974–10975.

Moore, D.D. 1987. Gene Synthesis: Assembly of Target Sequences Using Mutually Priming Long Oligonucleotides. In *Current Protocols in Molecular Biology*. (eds. F. Ausubel, R. Brent, R. Kingston, D.D. Moore, J.G. Seidman, J.A. Smith, and K. Struhl), pp. 8.2B - 8.3. John Wiley & Sons, New York.

Muchmore, D.C., McIntosh, L.P., Russell, C.B., Anderson, D.E., and Dahlquist, F.W. 1989. Expression and nitrogen-15 labeling of proteins for proton and nitrogen-15 nuclear magnetic resonance. *Methods Enzymol* **177:** 44-73.

Nakayama, S., Moncrief, N.D., and Kretsinger, R.H. 1992. Evolution of EF-hand calcium-modulated proteins. II. Domains of several subfamilies have diverse evolutionary histories. *J Mol Evol* **34:** 416-448.

Nestle, M., and Roberts, W.K. 1969. An extracellular nuclease from Serratia marcescens. II. Specificity of the enzyme. *J Biol Chem* **244:** 5219-5225.

Neuhoff, V., Arold, N., Taube, D., and Ehrhardt, W. 1988. Improved staining of proteins in polyacrylamide gels including isoelectric focusing gels with clear background at nanogram sensitivity using Coomassie Brilliant Blue G-250 and R-250. *Electrophoresis* **9:** 255-262.

Newton, D.L., Oldewurtel, M.D., Krinks, M.H., Shiloach, J., and Klee, C.B. 1984. Agonist and antagonist properties of calmodulin fragments. *J Biol Chem* **259:** 4419-4426.

Olsson, L.L., and Sjolin, L. 2001. Structure of Escherichia coli fragment TR2C from calmodulin to 1.7 Å resolution. *Acta Crystallogr D Biol Crystallogr* **57:** 664-669.

Onions, J., Hermann, S., and Grundstrom, T. 1997. Basic helix-loop-helix protein sequences determining differential inhibition by calmodulin and S-100 proteins. *J Biol Chem* **272:** 23930-23937.

Onions, J., Hermann, S., and Grundstrom, T. 2000. A novel type of calmodulin interaction in the inhibition of basic helix-loop-helix transcription factors. *Biochemistry* **39:** 4366-4374.

Osawa, M., Tokumitsu, H., Swindells, M.B., Kurihara, H., Orita, M., Shibanuma, T., Furuya, T., and Ikura, M. 1999. A novel target recognition revealed by calmodulin in complex with Ca^{2+}-calmodulin-dependent kinase kinase. *Nat Struct Biol* **6:** 819-824.

Pascal, S.M., Muhandiram, D.R., Yamazaki, T., Forman-Kay, J.D., and Kay, L.E. 1994. Simultaneous acquisition of ^{15}N- and ^{13}C-edited NOE spectra of proteins dissolved in H_2O. *J. Magn. Reson. Ser. B*: 197–201.

Pelton, J.T., and McLean, L.R. 2000. Spectroscopic methods for analysis of protein secondary structure. *Anal Biochem* **277:** 167-176.

Potter, J.D., and Gergely, J. 1975. The calcium and magnesium binding sites on troponin and their role in the regulation of myofibrillar adenosine triphosphatase. *J Biol Chem* **250:** 4628-4633.

Procyshyn, R.M., and Reid, R.E. 1994a. An examination of glutamic acid in the -X chelating position of the helix-loop-helix calcium binding motif. *Arch Biochem Biophys* **311:** 425-429.

Procyshyn, R.M., and Reid, R.E. 1994b. A structure/activity study of calcium affinity and selectivity using a synthetic peptide model of the helix-loop-helix calcium-binding motif. *J Biol Chem* **269:** 1641-1647.

Reid, R.E. 1987a. A synthetic 33-residue analogue of bovine brain calmodulin calcium binding site III: synthesis, purification, and calcium binding. *Biochemistry* **26:** 6070-6073.

Reid, R.E. 1987b. Total sequential solid phase synthesis of rabbit skeletal troponin C calcium binding site III. *Int J Pept Protein Res* **30:** 613-621.

Reid, R.E. 1990. Synthetic fragments of calmodulin calcium-binding site III. A test of the acid pair hypothesis. *J Biol Chem* **265:** 5971-5976.

Reid, R.E., and Hodges, R.S. 1980. Co-operativity and calcium/magnesium binding to troponin C and muscle calcium binding parvalbumin: an hypothesis. *J Theor Biol* **84:** 401-444.

Reilly, D., and Fairbrother, W.J. 1994. A novel isotope labeling protocol for bacterially expressed proteins. *J Biomol NMR* **4:** 459-462.

Rhoads, A.R., and Friedberg, F. 1997. Sequence motifs for calmodulin recognition. *Faseb J* **11:** 331-340.

Rink, H. 1987. Solid-phase synthesis of protected peptide fragments using a trialkoxy-diphenyl-methyl ester resin. *Tetrahedron Letters* **28:** 3787-3790.

Schagger, H., and von Jagow, G. 1987. Tricine-sodium dodecyl sulfate-polyacrylamide gel electrophoresis for the separation of proteins in the range from 1 to 100 kDa. *Anal Biochem* **166:** 368-379.

Schuck, P. 2003. On the analysis of protein self-association by sedimentation velocity analytical ultracentrifugation. *Anal Biochem* **320:** 104-124.

Schuck, P., Perugini, M.A., Gonzales, N.R., Howlett, G.J., and Schubert, D. 2002. Size-distribution analysis of proteins by analytical ultracentrifugation: strategies and application to model systems. *Biophys J* **82:** 1096-1111.

Schumacher, M.A., Crum, M., and Miller, M.C. 2004. Crystal structures of apocalmodulin and an apocalmodulin/SK potassium channel gating domain complex. *Structure* **12:** 849-860.

Schumacher, M.A., Rivard, A.F., Bachinger, H.P., and Adelman, J.P. 2001. Structure of the gating domain of a Ca^{2+}-activated K^{+} channel complexed with Ca^{2+}/calmodulin. *Nature* **410:** 1120-1124.

Sekharudu, Y.C., and Sundaralingam, M. 1988. A structure-function relationship for the calcium affinities of regulatory proteins containing 'EF-hand' pairs. *Protein Eng* **2:** 139-146.

Shaw, G.S., Golden, L.F., Hodges, R.S., and Sykes, B.D. 1991. Interactions between paired calcium-binding sites in proteins NMR determination of the stoichiometry of calcium binding to a synthetic troponin-C peptide. *J. Am. Chem. Soc* **113:** 5557-5563.

Shaw, G.S., Hodges, R.S., and Sykes, B.D. 1990. Calcium-induced peptide association to form an intact protein domain: 1H NMR structural evidence. *Science* **249:** 280-283.

Shaw, G.S., Hodges, R.S., and Sykes, B.D. 1992. Determination of the solution structure of a synthetic two-site calcium-binding homodimeric protein domain by NMR spectroscopy. *Biochemistry* **31:** 9572-9580.

Shaw, G.S., and Sykes, B.D. 1996. NMR solution structure of a synthetic troponin C heterodimeric domain. *Biochemistry* **35:** 7429-7438.

Smith, J.A. 1997. Suppose. Vanderbilt University, Nashville.

Strynadka, N.C., and James, M.N. 1989. Crystal structures of the helix-loop-helix calcium-binding proteins. *Annu Rev Biochem* **58:** 951-998.

Svensson, B., Jonsson, B., Thulin, E., and Woodward, C.E. 1993. Binding of Ca^{2+} to calmodulin and its tryptic fragments: theory and experiment. *Biochemistry* **32:** 2828-2834.

Szebenyi, D.M., and Moffat, K. 1986. The refined structure of vitamin D-dependent calcium-binding protein from bovine intestine. Molecular details, ion binding, and implications for the structure of other calcium-binding proteins. *J Biol Chem* **261:** 8761-8777.

Tjandra, N., Feller, S.E., Richard, W.P., and Bax, A. 1995. Rotational Diffusion Anisotropy of Human Ubiquitin from ^{15}N NMR Relaxation. *J. Am. Chem. Soc* **117:** 12562-12566.

Uhlmann, E. 1988. An alternative approach in gene synthesis: use of long selfpriming oligodeoxynucleotides for the construction of double-stranded DNA. *Gene* **71:** 29-40.

VanScyoc, W.S., and Shea, M.A. 2001. Phenylalanine fluorescence studies of calcium binding to N-domain fragments of Paramecium calmodulin mutants show increased calcium affinity correlates with increased disorder. *Protein Sci* **10:** 1758-1768.

VanScyoc, W.S., Sorensen, B.R., Rusinova, E., Laws, W.R., Ross, J.B., and Shea, M.A. 2002. Calcium binding to calmodulin mutants monitored by domain-specific intrinsic phenylalanine and tyrosine fluorescence. *Biophys J* **83:** 2767-2780.

Vetter, S.W., and Leclerc, E. 2003. Novel aspects of calmodulin target recognition and activation. *Eur J Biochem* **270:** 404-414.

Wang, C.K., and Cheung, H.C. 1985. Energetics of the binding of calcium and troponin I to troponin C from rabbit skeletal muscle. *Biophys J* **48:** 727-739.

Williams, T.C., Corson, D.C., Oikawa, K., McCubbin, W.D., Kay, C.M., and Sykes, B.D. 1986. 1H NMR spectroscopic studies of calcium-binding proteins. 3. Solution conformations of rat apo-alpha-parvalbumin and metal-bound rat alpha-parvalbumin. *Biochemistry* **25:** 1835-1846.

Wilson, M.A., and Brunger, A.T. 2000. The 1.0 Å crystal structure of Ca(2+)-bound calmodulin: an analysis of disorder and implications for functionally relevant plasticity. *J Mol Biol* **301:** 1237-1256.

Wishart, D.S., Sykes, B.D., and Richards, F.M. 1991. Relationship between nuclear magnetic resonance chemical shift and protein secondary structure. *J Mol Biol* **222:** 311-333.

Wishart, D.S., Sykes, B.D., and Richards, F.M. 1992. The chemical shift index: a fast and simple method for the assignment of protein secondary structure through NMR spectroscopy. *Biochemistry* **31:** 1647-1651.

Wittekind, M., and Mueller, L. 1993. HNCACB, a high sensitivity 3D NMR experiment to correlate amide proton and nitrogen resonances with the α– and β–carbon resonances in proteins. *J. Magn. Reson. Ser. B*: 201–205.

Wolff, J., Newton, D.L., and Klee, C.B. 1986. Activation of Bordetella pertussis adenylate cyclase by the carboxyl-terminal tryptic fragment of calmodulin. *Biochemistry* **25:** 7950-7955.

Wu, X., and Reid, R.E. 1997a. Conservative D133E mutation of calmodulin site IV drastically alters calcium binding and phosphodiesterase regulation. *Biochemistry* **36:** 3608-3616.

Wu, X., and Reid, R.E. 1997b. Structure/calcium affinity relationships of site III of calmodulin: testing the acid pair hypothesis using calmodulin mutants. *Biochemistry* **36:** 8649-8656.

Yamazaki, T., Forman-Kay, J.D., and Kay, L.E. 1993. Two-dimensional NMR experiments for correlating $^{13}C\beta$ and $^{1}H\delta/\varepsilon$ chemical shifts of aromatic residues in 13C labeled proteins via scalar couplings. *J. Am. Chem. Soc.*: 11054–11055.

Yamniuk, A.P., and Vogel, H.J. 2004. Calmodulin's flexibility allows for promiscuity in its interactions with target proteins and peptides. *Mol Biotechnol* **27:** 33-57.

Yap, K.L. 1995. Interhlx. University of Toronto, Toronto.

Yap, K.L., Ames, J.B., Swindells, M.B., and Ikura, M. 1999. Diversity of conformational states and changes within the EF-hand protein superfamily. *Proteins* **37:** 499-507.

Yap, K.L., Ames, J.B., Swindells, M.B., and Ikura, M. 2002. Vector geometry mapping. A method to characterize the conformation of helix-loop-helix calcium-binding proteins. *Methods Mol Biol* **173:** 317-324.

Yap, K.L., Kim, J., Truong, K., Sherman, M., Yuan, T., and Ikura, M. 2000. Calmodulin target database. *J Struct Funct Genomics* **1:** 8-14.

Yap, K.L., and Tomomori, C. 1999. CSI. University of Toronto, Toronto.

Zhang, M., Tanaka, T., and Ikura, M. 1995. Calcium-induced conformational transition revealed by the solution structure of apo calmodulin. *Nat Struct Biol* **2:** 758-767.

Zwahlen, C., Gardner, K.H., Sarma, S.P., Horita, D.A., Byrd, R.A., and Kay, L.E. 1998. An NMR experiment for measuring methyl-methyl NOEs in 13C-labeled proteins with high resolution. *J. Am. Chem. Soc.*: 7617–7625.

Appendix A

List of amino acids

Amino acid name	Three-letter code	One-letter code
Alanine	Ala	A
Arginine	Arg	R
Asparagine	Asn	N
Aspartic acid	Asp	D
Cysteine	Cys	C
Glutamine	Gln	Q
Glutamic acid	Glu	E
Glycine	Gly	G
Histidine	His	H
Isoleucine	Ile	I
Leucine	Leu	L
Lysine	Lys	K
Methionine	Met	M
Phenylalanine	Phe	F
Proline	Pro	P
Serine	Ser	S
Threonine	Thr	T
Tryptophan	Trp	W
Tyrosine	Tyr	Y
Valine	Val	V

Throughout this thesis whenever amino acids are referred to generally, the full name of that amino acid is used. When a specific amino acid is referred to with its sequence number the one-letter code is used immediately followed by the sequence number. When an amino acid is referred to as part of a motif the position number is given followed by the full name of that amino acid. The three-letter code is only used in Appendix C. The DNA bases adenine, guanine, cytosine, and thymine appear with their respective one letter codes (A, G, C, and T) in upper or lower case. It will be clear form the context of the figure or text weather the abbreviation is meant to mean amino acid or DNA base.

Appendix B

Thermal cycler programs used for PCR throughout this thesis. Times are in minutes followed by a colon and the seconds.

Thermal cycler programs

Modified "Touchdown" procedure

Cycle	Temperature °C	Time (min)
1	98	5:00
2	98	1:00
3	55	2:00
4	68	4:00
5	Go to cycle 2	5 times
6	98	1:00
7	50	2:00
8	68	4:00
9	Go to cycle 6	10 times
10	98	1:00
11	45	2:00
12	65	4:00
13	Go to cycle 10	10 times
14	98	1:00
15	40	2:00
16	65	4:00
17	Go to cycle 14	10 times
18	65	5:00
19	4	Indefinite

Typical PCR program

Cycle	Temperature °C	Time (min)
1	94	4:00
2	94	0:30
3	50	0:50
4	72	2:00
5	Go to 2	34 times
6	72	5:00
7	4	Indefinite

First stage of CaM2/3 gene synthesis

Cycle	Temperature °C	Time (min)
1	94.0	3:00
2	94to65 @0.5°C/s	0:58
3	65	0:30
4	72	1:00
5	Go to cycle 3	30 times
6	72	3:00
7	4	Indefinite

Second stage of CaM2/3 gene synthesis

Cycle	Temperature °C	Time (min)
1	94.0	3:00
2	94.0	0:30
3	94to53 @0.5°C/s	1:22
4	53	0:30
5	72	1:00
6	Go to cycle 2	35 times
7	72	3:00
8	4	Indefinite

Appendix C

Peptide purity and characterization.

This appendix shows the results of the LCMS studies described in Chapter 2. The first section has the chromatograms from the LCMS study with the retention times listed above the peaks in min. The next section has a table with the expected molecular weights and the experimentally determined molecular weights from the LCMS study described in Chapter 2. The final section has the results from the amino acid analysis studies.

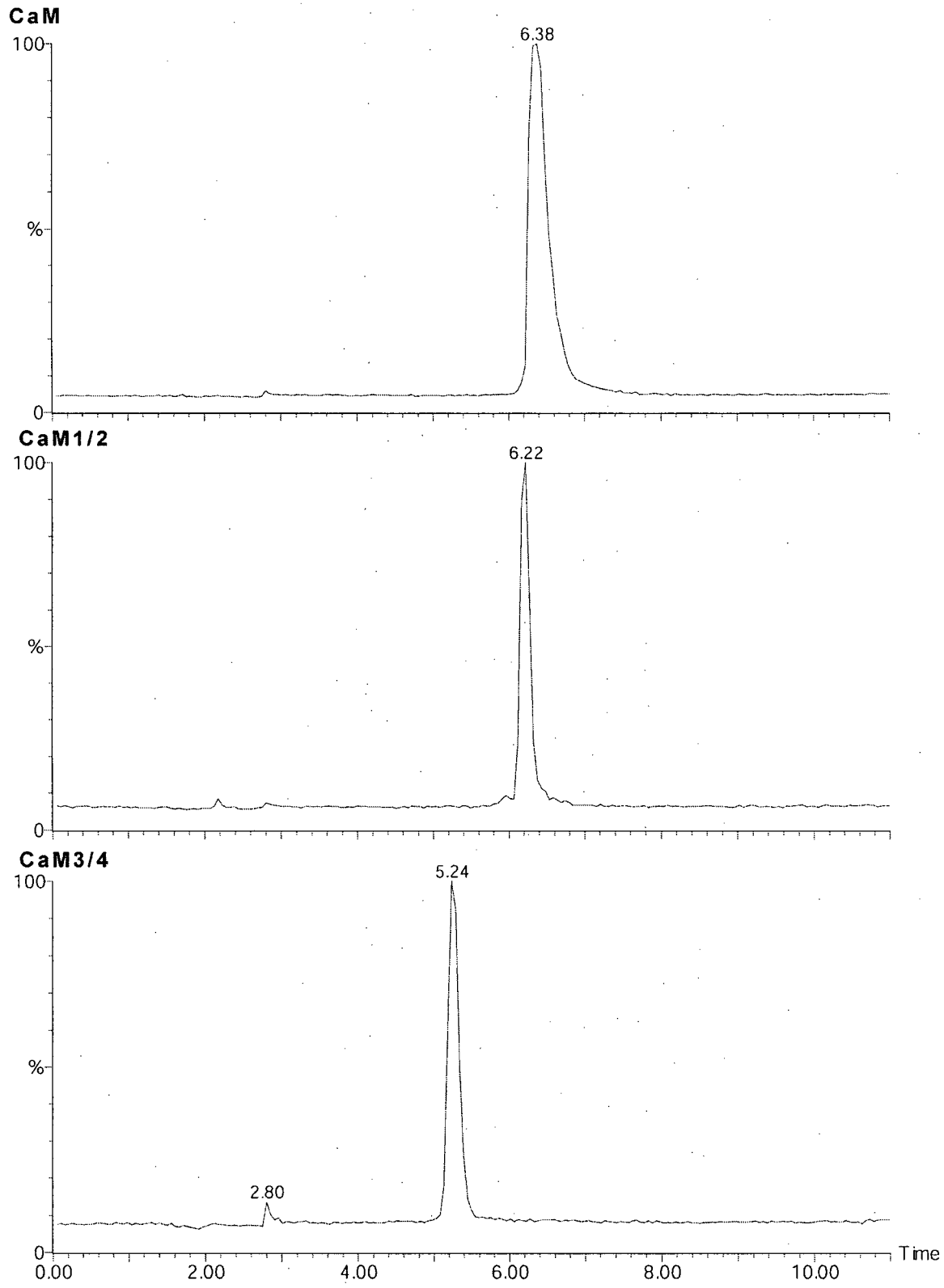
CaM
100
%
0
6.38
CaM1/2
100
%
0
6.22
CaM3/4
100
%
0
5.24
2.80
Time
0.00
2.00
4.00
6.00
8.00
10.00

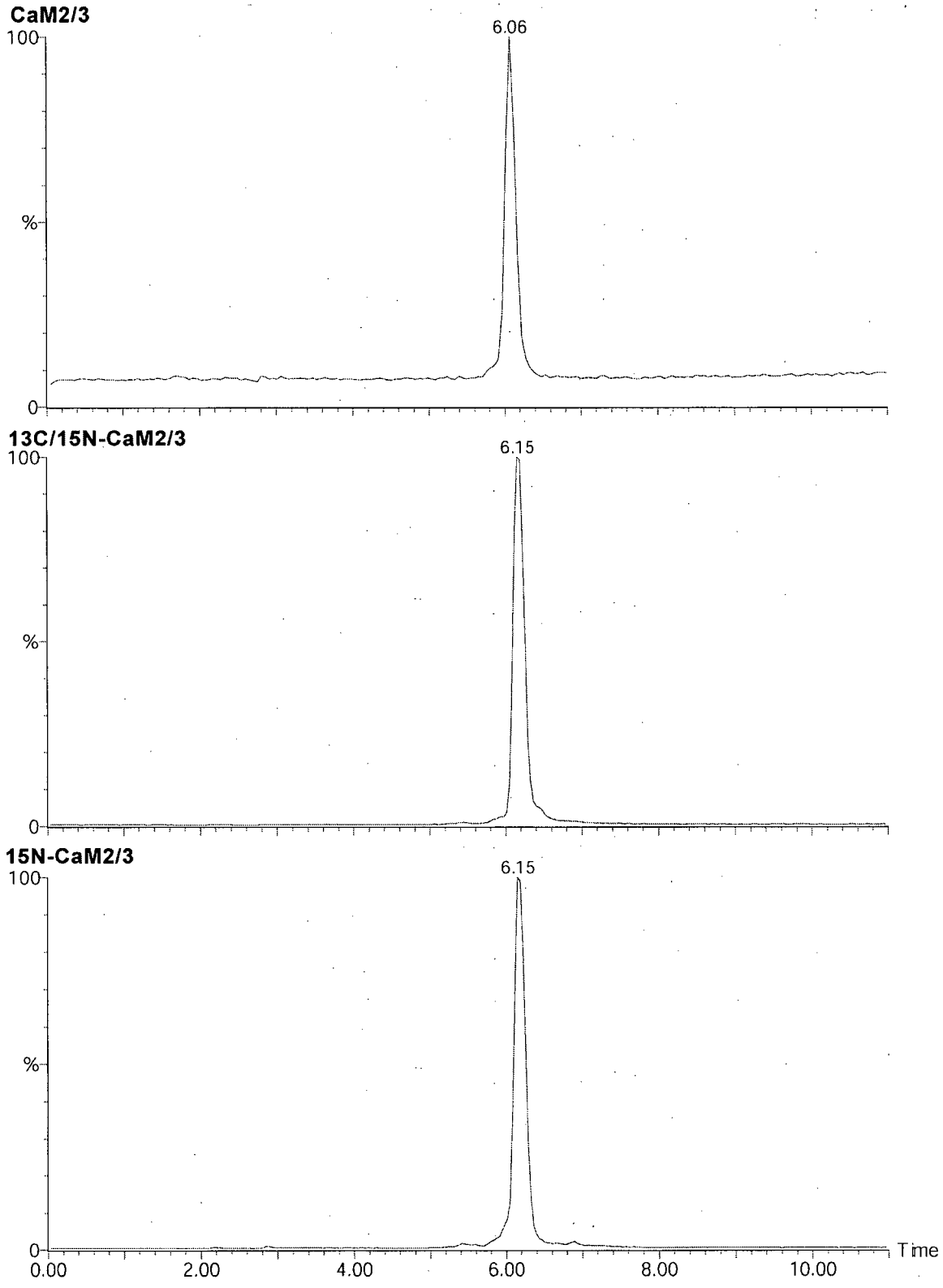
CaM2/3
100
%
0
6.06
13C/15N-CaM2/3
100
%
0
6.15
15N-CaM2/3
100
%
0
6.15
0.00
2.00
4.00
6.00
8.00
10.00
Time

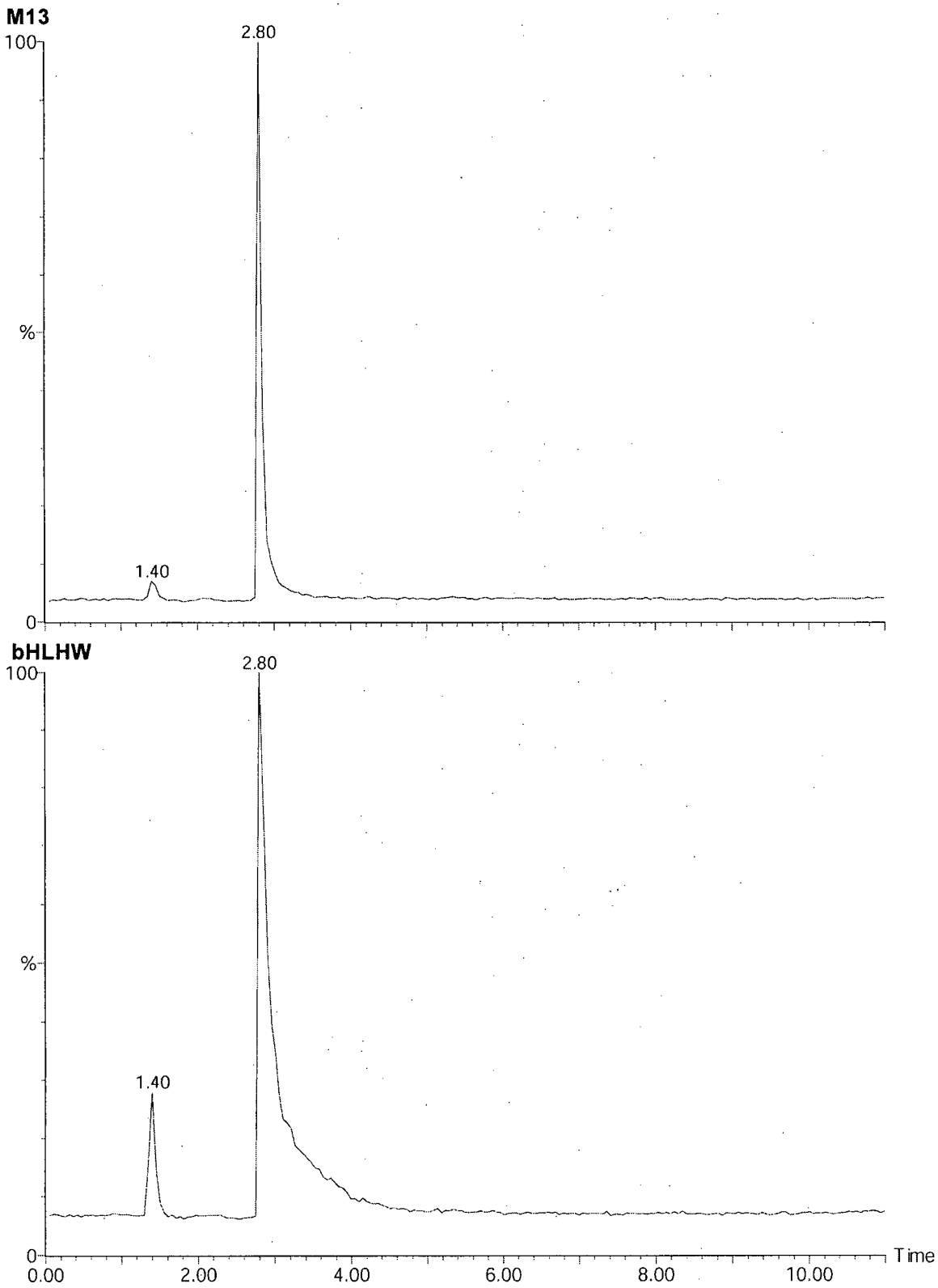
M13
100
2.80
%
1.40
0
bHLHW
100
2.80
%
1.40
0
0.00
2.00
4.00
6.00
8.00
10.00
Time

Peptide masses

Peptide	Expected Mass (a.m.u.)	Experimental Mass (a.m.u.)
CaM	16706.3	16708.3
CaM1/2	8908.0	8908.3
CaM3/4	7817.0	7817.0
CaM2/3	7700.6	7700.3
^{15}N-CaM2/3	7791.0	7790.3
^{13}C/^{15}N-CaM2/3	8119.0	8114
M13	2963.5	2963.3
bHLHW	5027.9	5027.0

Amino acid analysis

Amino acid analysis were performed according to Chapter 2 section 2.2.4. The peptide being analyzed is listed above each table. Amino acids are listed in three-letter code and AsX and GlX indicate Aspartate and asparagines, and glutamate and glutamine respectively. The pmol analyzed indicate the results of the analysis, the known comp. column lists the known amino acid composition of the listed peptide. The calculated comp. Column lists the calculated amino acid composition.

CaM

Amino Acid	pmol Analyzed	Known Comp.	Calculated Comp.
AsX	178909.545	23	23.5
GlX	212052.019	27	27.9
Ser	29777.1055	4	3.9
Gly	90173.801	11	11.8
His	9063.3885	1	1.2
Arg	53460.8715	6	7.0
Thr	89937.0815	12	11.8
Ala	89876.8325	11	11.8
Pro	19129.012	2	2.5
Tyr	11486.2255	2	1.5
Val	54879.734	7	7.2
Met	55511.531	9	7.3
Cys	327.94	0	0.0
Ile	58620.842	8	7.7
Leu	71750.4325	9	9.4
Phe	56146.5885	8	7.4
Lys	45315.5255	8	6.0

CaM1/2

Amino Acid	pmol Analyzed	Known Comp.	Calculated Comp.
AsX	114786	13	13.5
GlX	114918.6	13	13.5
Ser	16548.15	2	1.9
Gly	55276.76	6	6.5
His	0	0	0.0
Arg	19269.51	2	2.3
Thr	70863.03	9	8.3
Ala	54151.81	6	6.4
Pro	19470.07	2	2.3
Tyr	200.2765	0	0.0
Val	17905.47	2	2.1
Met	40826.19	5	4.8
Cys	124.6835	0	0.0
Ile	33566.23	4	3.9
Leu	52202.22	6	6.1
Phe	39808.35	5	4.7
Lys	31690.37	5	3.7

CaM3/4

Amino Acid	pmol Analyzed	Known Comp.	Calculated Comp.
AsX	213175	10	10.0
GlX	278473.3	14	13.0
Ser	41378.96	2	1.9
Gly	110606.1	5	5.2
His	23507.59	1	1.1
Arg	94281.22	4	4.4
Thr	62751.43	3	2.9
Ala	115611.5	5	5.4
Pro	0	0	0.0
Tyr	33634.85	2	1.6
Val	116084.4	5	5.4
Met	91621.84	4	4.3
Cys	43.156	0	0.0
Ile	88124.3	4	4.1
Leu	73358.82	3	3.4
Phe	65944.15	3	3.1
Lys	64895.52	3	3.0

CaM2/3

Amino Acid	pmol Analyzed	Known Comp.	Calculated Comp.
AsX	225097.2	12	11.9
GlX	171727.9	9	9.1
Ser	35188.61	2	1.9
Gly	97320.54	5	5.2
His	20376.65	1	1.1
Arg	81002.69	4	4.3
Thr	66957.27	4	3.5
Ala	116968.9	6	6.2
Pro	22556.11	1	1.2
Tyr	15078.93	1	0.8
Val	57973.12	3	3.1
Met	89827.29	5	4.8
Cys	532.655	0	0.0
Ile	74514.68	4	3.9
Leu	81161.88	4	4.3
Phe	74651.62	4	4.0
Lys	52385.07	3	2.8

^{15}N-CaM2/3

Amino Acid	pmol Analyzed	Known Comp.	Calculated Comp.
AsX	9159.17	12	12.5
GlX	5914.764	9	8.1
Ser	1592.344	2	2.2
Gly	3608.79	5	4.9
His	885.818	1	1.2
Arg	3731.915	4	5.1
Thr	2975.933	4	4.1
Ala	4154.14	6	5.7
Pro	1082.993	1	1.5
Tyr	653.5105	1	0.9
Val	2440.172	3	3.3
Met	3136.547	5	4.3
Cys	35.985	0	0.0
Ile	3205.075	4	4.4
Leu	1860.668	4	2.5
Phe	3184.437	4	4.4
Lys	2110.147	3	2.9

$^{13}C/^{15}N$-CaM2/3

Amino Acid	pmol Analyzed	Known Comp.	Calculated Comp.
AsX	12276.86	12	11.9
GlX	8195.358	9	7.9
Ser	2320.689	2	2.2
Gly	6197.037	5	6.0
His	1193.401	1	1.2
Arg	4442.562	4	4.3
Thr	4041.324	4	3.9
Ala	5934.068	6	5.7
Pro	1133.024	1	1.1
Tyr	1128.141	1	1.1
Val	3189.807	3	3.1
Met	4543.254	5	4.4
Cys	0.671667	0	0.0
Ile	4148.617	4	4.0
Leu	4325.581	4	4.2
Phe	4202.667	4	4.1
Lys	3042.918	3	2.9

M13

Amino Acid	pmol Analyzed	Known Comp.	Calculated Comp.
AsX	5632.874	2	1.8
GlX	0	0	0.0
Ser	13041.19	4	4.2
Gly	4370.125	1	1.4
His	847.001	0	0.3
Arg	7392.749	3	2.4
Thr	0	0	0.0
Ala	12539.12	4	4.0
Pro	0	0	0.0
Tyr	354.143	0	0.1
Val	2952.468	1	1.0
Met	35.702	0	0.0
Cys	0	0	0.0
Ile	6275.138	2	2.0
Leu	4132.358	1	1.3
Phe	6141.892	2	2.0
Lys	13747.35	5	4.4

bHLHW

Amino Acid	pmol Analyzed	Known Comp.	Calculated Comp.
AsX	13220.93	4	3.9
GlX	13503.28	4	4.0
Ser	0	0	0.0
Gly	21135.37	6	6.2
His	0	0	0.0
Arg	40795.5	12	12.1
Thr	0	0	0.0
Ala	13457.58	4	4.0
Pro	102.593	0	0.0
Tyr	0	0	0.0
Val	6616.693	2	2.0
Met	5202.815	2	1.5
Cys	153.028	0	0.0
Ile	0	0	0.0
Leu	6777.764	2	2.0
Phe	0	0	0.0
Lys	6221.549	2	1.8

Appendix D

Stability study

Prior to NMR studies we determined the stability of CaM2/3. A 50 μM solution of CaM2/3 was prepared in a buffer containing 20 mM Tris HCl pH 7.4, 50 mM KCl, and 10 mM $CaCl_2$. Two 100 μL samples were incubated at 37 and 30 °C for 10 days. After incubation an aliquot of each sample and a control sample were applied to a 16.5% Tris-Tricine gel according to the method in Chapter 3. The gel below shows that there is no visible degradation of CaM2/3 and that the CaM2/3 is stable in the above buffer.

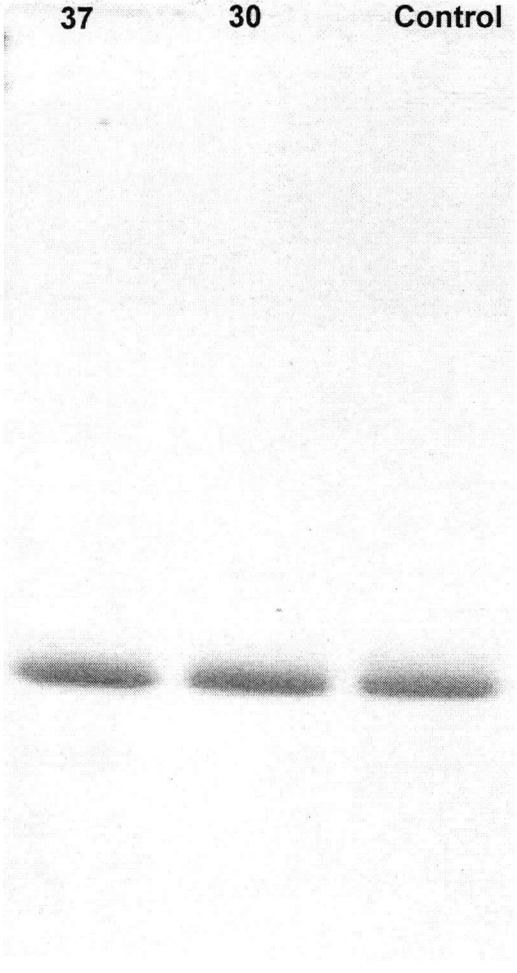

Appendix E

We used several experiments to show that CaM2/3 is monomeric in solution. These experiments included AUC, light scattering, measurement of τ_c, and an ^{13}C NOESY experiment. This appendix shows the results of both the light scattering and ^{13}C NOESY experiments.

Light scattering experiment

We initially used light scattering to determine if CaM2/3 was monomeric in solution. Natural abundance CaM2/3 was dissolved in a buffer containing 20 mM Tris HCl pH 7.4, 50 mM KCl, and 10 mM $CaCl_2$. The final concentration of CaM2/3 was 3 mg/mL. The protein sample was applied to a Superdex 75HR 10/30 gel filtration column (Amersham) that was pre equilibrated with the above buffer. The column was connected to a miniDAWN multi angle light scattering apparatus (Wyatt Technologies). Data analysis was carried out using the ASTRA software. The molecular weight is consistent with the monomeric molecular weight determined by mass spectrometry (7700 a.m.u.).

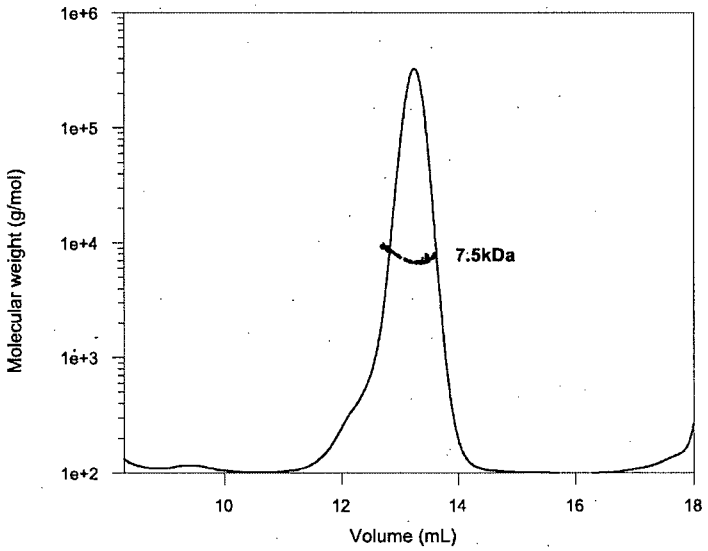

NMR Experiment

We used an isotope-filtered ^{13}C-HMQC-NOESY experiment to detect NOE's between uniformly labeled $^{13}C/^{15}N$-CaM2/3 and natural abundance CaM2/3 (Lee et al. 1994). If CaM2/3 is monomeric in solution it should not produce intermolecular NOE's under these conditions. Both uniformly labeled $^{13}C/^{15}N$-CaM2/3 and natural abundance CaM2/3 were mixed in equal concentrations (final concentration 0.3 mM) in NMR buffer and a ^{13}C-HMQC-NOESY was recorded on the 500 MHz spectrometer. The results are presented below and they show that there are no peaks that would be consistent with specific intermolecular contacts between $^{13}C/^{15}N$-CaM2/3 and CaM2/3.

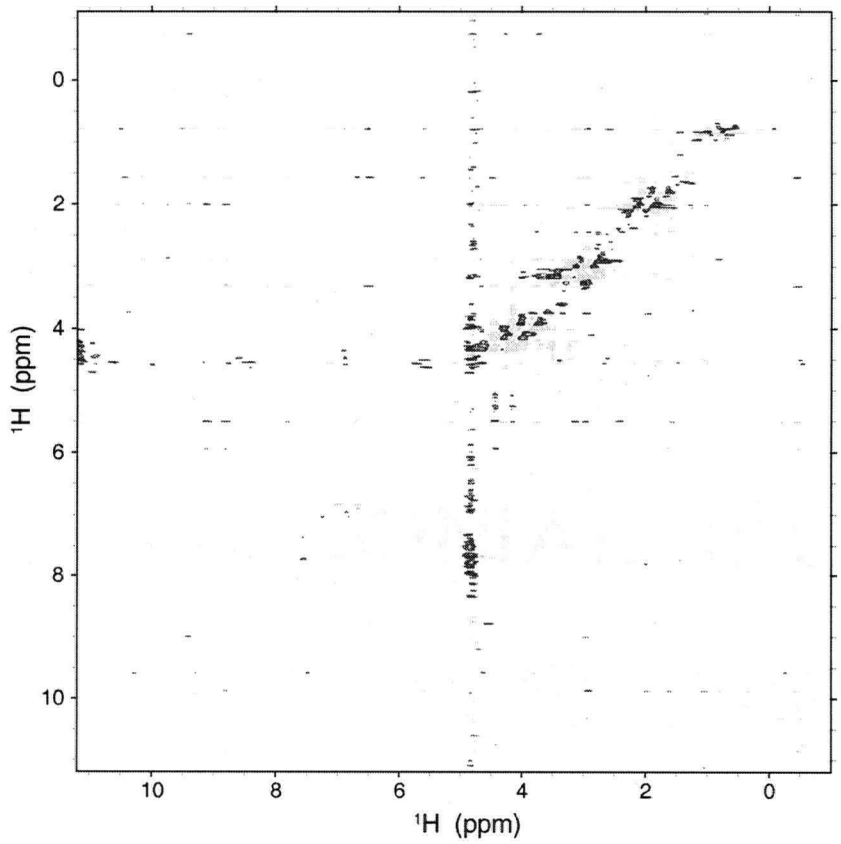

The black peaks are positive and the gray peaks are negative. There are no peaks consistent with a specific interaction between labeled and unlabeled CaM2/3

Appendix F

This appendix includes sequences from many EF-hand proteins showing the positions of aromatic residues involved in aromatic stacking interactions (highlighted). The sequences are aligned on the Ca^{2+}-binding segments.

EF	Protein	Sequence
		+ | +
1	CAMHS	EFKEAFSLF D K D GDGT I TTKELGTVMRSL
1	CAMSC	EFKEAFALF D K D NNGS I SSSELATVMRSL
1	CALCIB	RLGKRFKKL D L D NSGS L SVEEFMSLP EL
1	CALICE	EFREAFMMF D K D GNGT I STKELGIAMRSL
1	SPECI	EFKRRFKNK D T D KSKS I TAEELGEFFKST
1	TRACTIN	EIREAFDLF D T D GSGT I DAKELKVAMRAL
1	QUIDLN	EIKDAFDMF D I D GDGQ I TSKELRSVMKSL
1	aACTDD	EFKACFSHF D K D NDNK L NRLEFSSCLKSI
1	TPHUCS	EFKAAFDMF D A D GGGD I SVKELGTVMRML
1	TPHR	QFRAAFDIF VAD A KDGT I SSKELGKVMKML
1	TPAP1	ALQKAFDSF D T D SKGF I TPETVGIILRMM
1	MOPP1	QIQECFQIF D K D NDGK V SIEELGSALRSL
1	MOSWLE	EMKEAFSMI D V D RDGF V SKDDIKAISEQ~
1	MOSWLD	DLKDVFELF D FWDGRDGA V DAFKLGDVCRCL
1	MOHSA1	EFKEAFLLF D S T GDSK I ILSQVGDVLRAL
1	PVNESA	
1	PVNESB	
1	KLBOI	ELKGIFEKY A A K EGDPNQL SKEELKLLLQTE
1	BCBOIB	ALIDVFHQY S G R EGDKHKL KKSELKELINNE
1	2A9	LLVAIFHKY S G R EGDKHTL SKKELKELIQKE
1	PIOBT	TMMFTFHKF A GDKGYL TKEDLRVLMEKE
		+ | +
2	CAMHS	ELQDMINEV D A D GNGT I DFPEFLTMMARK
2	CAMSC	EVNDLMNEI D V D GNHQ I EFSEFLALMSRQ
2	CALCIB	LVQRVIDIF D T D GNGE V DFKEFIEGVSQF
2	CALICE	EILEMINEV D I D GNGQ I EFPEFCVMMKRM
2	SPEC1	QIDKMISDV D T D ESGT I DFSEMLMGIAEQ
2	TRACTIN	EIKKMISEI D K D GSGT I DFEEFLTMMTAK
2	QUIDLN	ELEEMIREV D T D GNGT I EYAEFVEMMAKQ
2	aACTDD	QLNQVISKI D T D GNGT I SFEEFIDYMVSS
2	TPHUCS	ELDAIIEEV D E D GSGT I DFEEFLVMMVRQ
2	TPHR	DLQEMIEEV D I D GSGT I DFEEFCLMMYRQ
2	TPAP1	HLQQVISET D E D GSGE I EFEEFAELAAKF
2	MOPP1	ELNTIKGEL NAKEF DLATFKTVYRKP
2	MOSWLE	ELTAML K E A PGP L NFTMFLS DK
2	MOSWLD	DVFAVGGTH K M G EKS L PFEEFLPAYEGL
2	MOHSA1	EVRKVLGNPSN E E LNAKKI EFEQFLPMMQAI
2	PVNESA	DINKAIHAF K A G EA F D FKKF VHLLGL
2	PVNESB	DIEAALSSV K A A ES F N YKTF FTKCGL
2	KLBOI	TLDELFEEL D K N GDGE V SFEEFQVLVKKI
2	BCBOIB	VVDKVMETL D S D GDGE C DFQEFMAFVAMI

```
2      2A9          EIARLMEDL D R N KDQE V NFQEYVTFLGAL
2      PIOBT        AVDKIMKDL D Q C RDGK V GFQSFFSLIAGL

                              +           |     +
3      CAMHS        EIREAFRVF D K D GNGY I SAAELRHVMTNL
3      CAMSC        ELLEAFKVF D K N GDGL I SAAELKHVLTSI
3      CALCIB       KLRFAFRIY D M D KDGY I SNGELFQVLKMM
3      CALICE       MIREAFRVF D K D GNGV I TAQEFRYFMVHM
3      SPECI        HYTKAFDDM D K D GNGS L SPQELREALSAS
3      TRACTIN      EILKAFRLF D D D NSGT I TIKDLRRVAKEL
3      QUIDLN       EMREAFRVF D K D GNGL I TAAELRQVMANF
3      aACTDD
3      TPHUCS       ELAECFRIF D R N ADGY I DPEELAEIFRAS
3      TPHR         ELSEAFRLF D L D GDG I G DELKAALDGT
3      TPAP1        ELKEAFRIY D R G GDGY I TTQVLREILKEL
3      MOPP1        EMLDAFRAL D K E GNGT I QEAELRQLLLNL
3      MOSWLE       TIRNAFAMF D E Q ENKK L NIEYIKDLLEDM
3      MOSWLD       DYMEAFKTF D R E GQGF I SGAELRHVLTAL
3      MOHSA1       DFVEGLRVF D K E GNGT V MGAELRHGLATL
3      PVNESA       DVTKAFHIL D K D RSGY I EEEELQLILKGF
3      PVNESB       QVKKVFDIL D Q D KSGY I EEDELQLFLKNF
3      KLBOI
3      BCBOIB
3      2A9
3      PIOBT

                              +           |     +
4      CAMHS        EVDEMIREA D I D GDGQ V NYEEFVQMMTAK
4      CAMSC        EVDDMLREV S D   GSGE I NIQQF AALLSK
4      CALCIB       IVDKTIINA D K D GDGR I SFEEFSAVVGGL
4      CALICE       EVDEMIKEV D V D GDGE I DYEEFVKMMSNQ
4      SPECI        KIKAIIQKA D A N KDGK I DREEFMKLIKSC
4      TRACTIN      ELQEMIAEA D R N DDNE I DEDEFIRIMKKT
4      QUIDLN       EISEMIREA D I D GDGM V NYEEFVKMMTPK
4      aACTDD
4      TPHUCS       EIESLMKDG D K N NDGR I DFDEFLKMMEGV
4      TPHR         EVDEMMADG D K N HDSQ I DYEEWVTMMKFV
4      TPAP1        NLDEIIEEI D E D GSGT I DFMEFMKMMTG
4      MOPP1        EVEELMKEV S V S GDGA I NYESFVDMLVTG
4      MOSWLE       EMR MTFKE A P V EGGK F DYVKFTAMIK G
4      MOSWLD       DEIISLTDL Q E D LEGN V KYEDFVKKVMAG
4      MOHSA1       EVEALMAG  Q E D SNGC I NYEAFVKHIMSI
4      PVNESA       ETKDLLIKG D K D GDGK I GVDEFTSLVAES
4      PVNESB       ETKAFLEAG D S D GDGK I GVDEFQALVR S
4      KLBOI
4      BCBOIB
4      2A9
4      PIOBT
```

The positions of key aromatic residues forming aromatic stacking interactions are highlighted. The abbreviations for calcium binding proteins: human CaM (CAMHS), yeast CaM (CAMSC), calcineurin-B (CALCIB), nematode Cal-1 gene (CALICE), sea urchin Spec1A protein (SPECI), flagellate caltracin (TRACTIN), squid squidulin (QUIDLN), slime mold α-actinin (aACTDD), human tropinin-C (TPHUCS), ascidian tropinin-C (TPHR), crayfish tropinin-C-1 (TPAP1), slim mold myosin ELC (MOPP1), scallop myosin ELC (MOSWLE), scallop myosin ELC-sk (MOSWLD), human myosin ELC-L1-sk (MOHSA1), amphiuma parvalbumin-α (PVNESA), amphiuma parvalbumin-β (PVNESB), bovine intestinal calcium binding protein (ICBP) (KLBOI), bovine S100-β, human calcyclin (2A9), bovine p10 (PIOBT) . The

positions of the first and last amino acid in the Ca^{2+}-binding loop is indicated with a + and the position 8, β-sheet forming residue in indicated with an |. This appendix was adapted from a similar appendix in (Moncrief et al. 1990).

Appendix G

A titration of ^{15}N CaM was performed with the bHLHW peptide using a Varian 600MHz spectrometer. ^{15}N-HSQC spectra were performed on CaM and CaM with increasing amounts of bHLHW. The graph below shows a binding plot for the titration of CaM using bHLHW by following residue K115 (open circles) and T44 (closed circles) here the stoichiometry for binding agrees with previous studies as the binding reaches a maximum around 0.5 bHLHW dimer : CaM or two CaM to one bHLHW dimer.